Computational model of normal and cancer cell collective mechanics and migration

By:

Ana Sofia dos Santos Leite Ferreira

A thesis submitted in partial fulfilment of the requirements for the degree of Doctor of Philosophy

The University of Sheffield

Department of Mechanical Engineering

Insigneo Institute for *in-silico medicine*

Sheffield, February 2018

Computational model of normal and cancer cell collective mechanics and migration

A.S.S.L. Ferreira

Supervisors:

Prof. Damien Lacroix

Dr. Dawn Walker

Examiners:

Prof. Hans Van Oosterwyck

Dr. Cecile Perrault

Sheffield, February 2018

Acknowledgements

Above all, I would like to thank my supervisors Doctor Dawn Walker and Professor Damien Lacroix for giving me the opportunity to enrol this PhD and for the knowledge shared and support provided throughout its duration. I am grateful for their mentorship and the experience I gained attending international conferences, summer schools, seminars and doing demonstrations at the University. *Thank you both.*

I would like to acknowledge the funding for this PhD provided by The Engineering and Physical Sciences Research Council (EPSRC) Frontier Engineering Award, FP7 EC Computational Horizons in Cancer (CHIC) project and the European Research Council (ERC).

This PhD work was developed at the Insigneo Institute for *in-silico* medicine in Sheffield. I am very thankful to everyone behind Insigneo for making it a place of solidarity, support and ambition. I am richer because of the opportunity I had to meet talented people from so many different countries and cultures. I am especially thankful to my close colleagues in Insigneo for the technical support and kind incentive, in particular from C+14: Jafar, André, Stefania and Ana. *Thank you all.*

The city of Sheffield became a second home thanks to my Sheffield friends. *Thank you for the inspiration and for representing the value of friendship.*

I would like to show gratitude to all my friends and family members for their unconditional encouragement and thank personally to Irene, Angelina, Francisca, Gosia, Kel, Mé, Paulina, Mitra, Miguel, Mario, Anita, my uncles, aunts and cousins, my godmather Ruca and my brother Zé Pedro. *Thank you all. Obrigada.*

I am grateful to my parents Ana and José for their guidance. *Obrigada por investirem em mim e acreditarem em mim.*

I would like to finish by thanking my young cousins Margarida, Bernardo, João, Tomás and Carlota and my grandparents Justa and Manuel for their sweet inspiration and motivation. *Obrigada.*

This thesis is dedicated to my grandfather Manuel C. Santos Leite

Ao meu avô

Eu sou porque tu foste,

Tu és,

Eu quero ser como tu foste,

Como tu és,

Porque tu és flor delicada e pedra dura,

És arte e ciência,

És música e princípio,

És pintura e és saber,

És curiosidade e és história.

Tu és espírito e suor,

És humildade e coragem,

Serves e crias,

Vês para além.

Tu és força maior,

Tu és inspiração.

E eu,

Eu quero ser como tu.

SF em 2016

Communications

Oral communication at the 21st Congress of the European Society of Biomechanics, Prague, Czech Republic, 5-8 July 2015 (Authors: Ana Sofia Ferreira, Dawn Walker and Damien Lacroix; Title: Multiscale modelling of normal and cancer cell biomechanics and behaviour)

Poster communication at the MEIBioeng 2015, Leeds, UK, 7-8 September 2015 (Authors: Ana Sofia Ferreira, Dawn Walker and Damien Lacroix; Title: Multiscale modelling of normal and cancer cell biomechanics and behaviour)

Poster communication at the Simulia Regional User Meeting, Warrington, 2-3 November 2015 (Authors: Ana Sofia Ferreira, Dawn Walker and Damien Lacroix; Title: Multiscale modelling of normal and cancer cell biomechanics and behaviour)

Oral communication at the 22nd Congress of the European Society of Biomechanics, Lyon, France, 10-13 July 2016 (Authors: Ana Sofia Ferreira, Dawn Walker and Damien Lacroix; Title: Computational modelling of normal and cancer collective mechanics and behaviour)

Oral communication at the Virtual Physiological Human Conference 2016, Amsterdam, Netherlands, 26-28 September 2016 (Authors: Ana Sofia Ferreira, Dawn Walker and Damien Lacroix; Title: Computational Modelling of Normal and Cancer Cell Collective Mechanics and Migration)

Oral communication at the 23rd Congress of the European Society of Biomechanics, Seville, Spain, 2-5 July 2017 (Authors: Ana Sofia Ferreira, Dawn Walker and Damien Lacroix; Title: Computational Modelling of the Mechanics of Migration of Normal and Cancer Cell Populations)

Abstract

Changes in the biological behaviours of cell migration and sorting are associated with cancer. Mechanistic and quantitative understanding of the mechanics of these biological processes can promote the development of anti-cancer treatments. Computational models can be used as platforms to generate this understanding and to test drugs *in-silico*. The heterogeneity of cancer cells constitutes one of the main drawbacks in the development of anti-cancer drugs. Cell heterogeneity must be comprehended and regarded when developing anti-cancer drugs. This heterogeneity can be accounted for using computational modelling. In addition, now that measurement technologies allow the determination of the mechanical properties of normal and cancer cells, computational models with higher mechanical fidelity are possible.

In this context, a quantitative and mechanistic computational model was developed in this work to investigate the role that the mechanical properties of cancer cells play in their migration and sorting.

The individual cell properties: Young's modulus, cell-cell adhesion and local microenvironment (neighbouring cells and position within the monolayer) were found to affect intercellular stress in the first hours following cell seeding. In addition, the presence of mechanically different normal and cancer cells in co-culture results in early sorting between them and higher variation of intercellular stress when comparing to normal and cancer monocultures.

Quantitative mechanical thresholds for the sorting of migrating normal and cancer cells in co-culture were defined. Sorting depended primarily on differences in the traction force of normal and cancer cells and absolute cell-cell adhesion levels, followed by the differential adhesion of normal and cancer cells. The predictions supported an integrated mechanism for the sorting of normal and cancer cells.

The model also predicted that different spatial distributions of cell mechanical properties can trigger different migration modes in cancer cell populations. This suggests that the plasticity of migration of cancer cell populations is related with the heterogeneity of cell mechanics. Since the sorting of normal and cancer cells in co-culture depends on the spatial distribution of their mechanical properties, mechanical

thresholds for cell sorting should additionally depend on the cell microenvironment. The effect of microtubule stabilizers on sorting was tested *in-silico* accounting for the changes induced in the mechanical properties of cancer cells. Microtubule stabilizers were predicted to reverse both the mechanical and migration properties of cancer cells to properties similar to the ones of normal healthy cells. The sorting of normal and cancer cells, is thereby, reduced.

This study shows that individual cell mechanical properties can explain a variety of population-scale measurements and behaviours. The results emphasize the importance of investigating the changes in cell mechanics that accompany malignant transformation and their role in cancer progression.

Index of Contents

List of Figures

Figure A.1. Intercellular force and cell velocity evolution for the three time step values considered. Force was computed as the sum of intercellular forces for all the cells modelled. Cell velocity was averaged for all the cells and the associated standard deviation is shown.

Figure A.2. Level of force per cell shows that force oscillates every iteration for time step 1. This is not observed for time step 2. Each line corresponds to the evolution of intercellular force for one cell. For normal cells intercellular force is in blue and for cancer cells intercellular force is in black.

Figure A.3. Cells with higher intercellular force are shown for four consecutive iterations using time step 1. These cells experience a repulsion/adhesion cycle. They are shown in different colour together with their intercellular force vector.

List of Tables

Symbols

A– Overlap area for a cell pair

d– Distance between the centre of two cells

E– Cell apparent Young's modulus

E_{eq}– Equivalent apparent Young's modulus for a cell pair

$\vec{F}$– Force driving cell movement

$F_{Adhesion}$– Adhesion force between two cells

$\vec{F}_{active}$– Active force for a cell

$F_{compress}$– Compressibility force for a cell pair

$\vec{F}_{drag}$– Extracellular drag force for a cell

F_{Hertz}– Hertz repulsion force between two cells

$\vec{F}_{intercellular}$ – Resultant intercellular force for a cell

$\vec{F}_{intercellullar\ pairwise}$– Intercellular force vector for a cell pair

F_{JKR}– JKR force between two cells

h– Contact penetration for a cell pair, same as $overlap$ in this work

K– Cell bulk modulus

μ – Medium viscosity

ν– Cell Poisson ratio

R– Cell radius

R_{eq}– Equivalent radius for a cell pair

σ– Intercellular adhesion energy for a cell pair

$Stress$– Cell stress

Δt– Time step

$\vec{u}$– Cell displacement

$\vec{v}$– Cell velocity

V– Cell volume

$V_{isolated}$– Isolated cell volume

$V_{overlap}$ – *Volume of the overlap region between two cells*

V_{target} – *Reference volume for a cell, in this work equal to* $V_{isolated}$

Chapter 1 - Introduction

Summary

This Chapter introduces the biological processes of collective cell migration and cell sorting, their importance in cancer and their relation with cell mechanics. The need to develop mechanistic understanding of the role of cell mechanics in collective migration and sorting is addressed, as well as the potential of computer models to satisfy that need. The thesis proposal is presented and the specific aims of each chapter are described.

1.1 Collective cell migration and sorting in cancer metastasis

Metastasis is the spreading of cancer from a primary tumour to secondary locations within the body. It is a complex process responsible for 90% of cancer deaths [1]. For metastasis, cancer cells detach from the primary tumour, migrate, invade other tissues, enter into the circulatory system and reach other sites where they create secondary tumours. Mechanistic understanding of metastasis is required to support the development of anti-metastatic treatments and reduce cancer mortality [2].

The migration of cells is affected in cancer metastasis. Cell migration is a normal process that is fundamental for the development and maintenance of multicellular organisms. It is involved in many diverse biological processes, from immune response to angiogenesis [3]. Cells can migrate individually or collectively, in coordination with other cells. When moving as a cluster, cells form a polarized multicellular unit and respond differently to directional cues than when moving in isolation [4]. Experimental data suggest that collective cell migration is regulated by intercellular interactions and large-scale propagation of signals, such as mechanical loading [5]. Therefore, the behaviour of a cell population emerges from the collective and cannot be predicted from the behaviour of single isolated cells.

Collective cell migration is particularly important in wound healing, morphogenesis and, in a diseased state, cancer metastasis [6]. A continuous transition seems to exist between individual and collective cell migration. Cells on the edge of a migrating cluster

present specific features that are similar to the ones found in cells that migrate individually. These enable them to direct the movement of the cluster [7]. This continuous spectrum of migration is also seen in cancer metastasis. Cancer cells are able to opportunistically switch migration mode, explaining why their migration is said to be plastic [8]. Cancer cells can detach from the carcinoma *in-situ* collectively and invade the surrounding tissues as a group [9], or individually, owing to a dynamic transformation to a more aggressive and migratory phenotype [10]. Therefore, cancer metastasis is related with the separation of cells of different type, or cell sorting.

The phenomenon of sorting requires collective cell migration and is not only involved in metastasis. Cell sorting is, for instance, naturally present in morphogenesis, allowing the segregation of the cells that will compose the different tissues [11], [12]. The separation of cells of different type can also be artificially triggered. One application is the development of primary tumour cell lines to test anti-cancer drugs. This requires the sorting of cells from mixed tumour samples [13]. Both collective cell migration and cell sorting are associated with cancer. Consequently, the investigation of these biological processes can favour the development of anti-cancer treatments.

In-vitro experiments have been developed to increase the understanding of collective cell migration and cell sorting. One of such experiments is the wound healing assay. After cell culture, the cell monolayer is scratched to create a wound and investigate the dynamics of the monolayer as the cells migrate to close the wound. These studies have shown that directionality and intercellular coordination are key aspects of collective cell migration [14]–[16]. Revealing the mechanism used by cells to coordinate their migration remains a challenge [17]. Furthermore, *in-vitro* experiments have confirmed the existence of a relationship between cell mechanics and cell migration. The forces actively exerted by adherent cells to migrate collectively on a substrate have been measured [16]. The results revealed heterogeneous and dynamic traction force fields. However, a clear relation between the forces measured and the collective movement observed is yet to be found [18].

The spontaneous sorting of cells of different types has been observed *in-vitro.* Cells of different types from the blood brain barrier co-cultured in mixed spheroids have shown spontaneous self-organization [19]. The cells were able to reproduce *in-vitro* a

multicellular architecture that resembles the one of the blood brain barrier. Spontaneous cell sorting has also been observed between normal and cancer cells in co-culture [20]. The *in-vitro* co-culture of normal and cancer cells was studied as a surrogate for tumour-host interactions. The observed segregation behaviour was related with the processes of tumour growth and metastasis *in-vivo*.

One mechanism suggested to explain cell recognition and sorting is the differential expression of cadherins. Steinberg [21], inspired by immiscible liquids, postulated that tissues should sort due to differences in their surface tension. Tissue surface tension is associated with cell-cell adhesion, seen as the force driving sorting. The theory is consistent with experimental observations [22]. However, differences in cortex tension [23] and motility forces [12], [24] have also been related to cell sorting. Therefore, other than intercellular adhesion forces, tension-producing forces seem to contribute to cell sorting [25].

1.2   Mechanics of normal and cancer cells

Single-cell measurements have shown that normal and cancer cells are mechanically different. Cancer cells are softer than normal cells and cell stiffness is now regarded as a biomarker of cancer [26]–[29]. Furthermore, the traction forces exerted by migrating cancer cells are higher than the ones exerted by normal cells [30], [31]. Measurements of cell mechanics have additionally shown that cancer cells of the same population can also be heterogeneous in stiffness [27], [29], [32] and traction force [33]. Besides mechanical properties, cancer cells within the same tumour can differ in morphology, proliferation, motility and metastatic potential [34]. Cell heterogeneity is a hallmark of tumours that is not completely understood, challenging the development of drugs [35]. In addition to dysregulated biological pathways, cancer is related with dysregulated cell mechanical properties, see Figure 1.1. Notwithstanding, it is not clear how the different mechanical properties found for cancer cells can contribute to their migration and invasion behaviours. The role that single cell mechanics plays in the biological processes of collective cell migration and sorting needs to be investigated.

Since the mechanical properties of cells are related with their malignancy, anti-cancer drugs can be developed to specifically target them. There is evidence that chemotherapeutic drugs designed to impair cancer cell division also affect the mechanical properties of cells. Microtubule stabilizers disturb the dynamics of the cytoskeleton, essential for cell division. The cytoskeleton greatly determines the mechanical properties of cells and microtubule stabilizers were found to change the cell stiffness and force generation properties [36], [37]. This interplay between cell behaviour and cell mechanics suggests that changes in cell mechanics could contribute to the therapeutic effect of chemotherapeutic drugs.
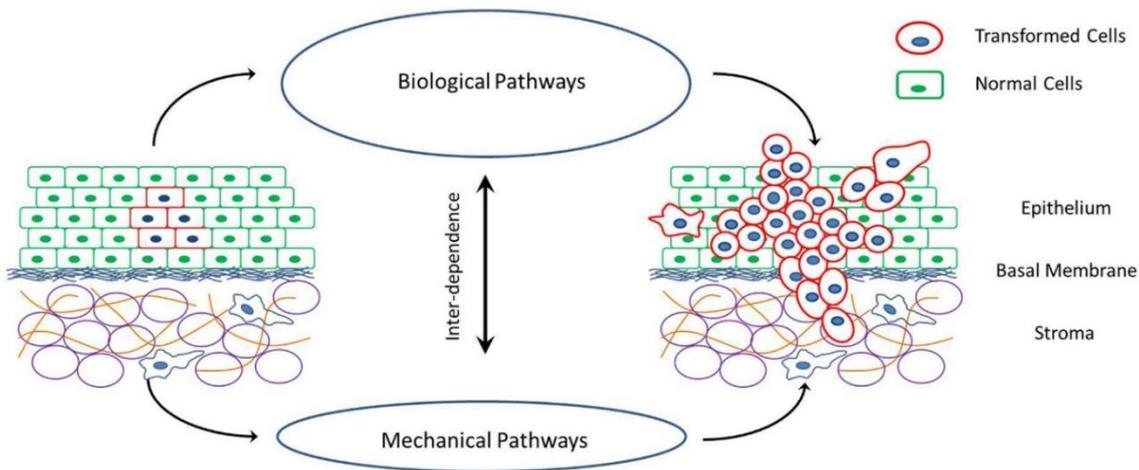
Figure 1.1 Schematic representation of cancer spreading from the primary tumour as resultant of an interplay of biological and mechanical pathways [38].

1.3 Thesis structure

Mechanistic and quantitative understanding of the mechanics of collective cell migration is required to support the development of anti-cancer drugs. Computational models that act as a platform for the testing of hypotheses can be used to test drugs *in-silico*. One of the challenges in cancer treatment is the heterogeneity of cancer cells. This heterogeneity must be understood and considered when developing anti-cancer drugs. Using computational modelling, features specific of the cells the tumour is composed of can be accounted for.

Many computational models of cancer focus on tumour growth [39], [40]. Even though cell migration and sorting are known to be important for cancer metastasis and invasion [41], [42], models investigating the underlying mechanisms are missing [42]. In addition, the different mechanical properties measured for normal and cancer cells should now support the development of cancer models with higher mechanical fidelity. The models will shed light on the role that the mechanical properties of cancer cells play in their migration and sorting. This understanding will, in turn, inform the development of anti-metastatic drugs targeting the mechanical properties of cells.

In this context, the aim of this thesis was to develop a mechanistic and quantitative computational model of the mechanics of collective cell migration and sorting in cancer. The model predictions will provide a mechanical perspective of collective cell migration with potential to help in the design of a novel class of anti-cancer drugs. The thesis is organized in seven Chapters:

- After introducing the context involving the thesis and its aims in this first Chapter, a review on collective cell migration and sorting models is presented in Chapter 2. Current theories and experiments are discussed with a focus on computational models.

- A computational model representing passive mechanical interactions between cells in the first hours after *in-vitro* seeding is presented in Chapter 3. Intercellular interactions are considered to govern cell spreading after seeding. The model is applied

to normal and cancer cells seeded in both monoculture and co-culture scenarios to predict population arrangement and mechanics.

- The computational model presented in Chapter 3 is extended to describe cell migration after cell spreading in Chapter 4. The model accounts for migratory traction forces actively exerted by cells. Mechanical and quantitative thresholds triggering the sorting of normal and cancer cells in co-culture are investigated.

- The computational model developed is used to investigate the migration of mechanically heterogeneous cell populations in Chapter 5. The model is applied to normal and cancer cells in both monoculture and co-culture scenarios. In addition, an *in-silico* drug test is performed to investigate the effect of the mechanical changes induced by microtubule stabilizers on the sorting of normal and cancer cells in co-culture.

- A general discussion of the results of the thesis is presented in Chapter 6. The results are discussed in an integrated perspective and compared with other works from the literature. The limitations of the model developed and future improvements are also covered.

- The thesis is concluded in Chapter 7. The predictions of the work are summarised and the main messages to take forward are highlighted.

Chapter 2 - Literature review

Summary

This Chapter reviews theories and state of the art mechanical models of collective cell migration and sorting. Both their knowledge contributions and limitations are discussed. Models addressing cancer are presented, as well as the changes in tissue mechanics known to be associated to the disease. The Chapter concludes discussing the gaps identified and the potential of the present work to fill them by investigating the role of cell mechanics in collective cancer cell migration and sorting.

2.1 Mechanics of collective cell migration: *in-vitro* insights

Collective cell migration is the coherent movement of cells. The directed and cohesive migration of a cell cluster requires cell-cell interactions involving chemical and mechanical crosstalk between individual cells [43].

The forces that a migrating epithelial cell sheet exerts on a substrate *in-vitro* have been measured, showing the relationship between cell mechanics and cell migration [16], see Figure 2.1. These traction forces emerge from the contraction of the cytoskeleton and are measured using a technique called Traction Force Microscopy (TFM). Cells are seeded on a polyacrylamide gel embedding fluorescent beads and coated with an adhesion-stimulating protein. Following adhesion to the gel, the cells generate migration forces that are transmitted to the substrate, leading to the displacement of the embedded beads. The displacement field can be measured using image registration techniques. Then, the traction forces exerted by the cells can be calculated using numerical methods. Traction force measurements on migrating monolayers revealed complex and heterogeneous force fields [16], [18]. In addition, higher traction force has been measured for individual cancer cells than for normal healthy cells [30], [31]. An interpretation of how the traction forces measured relate with the cells' migration behaviour is missing.
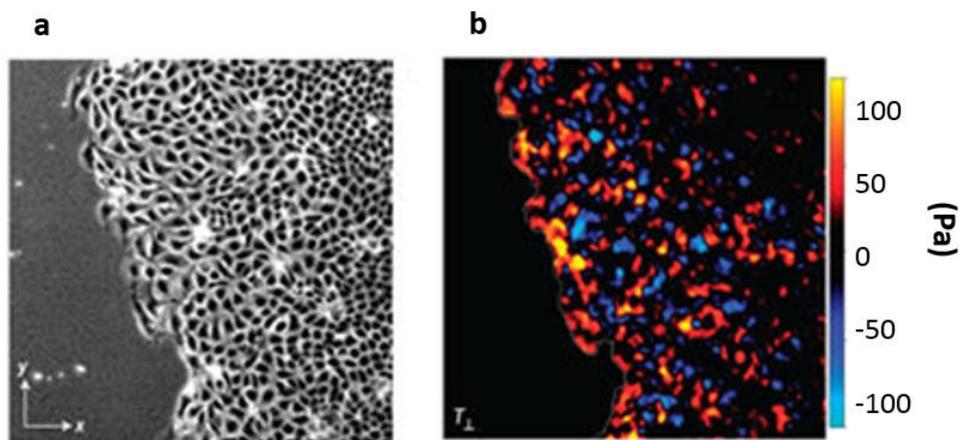
Figure 2.1. Migrating epithelial cell sheet: a) Phase contrast image and b) Traction forces normal to the edge. The field of view is of 750 µmx750 µm [16].

2.2 Mechanics of collective cell migration: computational models

Several computational models studied collective cell migration based on physical and mechanical principles [12], [44], [45]. Models are discussed in the following sections based on their spatial scale, description of intercellular interactions and cell polarity. Models that particularly investigate collective cell migration in cancer disease are also included.

2.2.1 Macroscale versus individual-based models

One of the approaches to model the complex behaviour of collective cell migration focuses on the macroscale [46]. These models establish a system of governing differential equations to describe the evolution of continuous variables in time and in space, such as the density of cells and concentration of chemicals. In other words, these models predict average population behaviour. An alternative approach is the use of individual-based models, in the case of collective cell migration, cell-based models. These do not rely on an explicit global equation, but on individual equations at the microscale giving rise to emergent macroscale behaviour. They can account for outliers, heterogeneity and stochasticity in behaviour. Therefore, individual-based models are powerful in modelling complex diseases, as the case of cancer. Both modelling

approaches can be combined, for instance to model the effect of a chemical gradient on collective cell migration [47]. The focus of this review is on individual-based models.

2.2.2 Modelling cell-cell interactions

Modelling the mechanics of collective cell migration using an individual-based model requires a description of cell-cell interactions. Cell-cell interactions can be defined by a pairwise potential. Different approaches have been considered such as models based on linear springs [48] and models based on the interatomic Lennard-Jones potential [49], that includes both cell-cell repulsion and adhesion, see Figure 2.2.
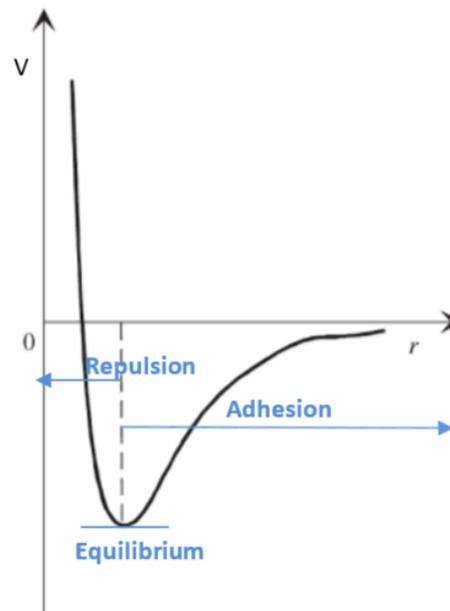
Figure 2.2. Interatomic Lennard-Jones potential: V is the potential energy of the particles and r is the distance between them [50].

Models inspired by contact mechanics such as the Hertz [51], [52] and Johnson-Kendall-Roberts (JKR) models [53] have also been implemented. These investigate intercellular contact mechanics based on cell elasticity properties measured with techniques such as micropipette aspiration [54], Magnetic Twisting Cytometry (MTC) [55] , Optical Tweezers (OT) [56] and Atomic Force Microscopy [57]. Atomic Force Microscopy (AFM), in particular, has emerged as a versatile and powerful technique. It is a type of scanning

probe microscopy. Along with high resolution imaging it provides the ability to investigate local mechanical properties, since it relies on the physical interaction between a probe and the sample being studied. In fact, AFM can be considered as an elastography technique. The sample, in this context the cell, is scanned or mechanically indented by a tip mounted on a cantilever whose deflection is determined using laser tracking. The cantilever's deflection is then converted to a force-distance curve that reflects the interaction between the tip and cell.

The Hertz contact model is the mechanical model most commonly used to fit Atomic Force Microscopy (AFM) experimental results and determine the cell apparent stiffness [58]. It defines the contact between two bodies, the cell and the AFM indentation probe, as following from their elastic deformation. The Hertz model is valid for small indentations, corresponding to 5 to 10% of the cell height, therefore on the order of hundreds of nanometres. On one hand, these small indentations avoid the influence of the substrate on the mechanical response observed [59]. On another, if these small indentations fall into the elastic regime of the cell mechanical response, the assumption made for cell elasticity is supported [60].

Roberts and Kendall experiments showed that attractive surface forces are present between smooth rubber spheres and glass spheres and are significant at low indentation forces. The attractive forces are explained based on the spheres' surface energy and supported the development of a new contact model, the Johnson-Kendall-Roberts (JKR) model [61]. Therefore, the JKR model differs from the Hertz model in that it accounts for the effect of adhesion and describes the contact force as resulting from a balance between the elastic energy stored and the surface energy lost upon contact, see Figure 2.3. The JKR force for two spheres, 1 and 2, is written as:

$$F_{JKR\,(1,\,2)} = \frac{E_{eq}r^3}{R_{eq}} - \sqrt{6\pi\sigma E_{eq}r^3} \qquad\qquad (\,2.1\,)$$

where r is the radius of the circular contact area, σ is the adhesion energy, and E_{eq} is the equivalent Young's modulus of the pair, function of the Young's modulus, E, and Poisson's ratio, ν:

$$\frac{1}{E_{eq}(1,2)} = \frac{4}{3}\left[\left(\frac{1-v_1{}^2}{E_1}\right) + \left(\frac{1-v_2{}^2}{E_2}\right)\right]$$ (2.2)

R_{eq} is the equivalent radius:

$$\frac{1}{R_{eq}(1,2)} = \left[\left(\frac{1}{R_1}\right) + \left(\frac{1}{R_2}\right)\right]$$ (2.3)

Measuring the force required to separate two cells using a micropipette, Chu et al [62] showed that the JKR model reasonably fits cell mechanics and can be used to model the contact between cells. The JKR model has been used in the development of several tissue models [63], [64]. Thereby, passive intercellular forces comprise a repulsive elastic force based on cortical tension and a cell-cell adhesion force due to adhesion complexes.
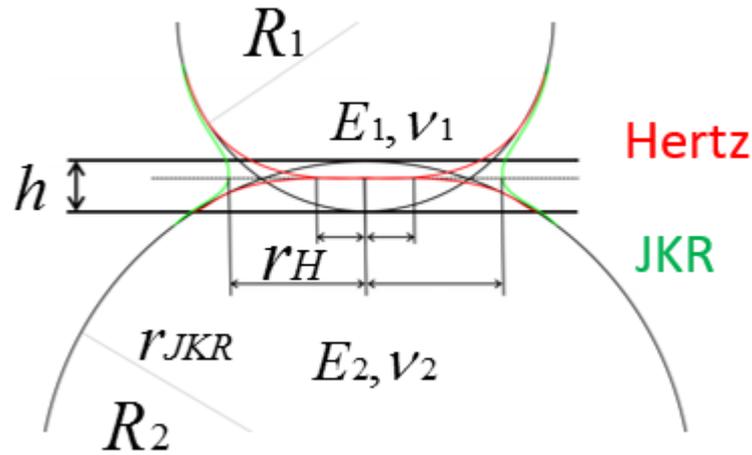
Figure 2.3. Contact region predicted by the Hertz and JKR models: h and r refer to the contact penetration and radius, respectively; R, E and ν *refer to the cells' radius, Young's modulus and Poisson's ratio [61].*

2.2.3 Modelling cell polarity

Single cell migration requires the establishment of front-to-rear cell polarity and a polarized arrangement of the cytoskeleton. At the front of the cell there is actin polymerization and formation of membrane protrusions, while, at the rear there is

contraction of the actomyosin machinery. Directed collective cell migration requires the establishment of front-to-rear polarity at both the cell and population scale. Several mechanisms have been proposed to explain the polarity of cells such as: polarity is guided by the direction of cell movement [65], polarity has a random component [66] and polarity follows the gradient of external signals [67].

Vicsek et al in 1995 proposed that collective movement emerges from the local alignment of self-propelled individuals [68]. More specifically, the movement of an individual depends on the average movement of its neighbours. Due to its phenomenological nature, Vicsek's model misses an explanation for this alignment. Nonetheless, the model has been applied to cell migration to represent the alignment of the actomyosin machineries of cells that migrate collectively. The model enabled the prediction of collective migration phenomena such as the rotation of bacterial cell clusters [69] and finger instabilities at the edge of monolayers [70]. Vicsek's model has been extended to include mechanistic aspects, for example force interactions [12], [71]. Furthermore, it motivated the development of cell sorting models, section 2.3.1 of this review.

2.2.4 Modelling cancer

Individual cancer cell migration is for example seen in leukaemia, lymphomas [3] and in the epithelium after EMT [72]. Nonetheless, several cancers, for instance melanoma [73], exhibit collective cell invasion when explanted *in-vitro.* This behaviour relies on the cells maintaining their expression of cell-cell adhesion molecules, such as cadherins. The migration of clusters of cells that maintain their cadherin-based cell-cell adhesions has also been studied *in-vitro* to investigate morphogenesis and tissue regeneration. These systems can be seen as *in-vitro* models to better understand collective invasion in cancer [74]. The mechanisms behind collective invasion in cancer are still much less understood than the ones behind morphogenesis and tissue regeneration. The fact that cancer is a long-term, multistep and complex process makes the design of appropriate microscopic experiments more difficult when compared to morphogenesis and tissue regeneration [75].

In this context, computational models have an important role in informing and inspiring experiments. Stichel et al [66] investigated the spatio-temporal behaviour of lung adenocarcinoma cells during *in-vitro* wound closure. An individual-based model was developed in order to interpret the experimental observations. Cell migration was considered as a result of active cell propulsion, random motility and cell-cell mechanical interactions. Since the model parameters considered were dimensionless and scaled a quantitative description was not possible. However, the results obtained confirmed that simple mechanical models are able to reproduce several features of the collective behaviour observed in experiments, such as speed dynamics and the detachment of individual cells. This stresses the need to comprehend the changes in tissue mechanics associated to cancer. Knowledge on this topic can enable the use of experimentally based model parameters and provide further mechanistic understanding of cancer cell migration.

It is known that the mechanics of the extracellular environment changes in the vicinity of a tumour. There is a stiffening of the extracellular environment associated to the malignant transformation of cells that seems to promote cancer progression [38], [76]. The mechanics of individual cells, focus of this review, is also affected. A decrease in cell stiffness is associated to the disease. This has been explained by changes in the cytoskeleton structure. Xu et al 2012 [26] reported longer actin fibres for normal cells, better aligned and better distributed throughout the cell body. Recent data also associates cell stiffness with the amount of fibres, and not only with the spatial organization of the cytoskeleton [77].

The relationship between cancer cell stiffness and migration has been investigated experimentally. Park et al [78] cultured normal and malignant fibroblasts, measured their apparent stiffness with AFM and tracked their movement. A correlation was found between the decrease in Young's modulus associated to the malignant transformation and higher motility. Many other studies suggest that lower cell stiffness enhances deformation and consequently the cell's ability to migrate and invade [79]. Friedl et al [80] investigated the role of the mechanical properties of the nucleus in migrating cells. The study showed that cells with more deformable nucleus are more motile. Owing to

its size and stiffness, the properties of the cell nucleus greatly determine the overall cell properties [81]. Therefore Friedl's work also suggests an inverse relationship between cell stiffness and motility. Decreased cell stiffness has also been found to be related with the cell's ability to invade neighbouring tissues in cancer metastasis [82]. However, there is conflicting evidence supporting that highly metastatic cells can be stiffer than less metastatic cancer cells [83]. Moreover, studies that used genetic modification [84], [85] that affect cell migration found higher motility for stiffer cells. Thus, more research is still required to further understand the relationship between cell stiffness and motility. Besides depending on the cells' ability to deform, migration depends on factors such as the cells ability to degrade or deform the extracellular matrix (dependent on the mechanical properties of the matrix itself) [86], the traction force exerted by cells to migrate [18] and the dynamics of focal adhesions [87]. The connection between all these factors is not necessarily obvious.

Katira et al [39] also investigated the relationship between the mechanical properties of cancer cells and their migration. Individual cells were modelled as liquid cores surrounded by viscoelastic shells representing the actin cortex. Cells were able to adhere to each other, proliferate and migrate to minimize the total energy of the system. The results suggest that the increased compliance of the cortex of cancer cells can explain their faster proliferation and that intercellular adhesion determines whether the tumour is more compact or spread out.

In addition to changes in stiffness, cancer cells also experience changes in the adhesion to other cells and the extracellular environment. However, these changes vary with the type of cancer and the stage of progression of the disease [38].

Since E-cadherin is responsible for the stability of cell-cell contacts in epithelial tissues, a decreased expression of E-cadherin is commonly associated with invasion. For example, Techasen et al in 2014 [88] found that the downregulation of E-cadherin in cholangiocarcinomas resulted in increased cell migration and invasion. In addition, the loss of E-cadherin has been linked to increased cell proliferation in tumours [89]. Other works investigate the role of other cadherins. For instance, Bryan et al [90] related increased P-cadherin expression to the invasion of bladder tumours.

The recent review from Friedl et al [91] discusses how the dynamics of cell-cell adhesion contributes to the broad range of migration modes shown by cells in different contexts. EMT supports cancer metastasis by reprogramming and weakening the adhesion between cells. Therefore, full EMT involves the dissemination of individual cells. However, intermediate levels of EMT have been suggested to explain the migratory behaviour adopted by cells that maintain their cell-cell contacts in collective migration. Therefore, the plasticity of cell-cell adhesions is directly related with the plasticity of migration of cancer cells.

When studying a particular type of cancer, it is important to investigate the specific expression of cell-cell adhesion proteins and the intrinsic dynamics of cell-cell adhesions. Furthermore, the development of quantitative models involves the quantification of intercellular adhesion forces. This further requires the identification of the mechanical roles of cell-cell adhesion proteins. Bazellières et al [92] suggested that, while P-cadherin is a good predictor of intercellular tension, E-cadherin is related to its time derivative. A quantitative and integrative understanding of the changes in the mechanics of cell-cell adhesion in cancer is still required.

2.3   Mechanics of cell sorting: analogy with phase ordering in fluids

The study of cell sorting has been inspired by the behaviour of immiscible liquids. Beysens et al [22] compared phase ordering in fluids and cell sorting in embryonic tissues. Both similar morphological patterns (Figure 2.4) and time evolution were found for the two processes. In fluids phase ordering the interfacial tension wall-liquid was lower than wall-gas. As a result, the liquid phase was found to wet the wall of the container and surround the gas phase. In cell sorting the interfacial tension culture medium-neural cells was lower than the interfacial tension culture medium-epithelial cells. For this reason, neural retinal cells wetted the tissue culture medium and surrounded epithelial cells.

This analogy is the base for the physical principles that have been considered to drive cell sorting, such as energy minimization [93]. Several theories interpret cell sorting based on tissue surface tension, differing on the way they explain surface tension as emergent from lower scale cell forces.

One theory is the Differential Adhesion Hypothesis (DAH) conceived by Steinberg [21]. The DAH proposes that tissue surface tension arises from cell-cell adhesion. Differences in both the type of cadherin expressed and the expression levels can result in different surface tension [94]. Following from the theory, for two contacting tissues, the tissue with lower surface tension should envelop the one with higher surface tension.

Another hypothesis is the Differential Interfacial Tension Hypothesis (DITH). The DITH developed from the work of Harris [95], Brodland [96] and Graner [97] and postulates that tissue surface tension is associated with the cortical tension of the individual cells.
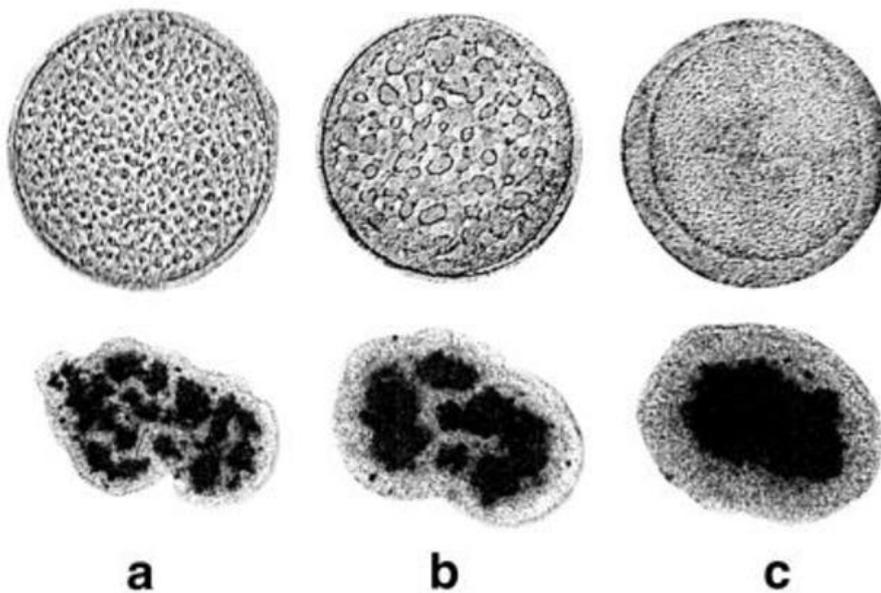
Figure 2.4. Phase ordering in fluids and cell sorting. (Upper) Gas and liquid phase ordering in sulfur hexafluoride under microgravity. The liquid phase wets the wall of the container and surrounds the gas phase. a, b, and c correspond to 120s, 275s and 3,960s after temperature quenching, respectively. (Lower) Sorting of chicken embryonic pigmented epithelial cells (dark) and chicken embryonic neural retinal cells (light). a, b, and c correspond to 17h, 42h, and 73h after the beginning of cell sorting, respectively [22].

In addition to intercellular adhesion and cortical tension, also differences in cell motility have been related to cell sorting [98]. Computational models of cell sorting exploring these ideas are discussed in the following sections.

2.3.1 Mechanics of cell sorting: computational models

2.3.1.1 Differential Adhesion Hypothesis

Based on the DAH hypothesis and the Potts model from statistical mechanics, Graner and Glazier [99] suggested a model to describe cell sorting, later named as Cellular Potts Model (CPM). This model became widely accepted and inspired the development of several models able to predict sorting in cell aggregates [94]. One example is the recent model from Sego et al [93] that predicts the spontaneous sorting of human induced pluripotent stem cells (iPSCs) and iPSC-derived neurons. The neural cells with lower cell-cell adhesion envelop the other cells, see Figure 2.5. This result is consistent with the experimental work of Beysens et al [22] (Figure 2.4).

The DAH crosses several scales by proposing that cell sorting arises from differences in tissue surface tension associated with differences in cell-cell adhesion. However, the connection between the forces at the cadherin level, the forces at the cell-cell adhesion level and the emergent surface tension forces leading to sorting at the tissue level is still under investigation [94].

| Simulation steps=0 | Simulation steps=1k | Simulation steps=20k | Simulation steps=200k |
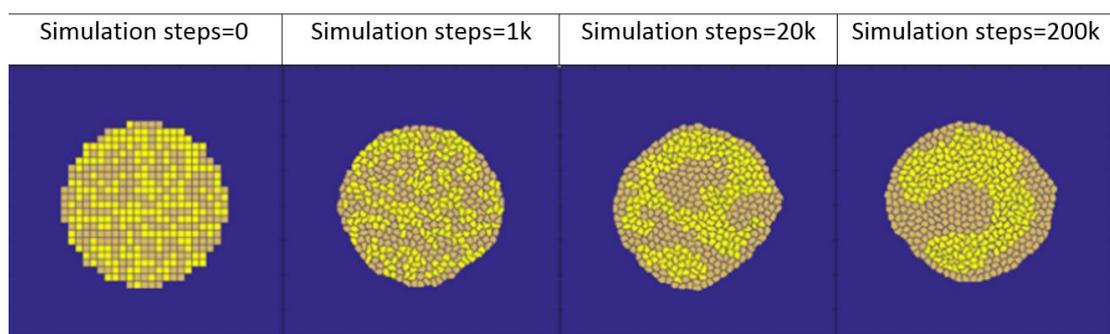
Figure 2.5. Simulation of the sorting between human induced pluripotent stem cells (iPSCs, in yellow) and iPSC-derived neurons (in brown) in equal proportion. Cell sorting is driven by differences in cell-cell adhesion (lower adhesion for the neural cells) [93].

2.3.1.2 Differential Interfacial Tension Hypothesis

Combining the DAH and the DITH, Krieg et al [100] explored the role of cell-cell adhesion and cortical tension in the sorting of germ-layer progenitors. AFM was used as a single-cell force spectroscope to measure cell-cell adhesion by recording the force required to separate two cells brought into contact. Cortical tension was extracted from AFM force-indentation curves of single cells using a mechanical model named cortical shell-liquid core model [23]. In addition, a computational model based on the Cellular Potts Model was developed to have an integrated understanding of the findings. The authors concluded that differences in cell-cell adhesion are not enough to explain the sorting of germ-layer progenitors and that differences in the actomyosin cortex tension are fundamental. Tissue surface tension is suggested to emerge from cell-substrate interactions dependent on cortical tension and cell-cell interactions dependent on both cortical tension and cell-cell adhesion.

Following the same idea, an analytical model integrating both DAH and DITH hypotheses was proposed by Manning et al [101]. The model supports the idea that cell sorting is driven by tissue surface tension with an energy contribution from cell-cell adhesion and from cortical tension. A crossover between an adhesion dominated regime and a tension dominated regime explained the shape of cell aggregates observed experimentally.

2.3.1.3 Role of cell motility in cell sorting

The role of cell motility in cell sorting has also been explored. Méhes et al [102] investigated the *in-vitro* sorting of keratocytes with different motility characteristics (Figure 2.6). The conclusion was that, in addition to differential adhesion, the different motility characteristics of the cells in co-culture are important and collective migration can speed up their sorting. Coupling collective cell migration and cell sorting computationally, Belmonte el al [103] developed a sorting model based on Vicsek's model [68] for collective movement. The aim was to investigate the role of coherent movement and differential adhesion in sorting for tissue regeneration. Following an analogy with fluid phase transitions, intercellular adhesion was represented by a scaling parameter defining the contribution of cohesive forces to cell migration. Sorting was quantified using a sorting index equal to the average ratio of cells of a different type

surrounding one cell. The sorting index decreases with time as cells segregate and the evolution was found to follow a power law. In addition, the more coherent the movement of cells the faster they segregate due to differential adhesion.

The computational work of Kabla et al [24] suggests that differences in cell motility are enough to explain cell sorting, even without differential adhesion. Similarly to the work of Belmonte et al discussed above, Kabla's work considered cell parameters that were not based on experimentally measured data. For the former, the scaling parameter for cell-cell adhesion and, for the latter, the differences in cell motility. As a consequence, only qualitative interpretations of the process of cell sorting were achieved.

There is a paucity of cell-based models investigating sorting in cancer metastasis. Brodland et al [42] developed a finite element model to investigate the mechanics of metastasis focusing on the dissemination step. The results suggest that for individual cancer cells to sort from the primary tumour they need to be mechanically different from neighbouring cells and have an appropriate surface tension. This is in accordance with the startling heterogeneity exhibited by cancer cells in various morphologic and physiological aspects. In fact, heterogeneity of the cell type has been recognized as another hallmark of tumours [34]. The model could be further improved in the future by accounting for experimentally measured mechanical properties of normal and cancer cells.
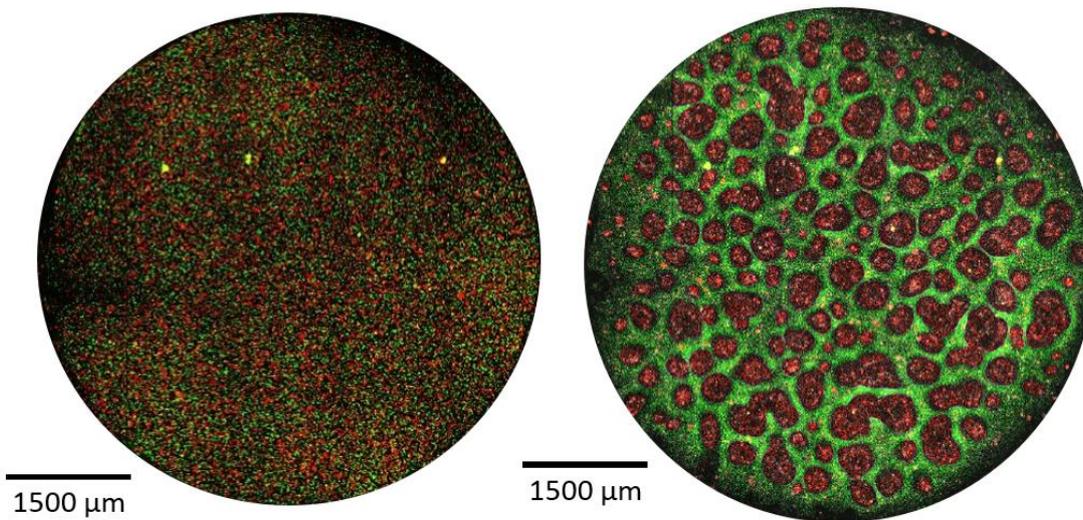
Figure 2.6. Cell sorting in a mixed co-culture of keratocytes with different motility characteristics: primary goldfish keratocytes (PFK, in red) and fish keratocyte cell line (EPC, in green). (Left) Initial configuration. (Right) After 17 hours [102].

2.4 Conclusion

Knowledge about the mechanisms behind collective cell migration and sorting can be used to better understand cancer dissemination. This knowledge is under development and gradually shifting from a descriptive perspective towards a more mechanistic and quantitative one [104]. Mechanistic mechanical models provide frameworks for the testing of hypotheses about the forces governing these processes [42]. The quantification of these forces can inspire and inform studies on the intracellular molecular events in their origin, thereby coupling cell mechanics and cell biology.

The development of mechanistic computational models relies on the availability of experimental parameters, pointing to knowledge gaps and the need for quantitative measurements [105]. Now that measurements of cell mechanics are increasingly used, cell-based models that have a higher degree of mechanical fidelity are possible. The use of experimentally based cell parameters, in opposition to scaling parameters, for instance, supports the development of mechanistic models. The different mechanics measured for different types of cells should be accounted for to appreciate the role of cell heterogeneity in collective migration and sorting [42]. Cell-based mechanical models

should account for experimentally measured properties such as cell traction force, apparent stiffness and intercellular adhesion.

Modelling in cancer has been mainly focused on cell proliferation and tumour growth. However, cell motility and cell sorting have proved to be important for cancer metastasis and invasion [41], [42] and their role needs to further explored. The computational model developed in the context of this thesis aims at filling the gaps presented. The model is a cell-based, mechanistic, mechanical model of collective cell migration and sorting. The purpose is to provide insight into the role that cell mechanics plays in these biological processes accounting for real mechanical properties measured for normal and cancer cells.

Chapter 3 - Modelling passive cell mechanics

Summary

In order to understand the several types of forces involved in cell migration it is common to distinguish between active and passive forces. Active forces are regarded as the forces exerted by cells in order to migrate. They involve cytoskeleton contraction and require energy. Passive forces, on the other hand, arise from intercellular contacts due to cell elasticity.

This work assumes that cell spreading is governed by passive forces in the first hours after in-vitro seeding and migratory propulsion forces are exerted by cells later.

The present Chapter concerns the modelling of the process of cell spreading following seeding. Cell movement is driven by intercellular interactions resultant from cell elasticity, intercellular adhesion and compressibility forces. The model was applied to normal and cancer cells with different mechanical properties and seeded in both monoculture and co-culture scenarios. It was found that volume and stress vary across a cell monolayer and depend on both the local level of cell packing and cell mechanical properties.

3.1 Introduction

Collective cell migration [106] and cell sorting [102] have both been observed *in-vitro.* In addition, it is already possible to measure the forces behind cell migration. However, the heterogeneous and dynamic fields found for these forces are not understood, nor their relationship with the cell movement observed [16].

The forces involved in cell migration can be categorized as active or passive [64]. Active forces are regarded as forces that are exerted by cells with the specific purpose of migrating, requiring the contraction of the cytoskeleton's actomyosin machinery and energy expenditure. On the other hand, passive forces are regarded as forces that arise from intercellular interactions. They are related with the cell's elastic elements, intercellular adhesion receptors and compressibility. This Chapter focuses on passive cell forces.

With the development of Atomic Force Microscopy (AFM), there is a wide range of comparable and complementary information on cell elasticity. The apparent Young's modulus of various cell types, including both normal and cancer cells has been measured [26], [107]. AFM results show that normal, non-cancerous, cells have a higher apparent Young's modulus than cancerous cells. However, the ratio between the Young's modulus of normal and cancer cells is highly dependent on the cell type. Normal breast cells have been reported as 1 to 2 times stiffer than their cancer counter parts [27], [28], while bladder normal cells as up to 32 times stiffer than bladder cancer cells [29]. The values found for the apparent Young's modulus of these cells are presented in Table 3.1.

Table 3.1 – Apparent Young's modulus for breast and bladder normal and cancer cells (average and standard deviation).

Cell type	Apparent Young's modulus (E, kPa)
Breast normal cells	2.26 ± 0.56 [27]
Breast cancer cells	1.24 ± 0.46 [27]
Bladder normal cells	9.7 ± 3.6 [29]
Bladder cancer cells	0.3 ± 0.2 [29]

Less experimental data are available to inform the adhesion forces between cells. Different metrics and methodologies are used to measure intercellular adhesion [108]. One of the approaches is to consider the tissue liquid properties and derive intercellular adhesion from the tissue surface tension [109]. The values reported in the literature vary from 0.05 [110] to 56 nN/um [111], found for *Xenopus* gastrula endoderm and brain cancer aggregates, respectively.

Cell elasticity has been modelled using numerical models such as the Johnson-Kendall-Roberts (JKR) model [61]. The JKR contact model was used in several tissue models [63], [64] to express the intercellular contact force from a balance between elastic repulsion resulting from cortical tension and cell-cell adhesion resulting from adhesion complexes. The model defines an equilibrium distance for a pair of cells, see Figure 3.1. The JKR

force is zero when the two cells are at the equilibrium distance, 2.9 µm in the example shown in Figure 3.1. A negative JKR force is associated with an overlap distance lower than the equilibrium one and an adhesive interaction between the cells. A positive JKR force is related to an overlap distance higher than the equilibrium one and a repulsive interaction between the cells.

However, several authors [63], [64] pointed out that, when applied to a cell population, the JKR model could predict an excessive level of compression for cells in the centre of a cell monolayer. In order to limit cell compression it has been proposed that the JKR should be combined with another model that accounts for the cell volume [63], [64].
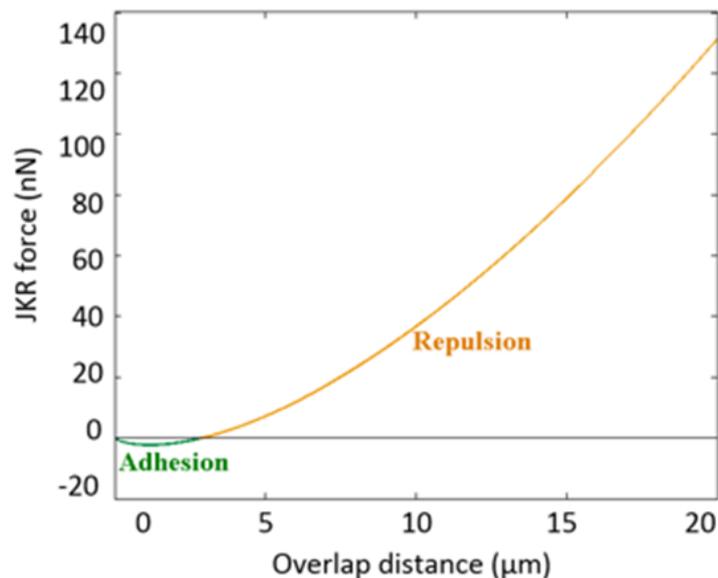
Figure 3.1. Example of JKR force-overlap curve for two cells with apparent Young's modulus of 1kPa, adhesion energy of 0.1 nN/µm, cell radius of 10 µm and Poisson's ratio of 0.47. The JKR model defines the contact equilibrium at an overlap of 2.9µm.

Aiming to develop a mechanistic understanding of collective cell migration, a preliminary model representing passive cell mechanics was developed and it is presented in this Chapter. The JKR model was applied to intercellular contact and complemented with a compressibility model. The purpose was to deconstruct cell mechanics and understand the role of passive cell forces. The model was applied to mechanically different normal and cancer cells in monoculture and co-culture. Co-

culture of normal and cancer cells is studied as a surrogate for tumour-host mechanical interactions. This Chapter answers the following scientific questions:

- How is intercellular stress distributed in cell a monolayer?
- How does intercellular stress change with the mechanical properties of the individual cells?
- Can passive cell mechanics explain the sorting of different cells in co-culture?

3.2 General methods

3.2.1 Passive model description

An individual-based model of collective cell migration was developed in Matlab (mathworks.com) [112]. Rules for cell movement derive from the laws of Newton assuming an overdamped approach. Since cell movement is associated with a low Reynolds number, acceleration can be neglected [75]. Three classes of forces are considered to play a role in cell migration in quasi-static equilibrium: passive intercellular forces; active propulsion forces and extracellular drag forces, Eq (3.1).

$$\sum \vec{F} \ = \ 0 \Leftrightarrow \vec{F}_{intercellular} \ + \ \vec{F}_{active} = - \ \vec{F}_{drag} \qquad (\,3.1\,)$$

The present Chapter focuses on passive cell movement, not considering active propulsion:

$$\sum \vec{F} \ = \ 0 \Leftrightarrow \vec{F}_{intercellular} \ = - \ \vec{F}_{drag} \qquad (\,3.2\,)$$

This model investigates the process through which cells spread and relax after *in-vitro* seeding. During *in-vitro* seeding cells deposit from suspension in random places within the seeding environment. They adhere, spread and establish intercellular contacts from the first hours to the end of the first couple of days, depending on the cell type and seeding density. After this time, cell migration and division start to take place. This

model investigates this time frame, hypothesizing that elastic forces dependent on cell mechanics govern cell spreading following *in-vitro* seeding.

Cells are considered as hemispheres adhered on a two-dimensional substrate. Neighbouring cells virtually overlap each other in the model, representing cell deformation due to intercellular interactions. The overlaps are translated into intercellular forces using a pairwise model described in section 3.2.2. A resultant intercellular force is obtained for each cell by computing the vectorial summation of the pairwise force contributions from the various contacting cells, referred as the cell's neighbours:

$$\vec{F}_{intercellular} = \Sigma_{neighbours} \vec{F}_{intercellullar\ pairwise} \qquad (3.3)$$

Cell movement is defined for each cell by a force balance between the intercellular resultant and extracellular drag, Eq (3.2). The extracellular drag due to the medium viscosity, μ, is described by the Stokes model [64]:

$$\vec{F}_{drag} = \vec{F}_{Stokes} = -6\pi R \mu \vec{v} \qquad (3.4)$$

where R is the cell radius and $\vec{v}$ is the cell velocity.

The positions of the cells at the next time point are determined integrating Eq (3.2) using the forward Euler method:

$$\sum \vec{F} = 0 \Leftrightarrow \vec{F}_{intercellular} = 6\pi R \mu \vec{v} \Leftrightarrow$$

$$\Leftrightarrow \vec{u} = \frac{\vec{F}_{intercellular}}{6\pi R \mu} \times \Delta t \qquad (3.5)$$

where $\vec{u}$ refers to the cell displacement.

Cells move synchronously for a specific number of iterations or until a specific criterion is met. At the end of each iteration, intercellular forces are computed to define cell movement in the next step.

Cells are represented as contacting hemispheres whose volume is approximated as the difference between the isolated cell volume and the sum of the volumes of the overlap regions [63]:

$$V = V_{isolated} - \sum_{neighbours} V_{overlap} =$$

$$= \frac{\frac{4\pi}{3}R^3}{2} - \sum_{neighbours} V_{overlap} \qquad (3.6)$$

$$V_{overlap\ (i,j)} = \frac{\frac{\pi}{12d}(2R-d)^2(d^2+4Rd)}{2} \qquad (3.7)$$

where d is the distance between the centres of cell$_i$ and cell$_j$. The volume of the overlap regions is determined as the sum of the two spherical caps of the intersection [113].

In order to investigate the distribution of stresses in the different scenarios investigated cell stress is computed as follows:

$$Stress = \frac{\sum_{neighbours} \pm |\vec{F}_{intercellullar\ pairwise}|}{2\pi R^2} \qquad (3.8)$$

It is regarded as the ratio between the scalar summation of the intercellular forces affecting a cell and the total cell's surface area [114], the surface area of a hemisphere. Cell stress illustrates the main type of intercellular interactions the cell experiences.

The positive sign is associated with repulsive pairwise forces whereas the negative one is associated to adhesive pairwise forces. Therefore, a microenvironment that is compressive in nature generates intercellular repulsions and positive cell stress. On the other hand, a microenvironment that is tensile in nature results in mainly adhesive forces, hence negative cell stress.

3.2.2 Intercellular pairwise model

3.2.2.1 Johnson-Kendall-Roberts contact model

Elastic contact interactions are described using the Johnson-Kendall-Roberts (JKR) model. In the JKR model [61] passive intercellular forces comprise a contact force based on cortical tension and intercellular adhesion. Following Schaller et al [63] in an approximation for small adhesion, the JKR pairwise force becomes a linear combination of the Hertz model and an intercellular adhesion model:

$$F_{JKR\,(i,\,j)} = F_{Hertz\,(i,\,j)} - F_{Adhesion\,(i,\,j)} =$$

$$= E_{eq}\sqrt{R_{eq}}h^{\frac{3}{2}} - \sqrt{6\pi\sigma E_{eq}R_{eq}^{\frac{3}{2}}h^{\frac{3}{2}}} \qquad (\,3.9\,)$$

where E_{eq} is the equivalent apparent Young's modulus of the cell pair, which is a function of the cells' apparent Young's modulus, E, and Poisson's ratio, v, see Eq (2.2). R_{eq} is the equivalent radius, Eq (2.3), σ is the cell-cell adhesion energy and h is the contact penetration, or virtual overlap:

$$h_{(i,j)} = R_i + R_j - d \qquad (\,3.10\,)$$

where d refers to the distance between the cells' centres. Eq (3.9) is valid as long as $\dfrac{\sigma}{E_{eq}R_{eq}} \langle\langle 1$ and is implemented to resolve passive intercellular forces in this work.

After determining the overlaps for each pair in contact the associated JKR force is determined using Eq (3.9). Each interaction between two cells is characterized by a force vector representing the cell response to that interaction. The vector has magnitude equal to the JKR contact force. The direction is dependent on the JKR force sign and defines whether the interaction is adhesive or repulsive. If the JKR force between two cells is negative, adhesive interaction, the force vector is assigned the direction of the vector between the centre of the cell and the contact point and points

towards the contact point. If the JKR force is positive, repulsive interaction, the force vector is assigned the same direction but points away from the contact point. Summing the force vectors across all the cell neighbours results in:

$$\vec{F}_{intercellular} = \Sigma_{neighbours}\, \vec{F}_{JKR} \qquad\qquad (3.11)$$

The intercellular resultant then defines cell movement according to Eq (3.5).

3.2.2.2 Compressibility model

The JKR model does not account for the cell level of compression due to multiple contacts. In order to accomplish that, a compressibility model proposed by Schaller et al [63] was implemented. Other authors proposed similar models (e.g. Beyer et al [115]).

The model is based on a repulsive force generated by the cell cytoskeleton due to the cell compressibility. For a cell pair the magnitude of this force is computed as:

$$F_{compress\,(i,\,j)} = A_{(i,\,j)}\left[K_i\left(1 - \frac{V_i}{V_{target}}\right) + K_j\left(1 - \frac{V_j}{V_{target}}\right)\right] \qquad (3.12)$$

where K is the cell bulk modulus:

$$K = \frac{E}{3(1-2v)} \qquad\qquad (3.13)$$

Cells feel a repulsion force towards a neighbouring cell proportional to the volumetric pressure of both cells of the pair. This pressure is associated with the cell volume deviation from V_{target} - the volume the cell naturally assumes when isolated from other cells. $A_{(i,j)}$ refers to the overlap area of the cell pair (i,j). Compressibility forces are, therefore, present for all non-isolated cells, regulating cell volume in response to surrounding cells.

The compressibility model presented was combined with the JKR model. The combined passive model accounts for volumetric pressures while considering cell-cell elastic interactions.

Summing the passive pairwise forces for each cell across all its neighbours results in:

$$\vec{F}_{intercellular} = \Sigma_{neighbours} \; (\vec{F}_{JKR} + \vec{F}_{compress}) \qquad\qquad (\,3.14\,)$$

The intercellular resultant then defines cell movement according to Eq (3.5).

3.2.3 Model parameters

Several cellular parameters need to be defined to apply the presented model to cell mechanics. The values considered are summarized in Table 3.2 and the explanation behind their choice follows.

Table 3.2 – Model parameters.

Cell bulk modulus (kPa)	5.5
Cell radius (µm)	10
Medium viscosity (kPa.s)	0.1

With regard to the cell bulk modulus, or resistance to compression, K, it can be computed using:

$$K = -V \; \frac{dP}{dV} \qquad\qquad (\,3.15\,)$$

In other words, depending on the cell initial volume, V, and on the change in pressure, dP, relative to the change in volume, dV.

The cell bulk modulus was determined based on the results of Zehnder et al [116]. Zehnder et al investigated the evolution of the projected area of Madin-Darby Canine

Kidney Epithelial (MDCK) cells of a monolayer with time-lapse microscopy. In addition, the cell thickness was measured with confocal microscopy. Computing the volume autocorrelation function it was found that the cell volume oscillates around its mean with an amplitude of 20% and a timescale of 4 hours. The authors suggested that volume oscillations can be understood by considering that cells of a monolayer exchange water with their neighbours through gap junctions. It was estimated that a cell with a permeability of 0.06 μm^3 $kPa^{-1}.s^{-1}$ can lose 20% of its own volume by generating a pressure of 1.1 kPa relative to its neighbours [116].

According to Eq (3.15) , if a cell generates a pressure of 1.1 kPa for a change in volume of 20% its bulk modulus has the value of 5.5 kPa. This is the fixed value considered for all the cells modelled in this work.

Different values for the apparent Young's modulus and intercellular adhesion energy are investigated throughout the Chapter.

The cell Poisson's ratio was determined depending on the apparent Young's modulus using the relation for homogenous isotropic materials:

$$\nu = \frac{3 - \frac{E}{K}}{6}$$

(3.16)

Softer cells are, hence, considered as more incompressible than stiffer cells.

Cells are adhered on the substrate and are all considered as hemispheres with a radius of 10 μm [116] (isolated volume of $\dfrac{\frac{4}{3}\pi 10^3}{2} \approx 2094\,\mu m^3$).

The extracellular environment was assigned a viscosity of 0.1 kPa.s [117].

3.2.4 Cell seeding and time step

Cell seeding precedes all simulations. Cells are randomly seeded in a circular region in five different replicates. The size of the region is determined assuming an ideal packing of circles in a circular environment to ensure cell proximity:

$$seeding\ environment\ radius = \sqrt{R^2 \times number\ of\ cells} \qquad (3.17)$$

After seeding, the cells move driven by intercellular forces within a boundary free region according to Eq (3.5). In order to define their movement, intercellular overlaps are determined for each pair of contacting cells as follows:

$$overlap_{(i,\ j)} = 2R - d \qquad (3.18)$$

where d refers to the distance between the cells' centres. The associated intercellular forces are obtained for each pair in contact using the model presented in section 3.2.2. The resultant force is computed for each cell and these initial forces are used to determine the time step of the simulation.

Cells are restricted to move a maximum distance equal to half of their radius per iteration. The aim is to prevent them from overcoming each other while moving, since no sense of intercellular contact establishment is provided during migration. In order to accomplish that, the time step is determined according to the maximum displacement allowed for the cells per iteration. Cells move according to intercellular forces; therefore, the maximum velocity possible in the model is associated to the maximum force. Immediately after seeding, the maximum intercellular force is in the order of magnitude of 10^3 nN. However, forces can temporarily increase during the simulation as the cluster relaxes and new intercellular contacts are created. As a result, the maximum possible force must be tuned to allow the cluster relaxation. Through trial and error experiments, it was found that a value for the maximum force ten times higher than the one measured after seeding ($\approx 10^4$ nN) enables a successful relaxation for all the cell populations investigated in this work. The simulation time step is determined based on the maximum force allowed using:

$$time\ step = \frac{maximum\ displacement}{maximum\ velocity} = \frac{0.5 \times R}{\frac{maximum\ force}{6\pi\mu R}} \qquad (3.20)$$

The computed time step is in the order of 10^{-3} seconds. In order to minimise computational time relaxation is broken down into two stages with increasing time step. The first relaxation, referred as pre-relaxation, is performed using the time step computed based on the initial forces. The time step for the second relaxation is computed based on the level of force during active migration which is the focus of Chapter 4. Through trial and error experiments, it was found that a maximum possible force in the model of 500-700 nN would allow the various populations investigated to migrate after complete relaxation. This force value corresponds to a time step on the order of magnitude of 10^{-1} seconds.

Force and volume distributions after seeding and after pre-relaxation for a 200 cell population are shown in Figure 3.2. After the random seeding cells were in an unrealistic compressed situation characterized by negative cell volumes. The maximum intercellular force (order of magnitude of 10^{3} nN) was in the centre due to cell crowding. The population was relaxed with a time step of the order of 10^{-3} seconds until the maximum force in the cluster was less than 50 nN. Intercellular forces became higher close to the border due to the influence of the monolayer edge. Cells have less neighbours around the border and therefore intercellular interactions do not balance each other as in the centre, leading to higher resultant forces. As force decreased the cell volume increased accordingly.

Afterwards, the second relaxation was performed with a time step on the order of 10^{-1} seconds. Model convergence for this second relaxation stage is investigated in section 3.3.2.1.
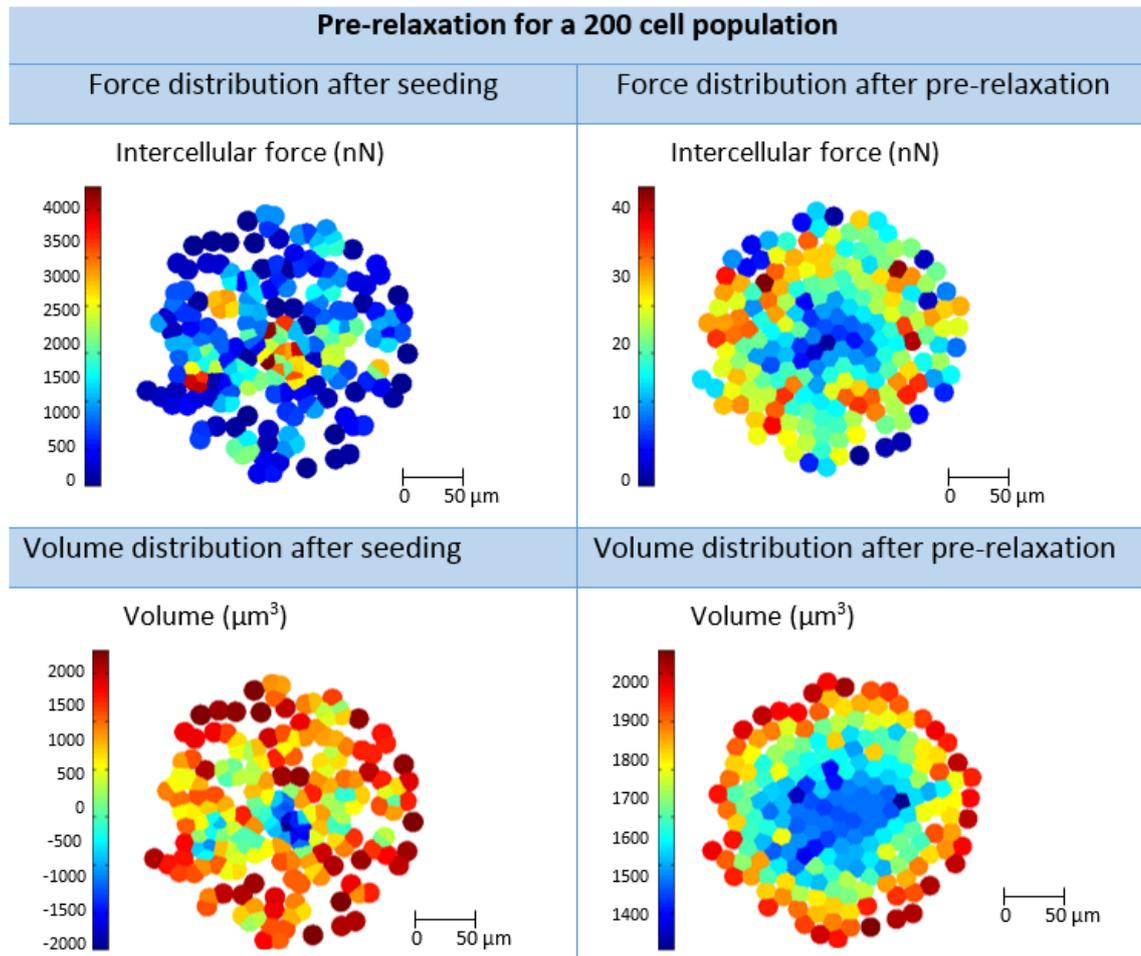
Figure 3.2. Pre-relaxation for a population of 200 cells with an apparent Young's Modulus of 1kPa and intercellular adhesion energy of 0.1 nN/µm: force and volume distributions after seeding and after pre-relaxation.

3.3 Simulations

The simulations were carried out serially using Matlab R2013a in the Iceberg cluster for High Performance Computing from The University of Sheffield.

3.3.1 JKR model

After seeding cell relaxation followed the JKR model. As a first step the JKR model was implemented in isolation, without the compressibility model.

In the literature, cancerous human breast epithelial cells are reported as 1 to 2 times softer than their non-cancerous counterparts [27], [28], [118]. Based on this evidence

two different populations were investigated in this first study, one with an apparent Young's modulus of 1 kPa [119], [120] and another with a lower value of 0.6 kPa, as shown in Table 3.3. Intercellular adhesion energy was assigned a baseline value of 0.1 nN/μm [64].

Table 3.3 – JKR model simulation cases.

Case	Apparent Young's modulus (E, kPa)	σ (nN/μm)
I	1	0.1
II	0.6	0.1

The JKR model defines an equilibrium overlap of 2.9 μm for two contacting cells with properties as in case I and 4 μm for cells with properties as in case II, see Figure 3.3. The JKR was numerically applied to cell populations of 200 cells.
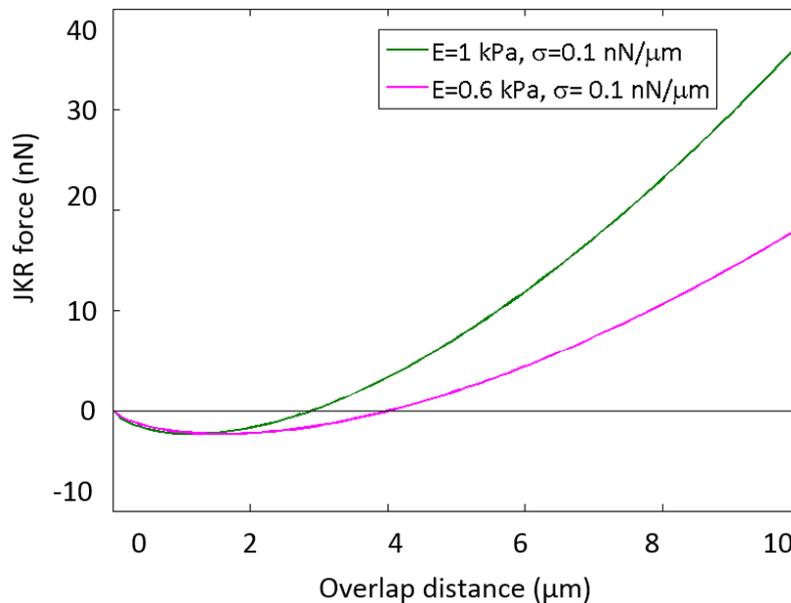
Figure 3.3 JKR force curves for contacting cells with apparent Young's Modulus of 1 and 0.6 kPa and intercellular adhesion energy of 0.1 nN/μm.

3.3.2 JKR and compressibility model

3.3.2.1. Convergence study

The JKR model was combined with the compressibility model to describe cell movement. Populations of 50, 100, 200 and 500 cells with an apparent Young's modulus of 1 kPa and intercellular adhesion energy of 0.1 nN/µm were considered. Model convergence was evaluated and the effect of the population size in cell volume and stress distributions was investigated.

3.3.2.2. Sensitivity

Experimentally reported values for quantities that characterize cell mechanics vary widely. This variability can be due to the different methodologies used for measurement but also due to cell type intrinsic differences. With regard to apparent Young's modulus, values as low as 0.02 kPa were reported for leukocytes and as high as 400 kPa for cells from the Organ of Corti [121]. Tissue surface tension can be considered as a measure of intercellular adhesion energy and has values between 0.05 nN/µm for *Xenopus* gastrula endoderm [110] and 56 nN/µm for cancer aggregates of ependymoma cells [111].

The existing variability drives the need for parameter studies to develop robust computational models. This section relies on the model developed to explore the effect of two parameters: cell apparent Young's modulus, E, and intercellular adhesion energy, σ, on passive cell mechanics.

The cell bulk modulus is considered fixed and equal to 5.5 kPa throughout the study, section 3.2.3. For values of the apparent Young's modulus equal or higher than 49.5 kPa, the cell Poisson's ratio becomes higher than one, Eq (3.16). As a consequence, the equivalent apparent Young's modulus of contacting cells becomes negative Eq (2.2), resulting in complex solutions Eq (3.5). For apparent Young's modulus between 16.5 and 49.5 kPa, the Poisson's ratio is smaller than one and therefore the model finds a real solution, though the Poisson ratio is still negative. Values of apparent Young's modulus smaller than 16.5 kPa result in a positive Poisson ratio and are, hence, worth investigating in the model as it stands. The interesting ranges for the cell apparent

Young's modulus and intercellular adhesion energy are therefore: 0.02-16 kPa and 0.05-56 nN/μm, respectively.

The combined model complements the JKR by accounting for compressibility forces that are associated with relative volumetric pressures between contacting cells. However, the model does not define a minimum cell volume. The maximum cell volume is the volume for an isolated cell, 2094 μm³. Assuming that cells vary their volume within a range of +/- 20% [64], the minimum volume in the model should be less than the maximum in 40%, 1257 μm³. As seen in section 3.4.2.1, cell volume varies across a packed monolayer, being lower for cells in the centre that have six neighbours. A minimum volume of 1257 μm³ corresponds to a maximum overlap value of 4 μm, using Eq (3.6), Eq (3.7) and Eq (3.18):

$$V \geq 1257 \quad \Leftrightarrow V_{isolated} - \sum_{neighbours} V_{overlap} \geq 1257 \Leftrightarrow$$

$$\sum_{neighbours} V_{overlap} \leq 837 \Leftrightarrow$$

$$V_{overlap} \leq \frac{837}{6} = 139.5 \quad \Leftrightarrow \frac{\frac{\pi}{12d}(2R-d)^2(d^2+4Rd)}{2} \leq 139.5 \Leftrightarrow$$

$$d \leq 24 \Leftrightarrow overlap \leq 4 \text{ μm}$$

The JKR force is a function of *E, σ* and the cell overlap, Eq (3.9):

$$F_{JKR}(overlap) = E_{eq}\sqrt{R_{eq}}\, overlap^{\frac{3}{2}} - \sqrt{6\pi\sigma E_{eq} R_{eq}^{\frac{3}{2}} overlap^{\frac{3}{2}}}$$

The compressibility force is a function of the cell overlap only, since the cell bulk modulus is fixed at 5.5 kPa. For two contacting cells with six neighbours it is:

$$F_{compress}\,(overlap) =$$

$$-200\cos^{-1}\left(1 - \frac{overlap}{20}\right) + \left(\frac{overlap}{2} - 10\right) \times \sqrt{400 - (overlap\text{ - }20)^2}$$

$$\times 33\,\frac{\dfrac{2000\pi}{3} + \dfrac{3\pi\,overlap^2 \times (overlap\text{ - }20)^2 - 40\,overlap + 800}{12\,overlap - 240}}{2000\pi - 11}$$

Solving for the cell overlap, Eq (3.14):

$$F_{JKR} + F_{compress} = 0$$

the overlaps predicted by the model for a cell in the centre of a monolayer are obtained as a function of E and σ (Figure 3.3). Five different test cases on the border of the valid parameter region were considered to verify the model behaviour, see Figure 3.4 and Table 3.4.
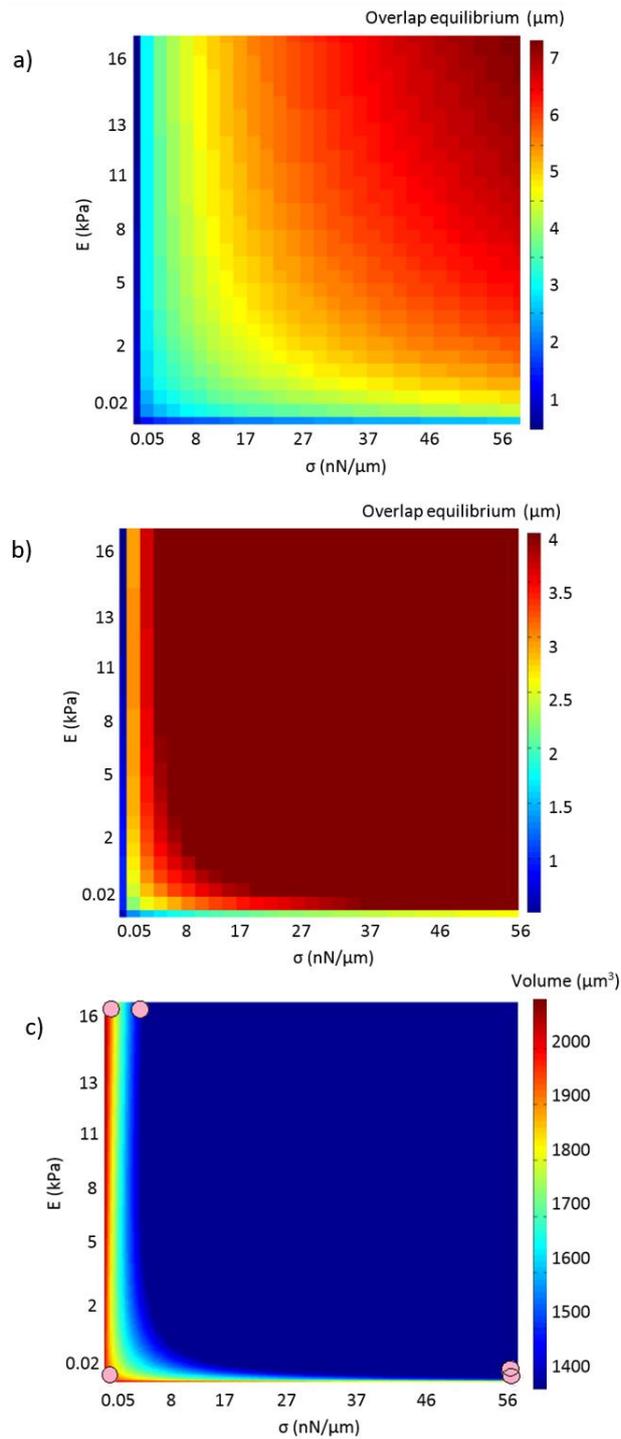
Figure 3.4 Overlap and volume solutions for a cell in the centre a monolayer as a function of E and σ: a) Overlaps coloured according to their value, b) Valid overlap solutions, overlaps lower than 4 µm, coloured according to their value. Overlaps equal or higher are coloured in dark red, c) Valid volume solutions. Volumes lower than 1257 µm³ are in dark blue. The five simulation cases implemented are represented as pink circles on the volume matrix.

Table 3.4 – Simulation cases for the combined model sensitivity study.

Case	E (kPa)	σ (nN/μm)	Overlap equilibrium (μm)	Minimum volume predicted (μm³)
I	0.02	0.05	0.71	2071
II	0.02	56	2.66	1778
III	0.12	56	3.7	1490
IV	16	0.05	0.34	2090
V	16	4.7	3.81	1454

The force curves associated to these cases are presented in Figure 3.5.
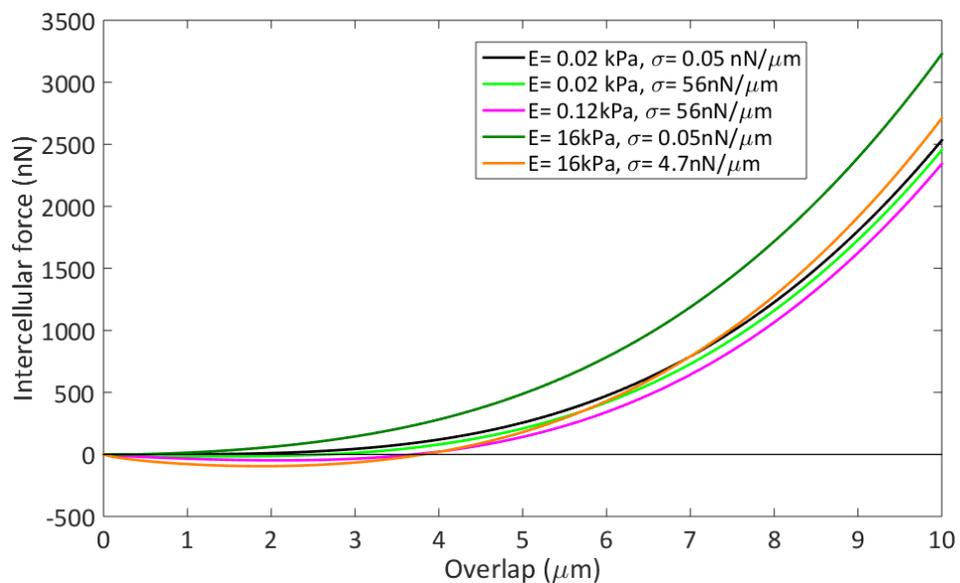
Figure 3.5 Combined model force curves for two cells in the centre a monolayer for the five simulation cases.

The effect of the cell Young's modulus and intercellular adhesion energy on cell volume and stress was investigated using 200 cell populations.

3.3.2.3 Mechanics of bladder and breast cell monocultures

After understanding the general model behaviour, cell-type specific parameters can be considered. The passive mechanics of monolayers composed of breast and bladder normal and cancer cells was investigated varying the cells' apparent Young's modulus and adhesion energy according to Table 3.5.

The apparent Young's modulus was varied according to the average value found in the literature for that cell type and the associated standard deviation, Table 3.1, thereby accounting for the variability. Concerning intercellular adhesion energy, no consistent cell type specific values were found in the literature. Therefore, the parameter was varied from the minimum to the maximum value in the valid parameter region, section 3.3.2.2. For cancer cells an extra intermediate adhesion value was considered for the average Young's modulus for comparison with normal cells.

The various simulation cases were implemented for 200 cell populations.

Table 3.5 – Mechanical properties considered for breast and bladder normal and cancer monocultures.

	E (kPa)	σ (nN/μm)		E (kPa)	σ (nN/μm)
Breast normal	1.7	0.05	**Bladder normal**	6.1	0.05
	1.7	7.5		6.1	4.7
	2.3	0.05		10	0.05
	2.3	7		10	4.7
	2.82	0.05		13.3	0.05
	2.82	6		13.3	4.7
Breast cancer	0.78	0.05	**Bladder cancer**	0.1	0.05
	0.78	13		0.1	56
	1.2	0.05		0.3	0.05
	1.2	7		0.3	4.7
	1.2	11		0.3	36
	1.7	0.05		0.5	0.05
	1.7	7.5		0.5	19

3.3.2.4 Mechanics of bladder and breast cell co-cultures

Three different types of normal and cancer cell co-culture were considered for breast and bladder cells. The co-cultures investigated different adhesion between normal cells and between cancer cells. Both the cases of maximum possible difference in adhesion and equal adhesion were explored. In the first case normal cells adhere more to each other than cancer cells, in the second case normal and cancer cells have equal adhesion and in the last case cancer cells adhere more to each other than normal cells. With regard to the adhesion between normal and cancer cells, it was considered as equal to the minimum between normal-normal adhesion and cancer-cancer adhesion. This is based on the idea that two cells of the same type should adhere to each other to a higher extent than two cells of different types [98]. The cases investigated are presented in Table 3.6. Populations of 200 cells in a 50% normal/cancer co-culture were studied.

Table 3.6 – Simulation cases for breast and bladder co-cultures.

Breast	Co-culture cases	Breast normal		Breast Cancer	
		E	σ	E	σ
		(kPa)	(nN/μm)	(kPa)	(nN/μm)
	1-Higher adhesion for normal cells	2.3	7	1.2	0.05
	2-Equal adhesion	2.3	7	1.2	7
	3-Higher adhesion for cancer cells	2.3	0.05	1.2	11
Bladder	Co-culture cases	Bladder normal		Bladder cancer	
		E	σ	E	σ
		(kPa)	(nN/μm)	(kPa)	(nN/μm)
	1-Higher adhesion for normal cells	10	4.7	0.3	0.05
	2-Equal adhesion	10	4.7	0.3	4.7
	3-Higher adhesion for cancer cells	10	0.05	0.3	36

3.4 Results

3.4.1 JKR model

After seeding cells move according to intercellular JKR forces. These were summed for all the cells of the population and the force evolution is shown in Figure 3.6. Force peaks due to the establishment of new cell contacts and decreases as the cells spread. For a value of the sum of forces lower than 10^{-1} nN, force lower than 5×10^{-4} nN per cell, there no more changes in cell contact and the model is considered to have converged.

Overlap and volume distributions at the end of the relaxation are shown in Figure 3.7. The results obtained across the various replicates are similar so only one of the replicates is shown.

As the cells relax, overlaps converge to the overlap equilibrium defined by the JKR for most of the cells of the cluster, 2.9 µm for case I and 4 µm for case II. However, few cells in the centre are over compressed, while others are under compressed. These appear in regions of lower cell connectivity within the monolayer. The overlaps vary around the equilibrium value by 28% and 38% for case I and II respectively. Case II is the case for which overlaps vary the most, being between -30 and +38% of the equilibrium value, 2.8-5.5 µm.

The cell volume changes depend on the cell position within the cluster and the number of surrounding cells, Eq (3.6). Cell volume is lower for over compressed cells and reaches a minimum of 1025 µm^3 for case II. Higher volumes are obtained for the under compressed ones.
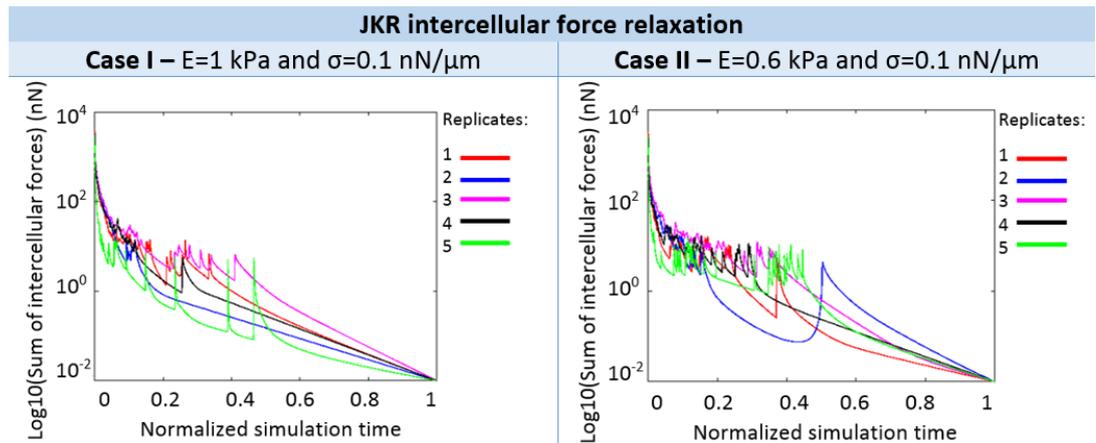
Figure 3.6: JKR model results for two populations of 200 cells with an apparent Young's Modulus of 1 and 0.6 kPa and intercellular adhesion energy of 0.1 nN/μm: intercellular force evolution.
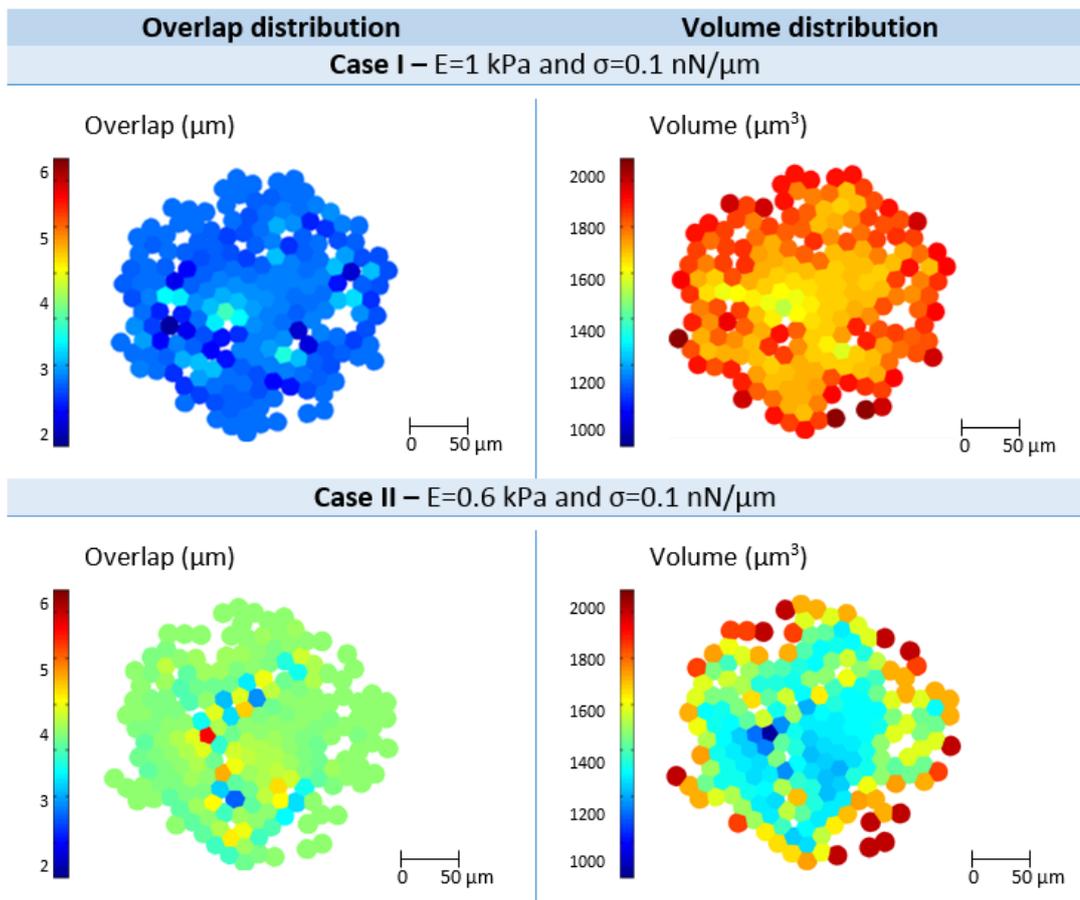

Figure 3.7: JKR model results for two populations of 200 cells with an apparent Young's Modulus of 1 and 0.6 kPa and intercellular adhesion energy of 0.1 nN/μm: overlap and volume distributions obtained.

3.4.2 JKR and compressibility model

3.4.2.1 Convergence study

Model convergence was evaluated for populations of 50, 100, 200 and 500 cells following the same protocol. The results obtained for the 200 cell populations are shown as an example.

Intercellular force, overlap and stress distributions after relaxation are shown in Figure 3.8. The evolution of the sum of intercellular forces for all cells, average overlap and average stress for the five replicates are also presented. Normalized simulation time is used since the different replicates took different time to relax.

Relaxation was stopped when the sum of intercellular forces for all the cells modelled reached 10^{-3} nN, with a force per cell on the order of 10^{-6} nN. Intercellular contacts are created as the cells spread after seeding, originating the force peaks observed in the force evolution curve. Below a value of 0.1 nN for the sum of the forces, blue line in Figure 3.8, no peaks are observed for none of the five replicates. In addition, the average overlap and the average stress are stabilized at this level of force. The change in the average overlap is in the order of 10^{-4} % and the maximum change in average stress is 18%, with an order of magnitude of 10^{-6} nN. For this reason, the model is considered to have converged for a value of 0.1 nN for the sum of intercellular forces. This corresponds to a force value of 5×10^{-4} nN per cell.

The model predicts different overlap and stress depending on the cell position within the monolayer. Overlap is generally higher on the border, where cells have less neighbours. In addition, the average overlap depends on the seeding, changing from replicate to replicate. As it happens for the overlap, there is a stress distribution. For a monolayer in intercellular equilibrium, resultant intercellular forces are low and cell interactions balance each other. This means that, at the cell scale, cells can be experiencing some degree of stress, as long as it is locally balanced by neighbouring cells. Although the average stress in the monolayer is low, of the order of 10^{-5} kPa, the maximum stress reaches a value that is two orders of magnitude higher.

Modelling five seeding replicates of a 200 cell population required globally 39 Gb of maximum virtual memory and 39 hours of CPU time. However, model convergence at a force value of 0.1 nN required 16 hours, a CPU time lower in 69%. The CPU time per

replicate changed considerably due to the random nature of the seeding (average of 3.2 ±1.2 hours).

In order to understand how the model results vary with the population size, volume and stress distributions obtained for populations of 50, 100, 200 and 500 cells are shown in Figure 3.9. These representative distributions are associated with one of the five replicates modelled.

Focusing on the results obtained for 50 and 100 cell monolayers first, volume and stress are uniformly distributed in the centre of the monolayer. Cells in the centre are in compression (positive stress values) and have 3% less volume than the cells on the border (2010 versus 2070 um^3). Stress is one order of magnitude higher close to the border of the monolayer reaching the order of the units of Pascal, 10^{-3} kPa. Volume varies the most in this region. Cells right on the edge have the highest volume and are in tension (negative stress values), while cells just behind have the lowest volume and are in compression.

The same generally holds for the 200 and 500 cell populations, except that volume and stress are not so uniformly distributed in the centre of the monolayer. Cells seem to be organized in several clusters and there are regions within the monolayer where cells are less packed. They resemble the monolayer edge: with higher volume variation and stress values predicted. The cells modelled are seeded randomly and find each other through passive spreading. This results in asymmetries in cell connectivity that are more probable the higher the number of cells considered. The predicted stress is on the same order of magnitude regardless of the size of the population.

Although cell configuration and asymmetries in packing are seeding dependent, the results reported hold for all the five replicates.
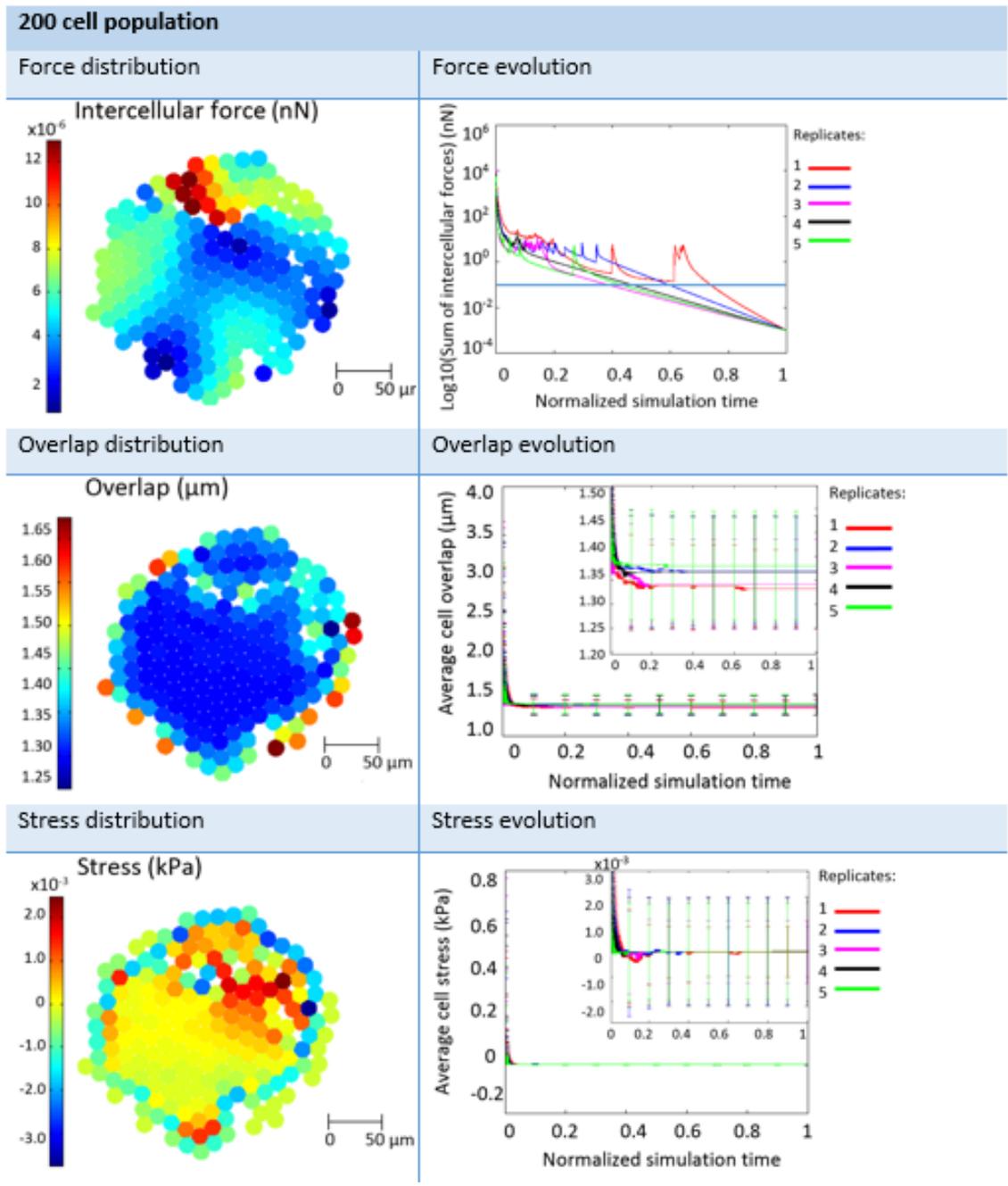
Figure 3.8 Convergence study for a 200 cell population with an apparent Young's modulus of 1 kPa and intercellular adhesion energy of 0.1 nN/μm: intercellular force, overlap and stress distribution and evolution. For overlap and stress evolution a zoomed image is included.
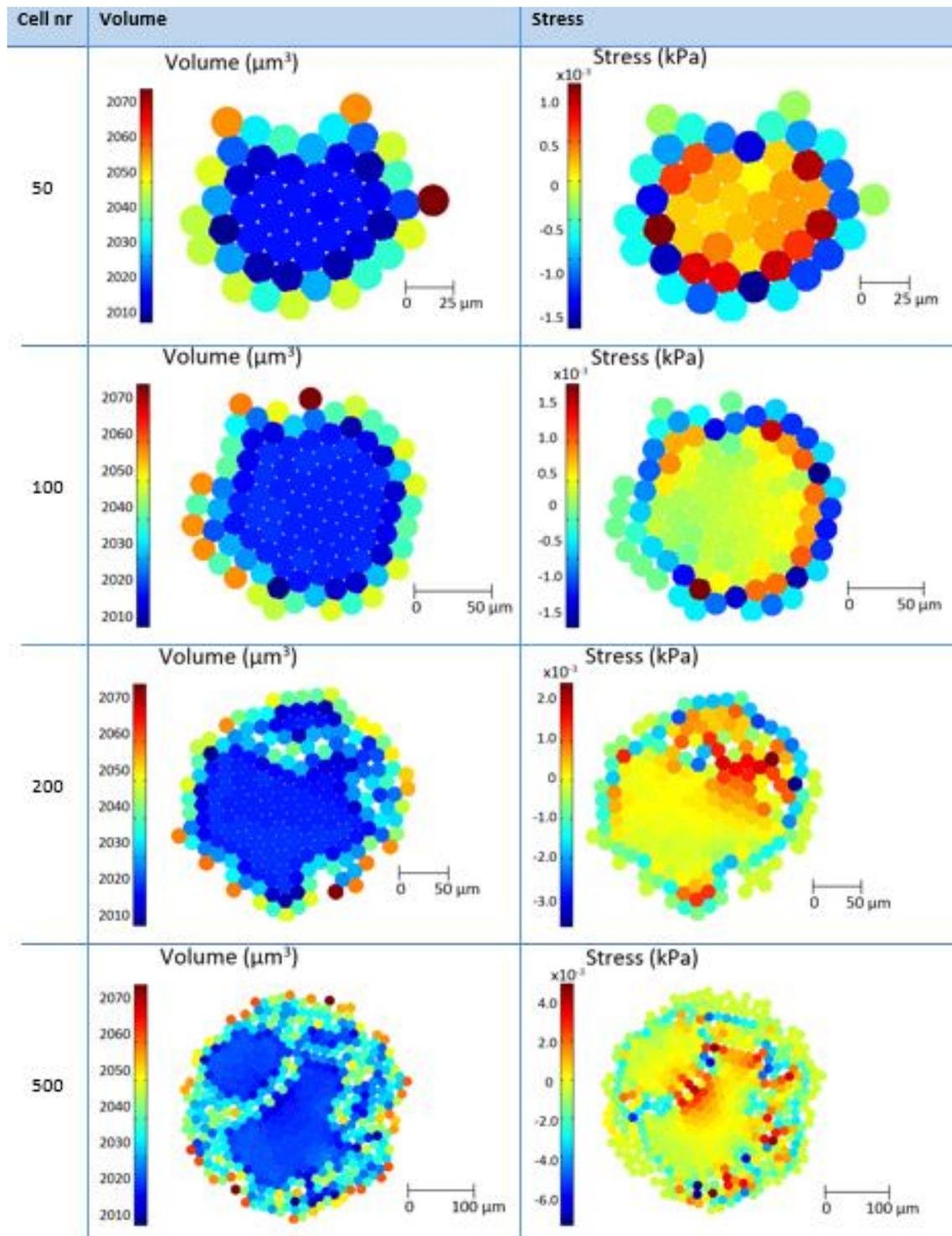
Figure 3.9 Volume and stress predicted for 50, 100, 200 and 500 cell populations with an apparent Young's modulus of 1 kPa and intercellular adhesion energy of 0.1 nN/μm.

3.4.2.2 Sensitivity

Model convergence for the populations investigated was verified as in section 3.4.2.1. Volume and stress distributions obtained for the various parameter cases are presented in Figure 3.10.

The stress is higher in the same regions of lower cell connectivity in the various populations, confirming the influence of cell topology. However, the stress magnitude changes depending on cell mechanics. The maximum stress in the monolayer has values with order of magnitude between 0.1-100 Pascal and increases with both the apparent Young's modulus and intercellular adhesion. Stress is highest for case V. Lower cell volume is associated with higher stress and it ranges between 1301 and 2094 μm^3 for case V, being always higher than the minimum allowed of 1257 μm^3.
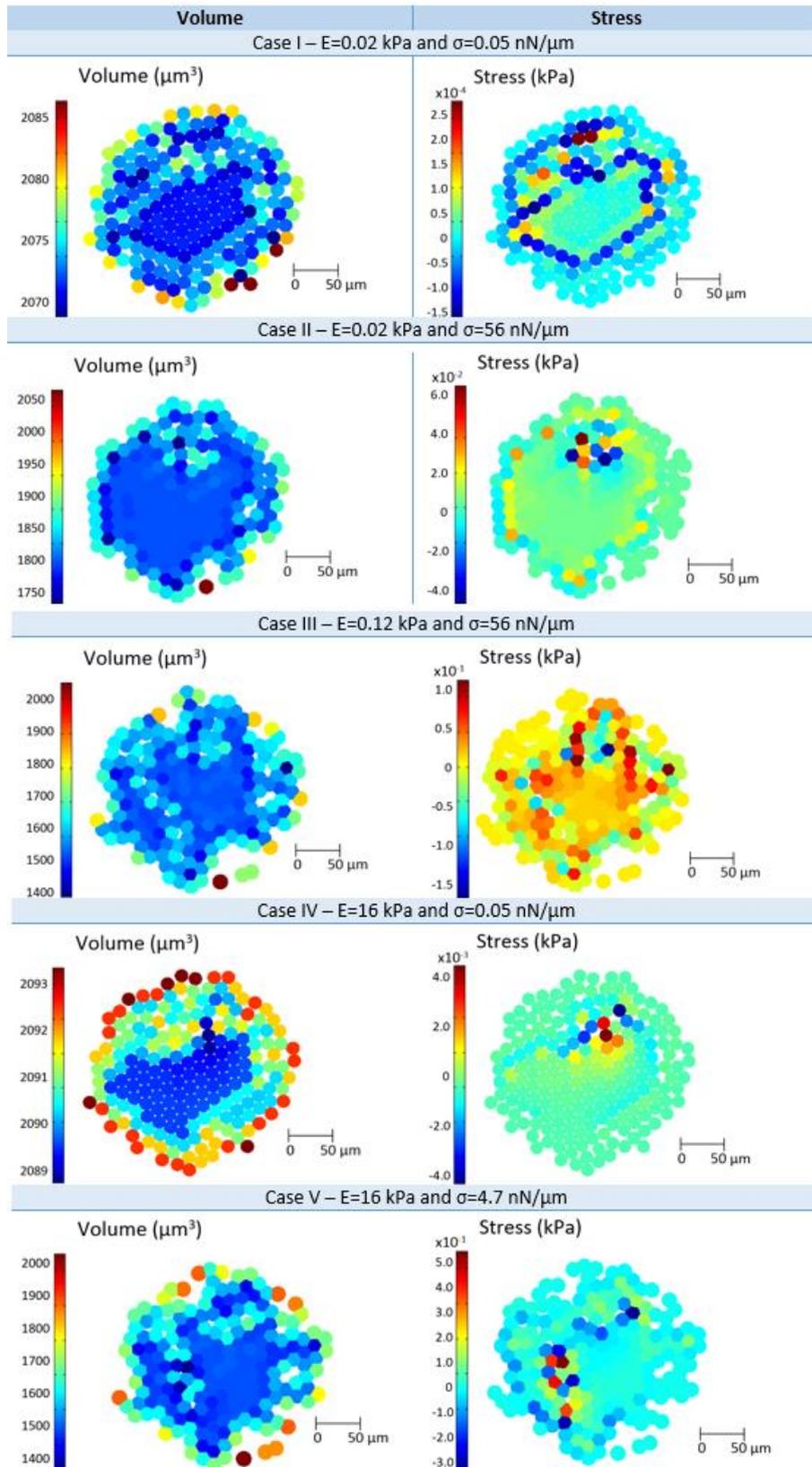
Figure 3.10 Volume and stress predicted for 200 cell monocultures with different mechanical properties.

3.4.2.3 Mechanics of bladder and breast cell monocultures

From the results obtained in the section 3.4.2.2 the maximum stress in a monolayer is not only dependent on topology but also on cell mechanics. In this section the relation between stress and cell mechanics is explored for two specific cell types: breast and bladder.

Compressibility forces depend on the cell volume and number of neighbouring cells, Eq (3.6). Therefore, the intercellular force curve for a pair of contacting cells depends on the local topology. The force curves in Figure 3.5, section 3.3.2.2, correspond to two contacting cells at the centre of a packed monolayer (surrounded by six neighbours each). The curves have zero force at different overlaps, depending on the cell Young's modulus and intercellular adhesion energy.

In the model, cell stress is related with overlap deviations from the equilibrium value. These overlap deviations are associated with different forces depending on the cell mechanical properties (Figure 3.5 in section 3.3.2.2). Therefore, it is expected that force variation around the overlap equilibrium value is related with cell stress.

For all the parameter cases modelled, the corresponding force curves were obtained and the derivative at the equilibrium point was computed. This quantity is regarded as a measure of the intercellular contact stiffness. Its relation with the maximum cell stress found in the monolayer was investigated, see Figure 3.11.

A relation between the maximum compressive stress and intercellular contact stiffness was found for the 24 cell-type specific cases modelled and the five cases investigating the parameter region boundary, section 3.4.2.2. The maximum stress in the monolayer increases with the intercellular contact stiffness following a power law of order 1.4981 with an R^2 of 0.9821 (Figure 3.11).
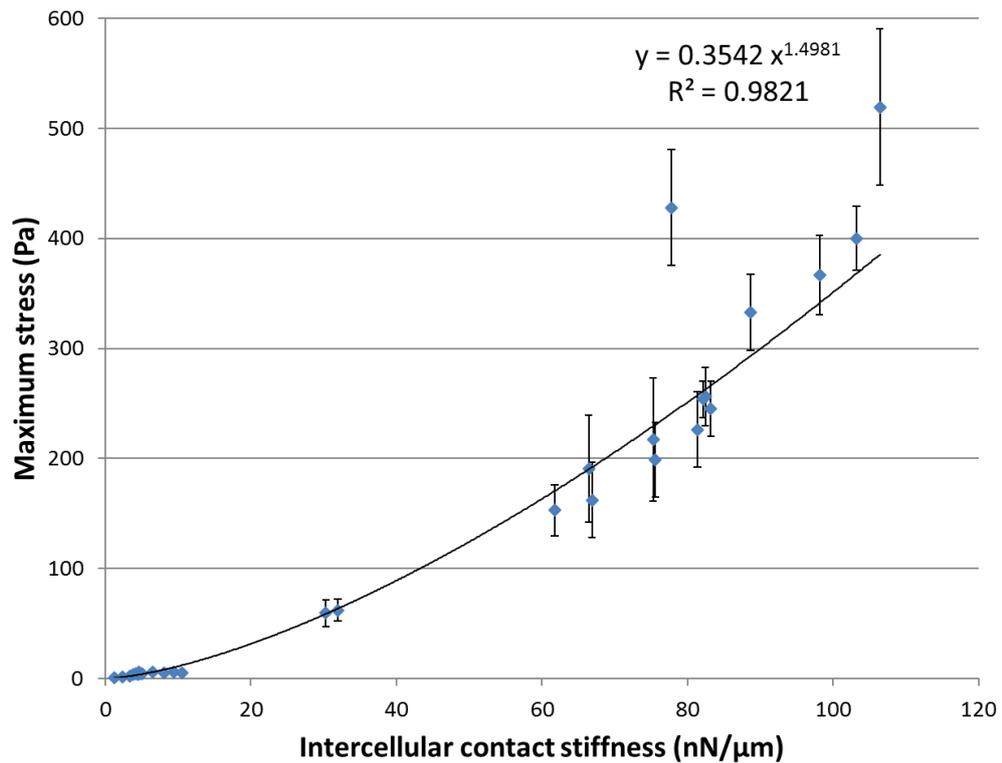
Figure 3.11 Maximum stress relation with intercellular contact stiffness for cell monocultures.

The error bars are associated with the five seeding replicates. Maximum stress changed a maximum of 36% between different seeding replicates.

The variation in stress with intercellular contact stiffness can be decomposed in the variation with apparent Young's modulus and intercellular adhesion energy. When changing the apparent Young's modulus within the complete range considered [0.02 – 16 kPa] for both low (0.05 nN/μm) and high adhesion (value dependent on the Young's modulus value) stress varies 58 and 59%, respectively. For the same apparent Young's modulus, if the adhesion is changed from low to high the variation in stress is between 75-99%. This means that the variation in stress is better explained by the variation in the adhesion than the variation in the Young's modulus.

In order to understand how the predicted stress changes with cell type specific mechanical properties, results for breast and bladder normal and cancer cultures are presented in Figure 3.12.

The figure shows stress distributions obtained for monocultures of normal and cancer cells with average apparent Young's modulus and the same level of adhesion. The distributions correspond to one of the five seeding replicates modelled. Higher levels of maximum compressive stress are found for normal cells than cancer, for both breast (2.4×10^2 Pa versus 1.3×10^2 Pa), and bladder (3.2×10^2 Pa versus 5.7×10^1 Pa). For bladder cells there is one order of magnitude difference in the maximum stress obtained for normal and cancer cell monocultures. The higher mismatch between the apparent Young's modulus of normal and cancer bladder cells results in a higher mismatch in the stress levels of the respective monocultures, for the same level of cell-cell adhesion.
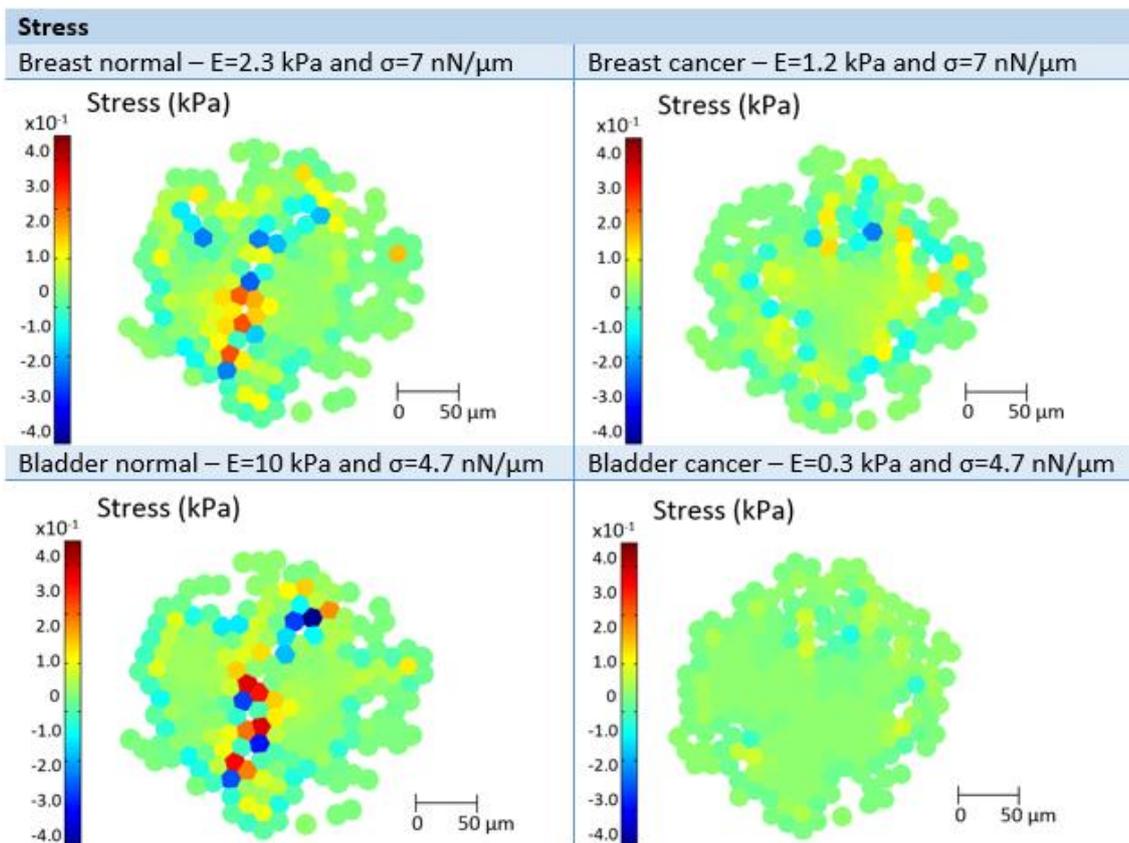
Figure 3.12 Stress distributions predicted for breast and bladder monocultures.

As already mentioned, there is a high stress variation associated with the uncertainty in intercellular adhesion, 75-99%. For this reason, stress variation with the cell type is analysed separately for minimum and maximum cell-cell adhesion, Tables 3.7 and 3.8. The maximum compressive stress for each population was obtained by averaging the maximum stress found for the five seeding replicates. The results for the different values

of Young's modulus considered for the same cell type were then averaged obtaining the values in Tables 3.7 and 3.8. The order of magnitude of stress increases from the order of Pascal to hundreds of Pascal from minimum to maximum cell-cell adhesion. Maximum compressive stress is higher for normal cell than for cancer bladder cell cultures. The difference observed in the maximum compressive stress of normal and cancer breast cell cultures is not regarded as relevant, considering the associated standard deviation.

Table 3.7 – Maximum compressive stress for breast and bladder monocultures with minimum cell-cell adhesion.

Minimum cell-cell adhesion				
Maximum stress (Pa)	**Breast cells**		**Bladder cells**	
	Normal	Cancer	Normal	Cancer
Average	4.9	4.6	5.5	2.5
Standard deviation	0.5	0.7	0.4	1.1

Table 3.8 – Maximum compressive stress for breast and bladder monocultures with maximum cell-cell adhesion.

Maximum cell-cell adhesion				
Maximum stress (Pa)	**Breast cells**		**Bladder cells**	
	Normal	Cancer	Normal	Cancer
Average	3.1×10^2	2.9×10^2	3.7×10^2	2.0×10^2
Standard deviation	84	98	28	33

3.4.2.4 Mechanics of bladder and breast cell co-cultures

Contrary to monocultures, in co-cultures both cells in compression and in tension are found in the centre of the monolayer. Normal and cancer cells have different overlap equilibrium resulting in them adhering to different extents (Figure 3.13).

Distributions obtained for one replicate of the three types of co-culture investigated, see Table 3.6 in section 3.3.2.4, are presented for breast (Figure 3.14) and bladder (Figure 3.15). Two different distributions are shown for each case. In the first, a), the cells are coloured according to their type: green if normal and black if cancer. In the second, b), the cells are coloured according to their level of stress: red if in compression, blue if in tension and light green if the stress magnitude is lower than 1Pa. Although cell stress depends on the local cell surroundings, as observed before, it also depends on the type of cell. Therefore, the distribution of normal and cancer cells in the co-culture, a), can be compared with the distribution of cell stress, b).

For type 1 and 3 co-cultures the intercellular adhesion energy values assigned to normal and cancer cells differ in two and three orders of magnitude, respectively. This results in visible sorting according to the cell type. Since there is low adhesion between normal and cancer cells (minimum between normal-normal adhesion and cancer-cancer adhesion), cells adhere to each other much less globally. For this reason, stress is low for most of the cells of the monolayer, less than 1 Pa. One exception is when a cell is surrounded by others of different type, as in Figure 3.14 b) and Figure 3.15 b) for type 3 co-cultures. The much higher intercellular adhesion energy value assigned to cancer cells in type 3 co-cultures results in them wanting to adhere to a higher extent than normal cells (higher overlap equilibrium, see Figure 3.13). Cancer cells are in tension and compress normal cells, explaining the higher level of stress locally. Higher levels of stress are also observed for clusters of cells with high adhesion, as in Figure 3.14 c) and Figure 3.15 c) for normal cells in type 1 co-cultures.

For type 2 co-cultures there is higher normal-cancer cell adhesion and cells adhere more to each other globally. This results in higher level of stress and less sorting comparing to type 1 and 3 co-cultures. Cancer cells are in compression and normal cells in tension. Even if the intercellular adhesion energy is the same for normal and cancer cells for a type 2 co-culture, the difference in apparent Young's modulus results in cancer and normal cells wanting to adhere to different extents (different overlap equilibrium values in Figure 3.13).
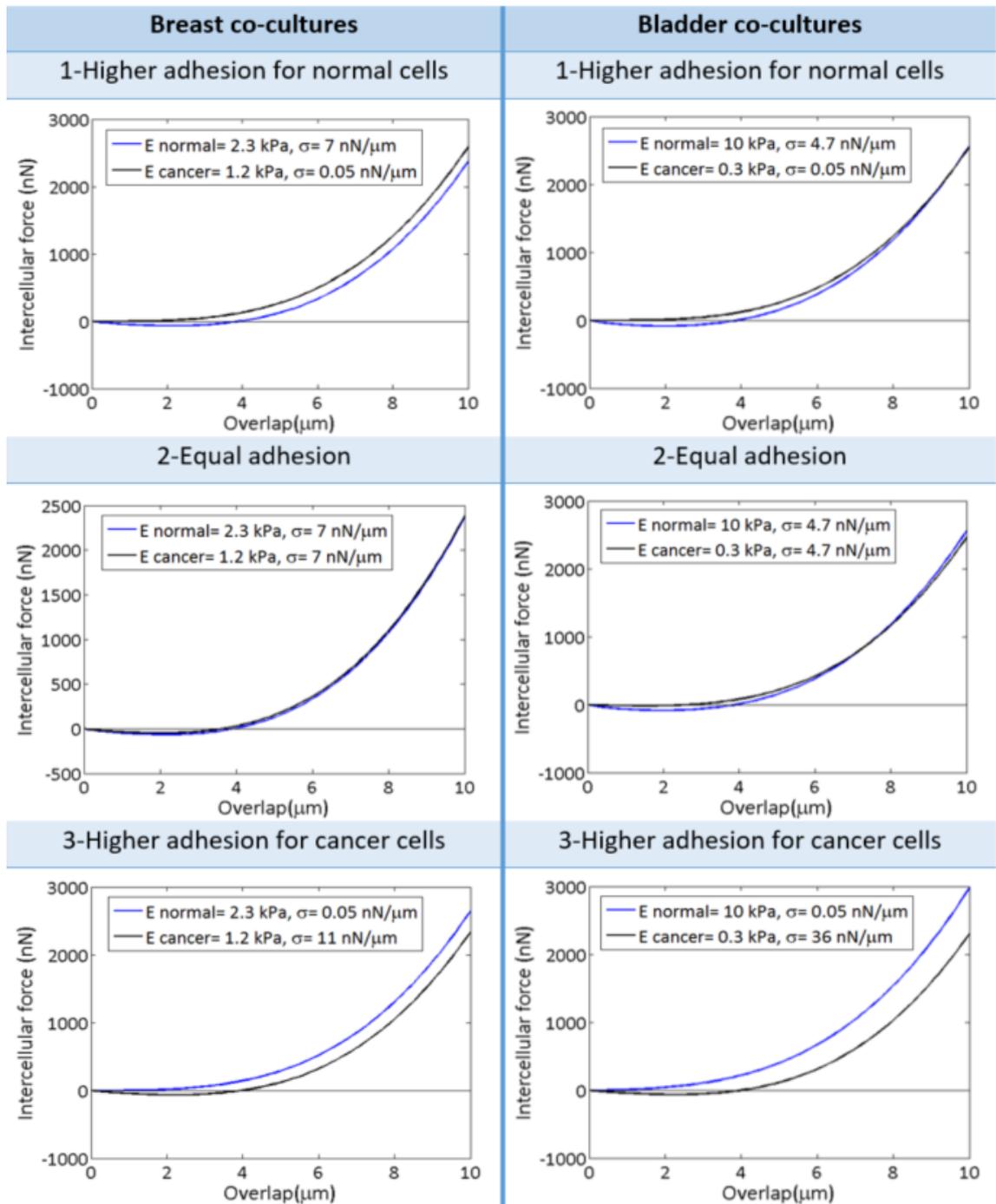
Figure 3.13 Force curves for two contacting cells in the centre of the various co-cultures.

Normal-normal cell interaction in blue and cancer-cancer cell interaction in black.
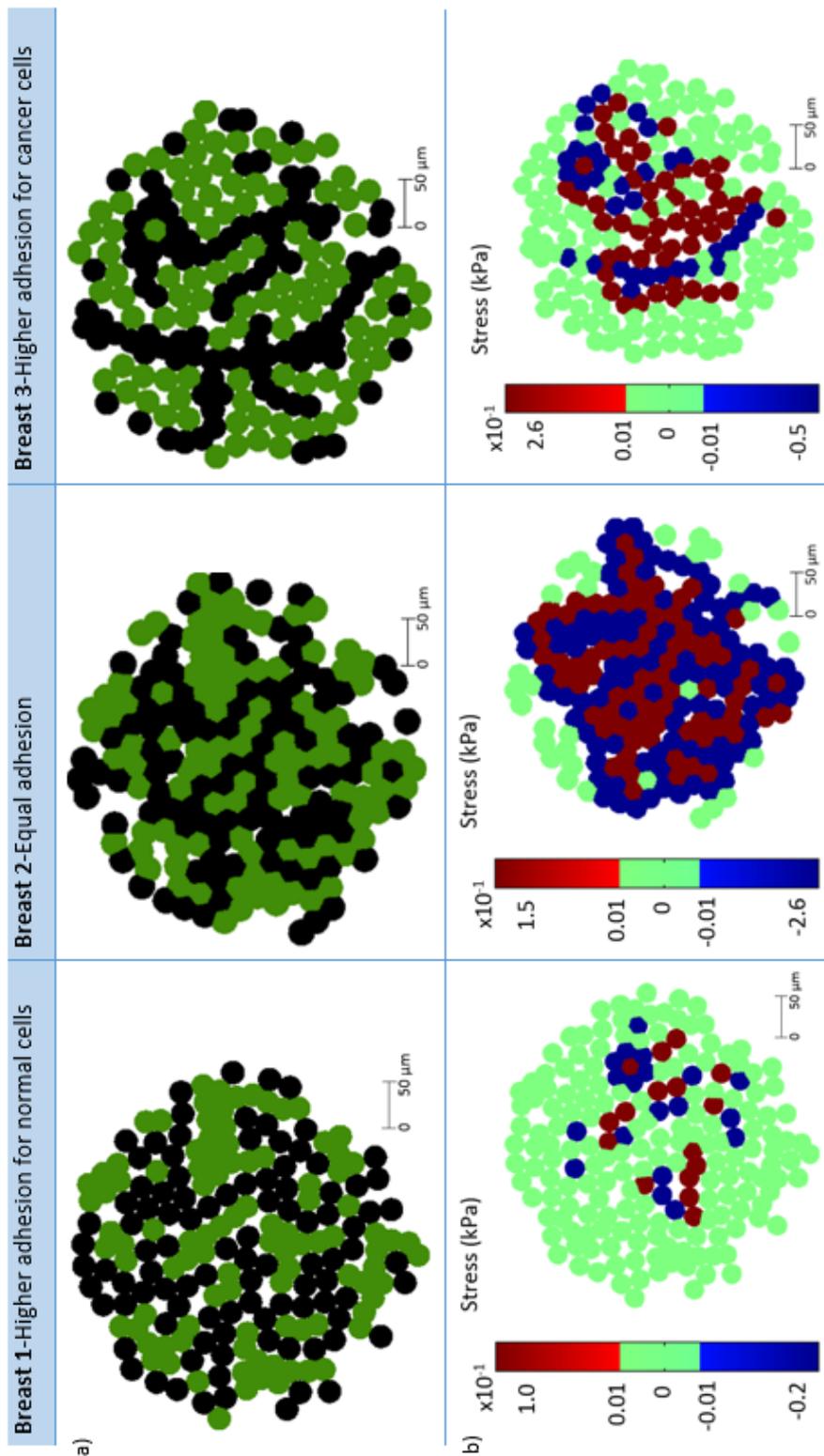
Figure 3.14 Breast co-cultures: a) normal (green) and cancer (black) cell distribution and b) stress.
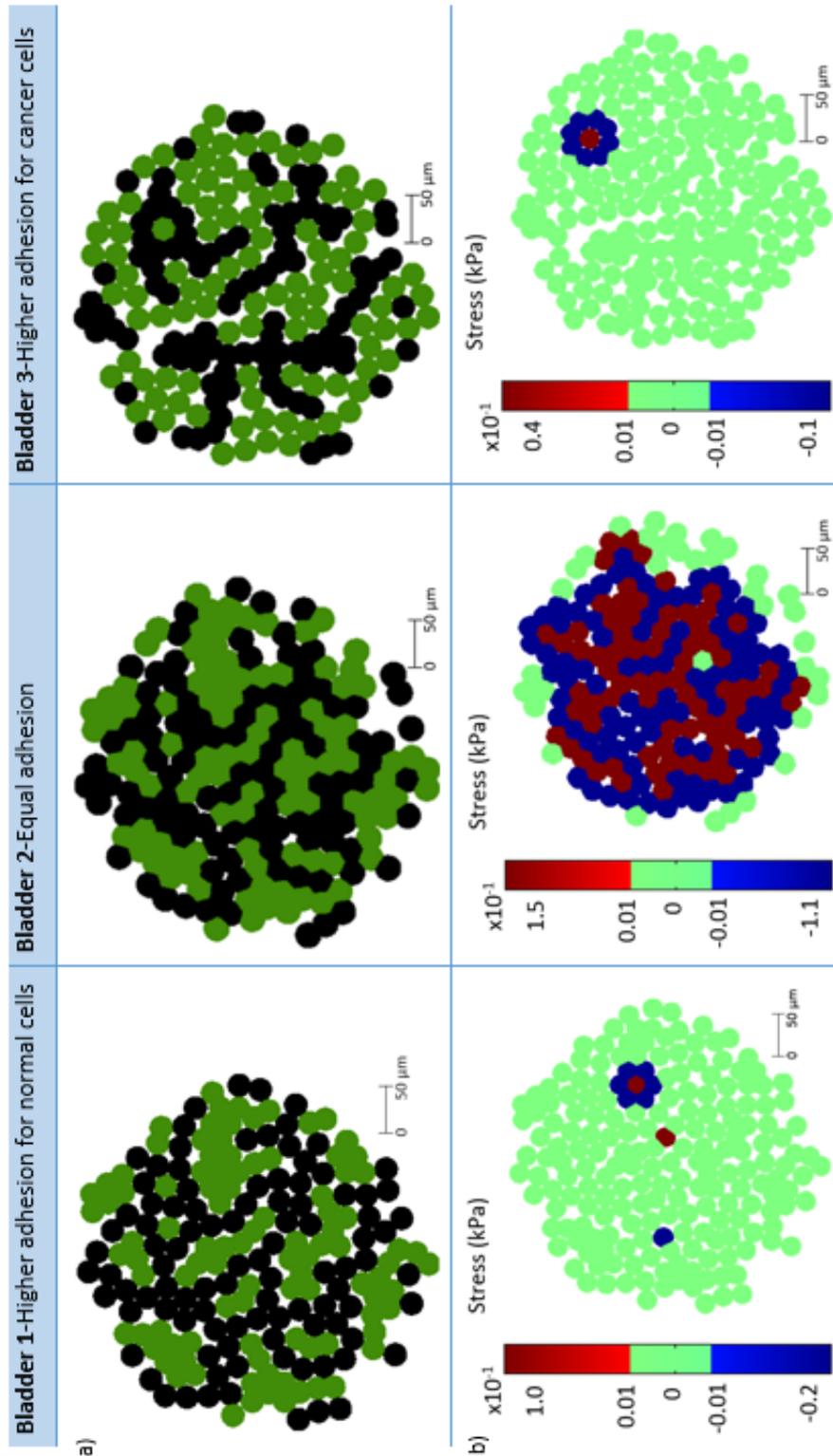
Figure 3.15 Bladder co-cultures: a) normal (green) and cancer (black) and b) stress.

The maximum compressive stress obtained for the various types of co-cultures was averaged across the five seeding replicates to understand how stress changes regardless of the seeding topology. The results are presented in Table 3.9.

When comparing breast and bladder co-cultures there is no clear difference in maximum compressive stress. However, between co-culture types there is a clear difference. The results confirm that type 2 co-cultures have higher stress than type 1 and 3 and that cell stress is highly dependent on cell-cell adhesion.

The high standard deviations reflect the stress variation with the seeding configuration. The variation is particularly relevant for co-cultures 1 and 3. Cells sort according to their type due to the adhesion mismatch between normal and cancer cells. However, sorting depends on the seeding configuration, happening to a greater extent in some replicates than in others. Consequently, different configurations are obtained and different levels of maximum stress. The replicates for which sorting is higher were able to relax more decreasing the level of cell stress. Sorting depends on the seeding and is, for example, not possible when cancer or normal cells are completely surrounded by cells of other type. Through passive spreading these cells are not able to sort and stay in a considerably higher state of stress than the rest of the cells in the monolayer. The results obtained for another seeding replicate of the bladder co-culture 3 are shown as example (Figure 3.16). This seeding replicate allowed a higher sorting of normal and cancer cells and a lower state of stress to be reached (maximum on the order of magnitude of 10^{-2} Pa).

Table 3.9– Maximum stress for breast and bladder co-cultures.

Maximum compressive stress (Pa)	Breast cell co-culture			Bladder cell co-culture		
	1	2	3	1	2	3
Average	63	233	147	92	184	86
Standard deviation	50	52	81	88	80	91
Standard deviation as % of the mean	80	22	55	96	43	106
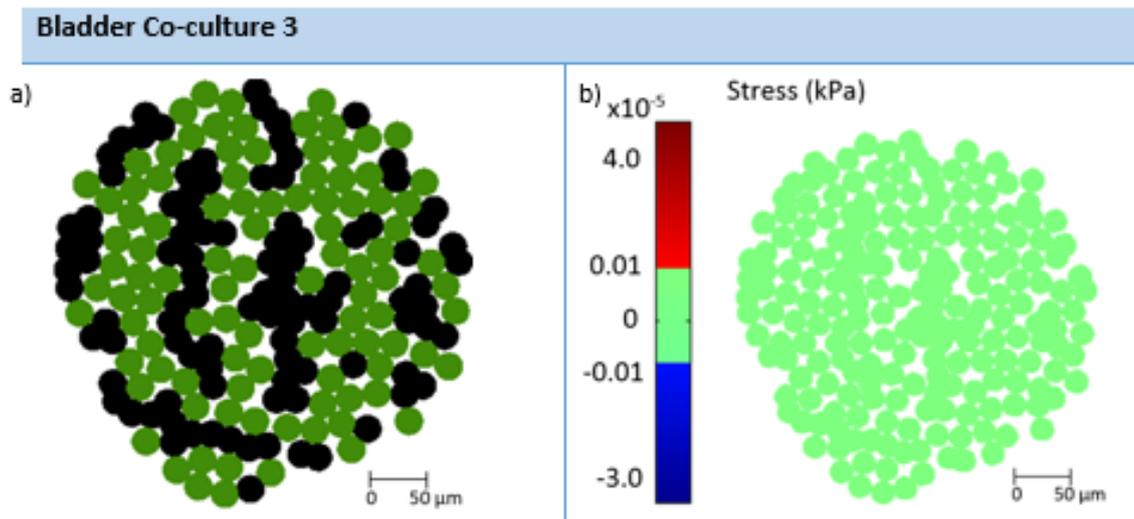
Figure 3.16 Bladder co-culture 3: a) normal and cancer cell distribution and b) stress.

3.5 Discussion

3.5.1 JKR model

The JKR model as implemented here is an approximation for small adhesion sometimes referred as the modified Hertz model. The original JKR model [61] needs to be solved iteratively requiring more computational resources. It accounts for intercellular contact hysteresis, not considering intercellular contact formation as a reversible process, in thermodynamics' terminology. As Schaller et al proposes [63] a possible workaround could be to make the intercellular adhesion energy time dependent. Furthermore, cells are considered as homogenous and purely elastic spheres. The polarized nature of the cytoskeleton, its viscoelastic behaviour and dynamics are not considered [63].

With relaxation not all cells of the cluster reach the equilibrium overlap defined by the JKR model (Figure 3.3). Over and under compressed cells are found in regions of lower cell connectivity.

The seeding method consisted of randomly seeding the cells within the seeding region. After seeding there was an asymmetric cell distribution, some cells on the border had none or very few neighbours, while others in the centre had too many, more than six. Through relaxation the cells increase their surface area and cell density becomes more uniform. However, since the level of compression due to multiple neighbours is not

accounted for, it is possible that few cells remain over compressed after passive relaxation.

A possible explanation for this result lies on the fact that the JKR model is a pairwise model here applied to several bodies in contact [63], [64]. The JKR defines the contact force based on the overlap between two bodies. When applied to several bodies the multiple overlap regions may overlap each other. This leads to an incorrect estimation of the force, assumed to be pairwise additive. The result is the presence of cells that are too compressed in the middle of the monolayer, not able to exert enough repulsion force. Near these cells there are under compressed cells for force balance. The JKR model assigns higher repulsion forces to cells with higher apparent Young's modulus. Therefore, according to this explanation, less overlap variation is expected for monolayers of cells with higher apparent Young's modulus. In fact, overlap variation increased from case I to II, see Figure 3.7. This confirms that overlap convergence is dependent on the cells' ability to exert enough repulsion forces and reduce the effect of the overlapping of overlap regions.

The cell level of compression was limited by including the compressibility model in a combined passive model, section 3.3.2.

3.5.2 JKR and compressibility model

3.5.2.1 Convergence study

Cell overlap and stress are stabilized for a sum of intercellular forces of 10^{-1} nN, see Figure 3.8. No cell rearrangements are observed from this point on and the monolayer is considered to be at a state of intercellular equilibrium. Thereby, when including active cell migration, intercellular contact changes can be interpreted as resulting from active cell behaviour and not residual passive forces from the relaxation step.

The JKR model defines equal overlap for all the cells of a cluster, as long as they have similar mechanical properties. When including the effect of cell volume with the compressibility model, the equilibrium value for the cell overlap is different depending on the number of contacting cells. Cells with less neighbours have higher overlaps than cells that are completely surrounded by other cells.

There is an edge effect for cell volume as well. It is 3% lower for cells in the centre of a monolayer. In reality cells may change their height to conserve their volume when within a monolayer. This was not accounted for in this work and volume was considered to change whenever the projected area of cells changed. In addition, it was considered that compressibility forces are present for all non-isolated cells, Eq (3.12). Therefore, the equilibrium for a cell is characterized by a balance between compressibility and elastic contact forces, Eq (3.14). It is relevant to point out that, although the JKR model represents both intercellular elastic repulsion and adhesion, it is the JKR adhesive nature that balances the repulsive compressibility forces in the combined model. As mentioned by Liedekerke et al [122], an alternative way of combining both models would be to let the compressibility model alone define the repulsive interactions and remove them from the JKR model. However, this is not straightforward. It is not obvious what the most sensible way to combine both models is: the choice of the target volume and whether or not compressibility forces should be present for all cells within the monolayer.

The JKR and compressibility resultants balance each other for each cell. However, the stress, being a scalar summation of these forces, reflects the level of cell compression. Therefore, passive cell stress can exist in a monolayer in force equilibrium. The various cell-cell interactions can balance each other, depending on the topology and direction of intercellular forces. When a cell is contacting two others only, this is not so probable, as it implies that the three cells would have to be in line. In this case, for intercellular equilibrium, the cell has to be in a state of zero stress (overlaps equal to the equilibrium value, adhesion forces equal in magnitude to compressibility forces), explaining the zero stress cells found on the monolayer border (Figure 3.8).

Compressed cells, with positive stress, are found at the centre of the monolayer revealing that compressibility forces are higher than adhesion forces (Figure 3.8). Compressibility forces have a predominant role in this region since cell volume is lower. Close to the border the stress is two orders of magnitude higher. Adhesive forces towards the cluster centre are sensed by cells in tension that assure its cohesiveness. Before this line of border cells in tension, there are cells experiencing compression from

the cluster and balancing this region. Cell stress reaches a magnitude in the order of the units of Pascal independently of the population size.

Some simplifications were considered when computing cell volume, Eq (3.6), and stress, Eq (3.8). The fact that overlap regions can intersect each other was not accounted for when determining cell volume, therefore this is underestimated. The total surface area of the cell was considered when determining cell stress, although another choice could have been the area of the overlap regions. Nevertheless, these simplified computations are able to provide an insight into how compressed the cells are.

For populations of higher cell number (200 and 500), cells are distributed less uniformly (Figure 3.9). During relaxation, the cells relax passively, moving according to intercellular contact interactions. Therefore, the seeding procedure in defining the initial cell connectivity influences the final cell distribution. Due to its random nature, regions of less cell connectivity are more probable for populations of higher cell number. In order to make the results less seeding dependent, the seeding could have been more controlled. Maximum and minimum limits could have been set to the initial cell overlap controlling cell connectivity. This would probably force more uniform cell distributions from the beginning. However, there is a random nature associated to cell deposition from suspension. Asymmetric cell distributions can be obtained in *in-vitro* cell seeding. Cells can fall on top of each other and need to find space with time. In order to achieve a more uniform cell distribution external force can be applied to shake the culture plate and spread the cells more evenly.

Seeding affected cell stress as well. More cells were seeded in the centre of the seeding region than at its periphery. Since cells at the periphery start to have higher intercellular force resultant they adapt creating tension that balances the compressed cluster. Following this line of thought, the compression found in the centre of relaxed monolayers can be seen as reminiscent from the seeding. If the resultant intercellular force governs passive cell behaviour, localized stress can exist in a monolayer. Another modelling approach would be to consider that cells move passively according to a scalar summation of intercellular forces or stress. Even if the final distributions depend on the cell connectivity defined by the seeding procedure, the model prediction that the cell stress is higher on the monolayer border and in regions of low cell connectivity holds.

During *in-vitro* seeding cells deposit from suspension in random places within the seeding environment. Drawing a parallel with experiments, the cell density asymmetries predicted by the model suggest that passive relaxation may not be enough for cells to find each other after seeding. This explains the changes in the level of cell packing within the monolayer. In reality, cells can sense the ones they are not in contact with through mechanisms not here considered such as signalling and lamellipodia formation and close monolayer wounds [123]. Nonetheless, the model suggests that these regions can be temporary regions of high passive cell stress. It is actually possible that passive stress is in the origin of an active cell response that maintains monolayer uniformity and integrity. As Mertz et al [124] suggests, a feedback may exist between intercellular adhesion forces and active traction forces.

In summary, the results suggest that some degree of passive cell stress exists to balance a stationary monolayer. Cells in higher level of stress are present at the border and in inner regions where the monolayer is less cohesive.

3.5.2.2 Sensitivity

From the results obtained in section 3.4.2.2, cell stress is not only dependent on the cell position within the monolayer but also on the cell mechanical properties, see Figure 3.10.

Different values for the parameters (apparent Young's modulus and intercellular adhesion energy) were investigated. The simulations were performed fixing the cell bulk modulus at 5.5 kPa and changing the Poisson's ratio adequately, Eq(3.18). However, numerical problems associated with the Poisson's ratio limited the possible values for the apparent Young's modulus. An alternative approach could have been to fix the Poisson's ratio and change both the apparent Young's modulus and the bulk modulus. The cell bulk modulus was determined in this work based on water transport experiments through permeable gap junctions [116]. This can constitute a limitation as an instantaneous elastic property was related with the time-dependent flow of water through cell-cell junctions. In addition, this explains the discrepancy between the value of bulk modulus used in this work and values reported in the literature, however limited,

measured using acoustic microscopy [125] and radiation [126], 2-3 GPa. The model developed predicts different volume for cells within a monolayer. However, its formulation does not define a minimum value for this volume. Therefore, unrealistic cell volumes were avoided by restricting the possible values for the parameters. An alternative would be to include a minimum cell volume within the model formulation, for instance, by accounting for changes in cell height. Another option would be to include another repulsive force dependent on the absolute cell volume, rather than on relative volume pressures existent between cells.

The maximum stress predicted has values with order of magnitude between 0.1-100 Pa and increases with both the apparent Young's modulus and intercellular adhesion (Figure 3.10). When comparing the stress distributions obtained in this work with experimental results from the literature one must consider the intercellular and passive nature of the cell stress here predicted. Active cell tractions that drive cell migration were not included. This fact constitutes a barrier to validation as passive and active cell contributions are difficult to differentiate experimentally and may even be related [124]. Although this fact is a barrier to validation, it also shows one of the strengths of computational modelling in comparison with experimental work: the possibility of isolating the contribution from different factors and increase mechanistic understanding. Nonetheless, studies like the one of Trepat et al [16] on Madin-Darby Canine Kidney Epithelial Cells (MDCK) can be analysed as a reference. The stress within a migrating monolayer was theoretically computed based on experimentally measured traction forces. Although higher traction stress was measured for cells at the leading edge (20 Pa), considerable traction was measured for cells many rows behind it (5 Pa for cells at a distance of 200 μm). Assuming that the traction stress generated by migrating cells is balanced by an intercellular stress carried within the monolayer, it was possible to determine the intercellular stress using a force balance. This intercellular stress was found to be maximum for cells far away from the leading edge, reaching an order of magnitude of hundreds of Pa. The hypothesis suggested by the authors is that part of the high traction force exerted by cells at the border is transmitted to inner cells. This explains the build-up of forces towards the centre of the monolayer and the higher stress found in this region. In contrast with these results, in this work higher intercellular

stress was predicted for cells on the border of the monolayer. The reason behind this difference lies in the fact that no migratory traction forces were included and instead of a directional migration, cell movement followed a radial expansion after cell seeding based on elastic forces. In agreement with the results obtained in this work, the same authors found that cells in tension and cells in compression can be in close proximity in the same monolayer.

3.5.2.3 Mechanics of bladder and breast cell monocultures

A power-law relation between the maximum compressive stress and intercellular contact stiffness was found for all the cells modelled with a good coefficient of determination, see Figure 3.11. It is reasonable that stress increases with the stiffness associated with cell-cell contact. In addition, higher stress was found for monolayers of bladder normal cells than for monolayers of bladder cancer cells, Table 3.7 and Table 3.8. The high mechanical mismatch between individual bladder normal cells and bladder cancer cells results in different maximum compressive stress at the population level.

The variation in stress found for cells of the same type reflects the variation in apparent Young's modulus and intercellular adhesion. However, the variation in adhesion is much more relevant. Maximum stress levels increase from the units of Pa for minimum adhesion to hundreds of Pa for maximum cell-cell adhesion, Table 3.7 and Table 3.8. The variation in Young's modulus is based on measurements for the same cell type reported in the literature. On the other hand, the variation in adhesion relied on measurements performed for different cell types, being much higher.

Alternative metrics for the cell-cell adhesion could have considered. For instance, in AFM force spectroscopy the force at which two cells detach is measured using a cantilever. However, due to the current difficulty in tracking the contact area between two cells, this technique lacks a method for normalizing the forces measured [127]. In addition to the problem of limited data for the adhesion between cells of specific type; model inputs require data from the literature to be comparable and compatible with the model formulation. In this case, the JKR model requires the work associated with cell-cell contact and not adhesion forces as reported by some authors [33]. Given that the

development of simulation models is dependent on the development of accurate measurement technologies, the development of models should be considered in parallel with the available measuring tools to inform the models.

3.5.2.4 Mechanics of bladder and breast cell co-cultures

Differences in cell packing and sorting were observed for co-cultures of cells with different mechanics (Figure 3.15 and Figure 3.16). This evidences the role of intercellular contact and compressibility forces within the first hours after seeding. Unpublished data collected by PhD student Marzieh Tehrani (Insigneo, University of Sheffield) confirms that differences in cell shape and clustering are observed for normal and cancer cells within this time frame. The following microscope image was taken 10 hours after seeding, before cell migration and division start:
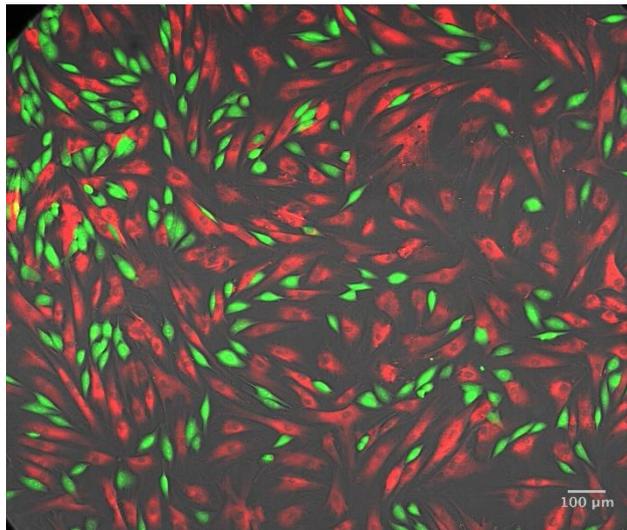
Figure 3.17 Microscope image taken 10 hours after the seeding of an in-vitro co-culture of mesenchymal stem cells, in red, and bone cancer cells, in green.

Asymmetries in cell packing are visible, there is higher cell density on the top left of the image. In particular, there is a high cancer cell density in this region when comparing to the rest of the image. This suggests that cells are clustering according to their type. The results of this work indicate that the seeding procedure and the mechanics of the cells cultured can play a role in cell packing asymmetries and cell sorting.

Cells in tension and in compression were found in the centre of heterogeneous monolayers in this work. This was reported by Trepat et al. [16] for migrating populations. Since the populations studied by Trepat correspond to monocultures, the heterogeneous stress fields measured suggest that either differences in cell packing or cell mechanics exist within a monoculture. The authors proposed that mechanically different cells may be present, which is reinforced by the results obtained in this work. In order to take more conclusions with regards to how much of the stress is determined by cell mechanics or cell local topology, monolayers with more cells could be investigated in the future with the model developed.

Three different types of co-culture were implemented: higher adhesion for normal cells, equal adhesion for normal and cancer, higher adhesion for cancer cells. In addition to the question of whether cell-cell adhesion is higher for normal or cancer cells, there is the question of whether cell-cell adhesion is different at different stages of cancer development [128]. It is possible that cancer cell adhesion changes during the process of detaching from the primary tumour, migrating and attaching to other secondary tissues for metastasis. The same applies to the Young's modulus. It is possible that cell mechanical changes are necessary for cell function and adaptation to the environment. In the future, the dynamics of cell adaption could be considered in the model developed. A feedback could be included between the level of stress experienced by the cell and the consequent change in its mechanical properties.

Active cell tractions that drive cell migration are included in Chapter 4 of this thesis. The aim is to investigate the relative role of passive and active cell mechanical properties in the migration of breast and bladder cell co-cultures.

3.6 Conclusion

In conclusion, a computational model representing the process of cell spreading within the first few hours of *in-vitro* seeding was developed. Cell spreading is considered to be governed by intercellular contact and compressibility forces. Thereby, cell volume and intercellular stress can be predicted for cells within a population.

The model was applied to normal and cancer cell cultures accounting for the different individual cell mechanics associated with malignant transformation. Intercellular stress in a monolayer was found to depend on both the cell mechanical properties (Young's modulus and intercellular adhesion) and those of neighbouring cells. Intercellular stress varies more within a co-culture of mechanically different normal and cancer cells than within monocultures. Furthermore, the different mechanical properties of normal and cancer cells explain their early sorting in co-culture.

The predictions of the model show that the mechanical properties of individual cells reflect at the population level. This evidences their potential to be used as targets to treat diseases that affect the mechanics of tissues, such as cancer.

The results of this Chapter demonstrate the robustness of the computational model developed. This is the first step in developing a collective cell migration model which is extended to include active traction forces – Chapter 4. By investigating passive forces at a first step, it will be possible to understand the relative role of passive and active forces in the mechanics and migration of cell populations.

Chapter 4 - Modelling active mechanics of cell migration

Summary

Cancer cells in the body sort from the normal tissue and tend to cluster enabling metastasis. Similar sorting behaviour has also been observed in-vitro. In addition, normal and cancer cells have been shown to be mechanically different. However, it is not understood how these different mechanical properties affect collective cell migration and sorting in cancer.

In this Chapter a computational model was developed to investigate the mechanics of migration of normal and cancer cells in co-cultures. Cell movement is governed by passive forces, the subject of Chapter 3, in the first hours after seeding and migratory traction forces are exerted by cells later.

The results of this new model indicate that the sorting between normal and cancer cells in co-culture is more influenced by differences in the traction of normal and cancer cells and cell-cell adhesion levels, followed by differential adhesion of normal and cancer cells.

4.1 Introduction

As discussed in Chapter 2 of this thesis, cell sorting is related with cancer spreading *in-vivo*, as cancer cells sort from the normal tissue and cluster for metastasis. Spontaneous sorting of normal and cancer cells in co-culture has also been observed in *in-vitro* experiments [20], [129].

The study of cell sorting has been inspired by the same physical principles as the ones governing the behaviour of immiscible liquids [22], [93]. These principles are the basis of theories such as the Differential Adhesion Hypothesis (DAH) [21]. However, also differences in cell motility have been proposed to play a role in cell sorting and collective behaviour. There is experimental evidence of the sorting of keratocytes with different motilities [102] and computational work supporting this idea [24], [98].

The measurement of parameters characterizing cell mechanics, such as the apparent Young's modulus, intercellular adhesion and traction force was presented in Chapter 3. At the same time, a recent review on collective cell migration shows the great variety of

computational models developed to understand this phenomenon [44]. However, the connection between the emergent collective behaviour and individual cell mechanics is missing. The traction forces exerted by collectively moving cells are heterogeneous and dynamic and a clear relation between the movement observed and the forces measured is yet to be found [18]. In addition, despite the importance of collective cell migration and sorting in metastasis [41], [42], cell-based models investigating these processes in cancer lack [42].

The aim of this Chapter was to investigate the mechanics of collective cell behaviour and cell sorting in cancer. The model presented in Chapter 3 was expanded to include migratory traction forces. It was applied to co-cultures of mechanically different normal and cancer cells as a surrogate for tumour-host mechanical interactions. The main scientific questions that are addressed in this Chapter are:

- What is the relation between cell sorting and intercellular forces?

- What is the relative role of differences in motility and cell-cell adhesion in the sorting of normal and cancer cells in co-culture?

- Can the Differential Adhesion Hypothesis explain the sorting of normal and cancer cells in co-culture?

- Can cell mechanics inspire a mechanistic explanation for cell sorting?

4.2 General methods

4.2.1 Model description

This work regards cell movement as governed by passive intercellular forces in the first few hours after cell seeding. Passive relaxation is characterized by a decrease in intercellular forces and cells reaching a state of equilibrium, subject of Chapter 3. In this Chapter, active traction forces exerted by cells to migrate are included in the model, Eq (3.1). Intercellular forces, cell position, volume and stress are all computed as described in Chapter 3 – section 3.2.1.

It is assumed that cells start migration as being polarized in a random direction. Therefore, at the beginning cells are assigned random angles for their active forces.

Following the minimal model of Vicsek [68], it is considered that, during migration, cells align the direction of their active machineries with neighbouring cells in order to migrate collectively. Neighbouring cells align their active machineries with time, while showing some degree of persistence in their movement:

$$\alpha_{cell}(t + 1) = \ 0.98 \ \alpha_{cell} \ (t) + 0.02 \ \alpha_{neighbours} \ (t) \qquad (\ 4.1\ )$$

in which α_{cell} refers to the active force angle for a particular cell and $\alpha_{neighbours}$ is the average angle for neighbouring cells. Isolated cells, without neighbours, keep migrating in the same direction. This alignment rule results in a 200 cell population having a coordinated movement after 15-30 minutes of real time migration.

The active traction force magnitude is tuned to *in-vitro* measurements of the velocity of individual cells. Modelling drag using the Stoke's model [130] and following from Eq.(3.1), the active force can be computed for an isolated cell, for which intercellular forces are not present, based on its velocity v_{active}, radius R and the extracellular environment viscosity µ:

$$F_{active} = 6\pi R \mu v_{active} \qquad (4.2\ )$$

It is assumed that cells preserve the magnitude of the active force when surrounded by other cells.

This Chapter investigates sorting between normal and cancer cells in co-culture, quantified using a metric called *sorting index* (SI). This is computed as the number of cells of different type, $\eta_{\neq}$, over the total number of cells surrounding a particular cell, $\eta_{\neq} + \eta_{=}$ [102].

$$SI = \frac{n_{\neq}}{n_{\neq} + n_{=}} \qquad (\ 4.3\ )$$

4.2.2. Model parameters

Bladder and breast normal and cancer cells were assigned the average apparent Young's modulus considered in Chapter 3, Table 4.1. Intercellular adhesion energy was varied within the valid range found in Chapter 3 – section 3.3.2.2 according to cell volume restrictions. The bulk modulus for all the cells, the cell radius and the medium viscosity were kept constant at 5.5 kPa, 10 μm and 0.01 kPa.s respectively. As in Chapter 3, the Poisson's ratio was determined depending on the apparent Young's modulus and assuming that cells behave as homogenous isotropic materials (Eq. 3.16).

In the studies in which intercellular adhesion was different for the homotypic cell interactions normal-normal and cancer-cancer, the magnitude of adhesion for the interaction normal-cancer was assumed to be equal to the minimum of the last two. This is based on the idea that two cells of the same type should adhere to each other to a higher extent than two cells of different type [98].

Velocity values of single migrating cells have been reported to be in the order of magnitude of 0.1-5 μm/min [131]. In this study, single normal cells were considered to migrate at a velocity of 5 μm/min. This velocity was converted to an active traction force as described in section 4.2.1, Eq (4.2).

Higher traction forces have been measured for cancer cells than for normal cells, between 20 to 100% higher [30], [31]. The active velocity, and therefore traction force, for cancer cells was determined in this work considering this mismatch in traction found between normal and cancer cells. Assuming that active force in the model is a proxy for cell traction force, active force mismatches within this range were applied between normal and cancer cells throughout this work.

Table 4.1 – Model parameters.

	Young's modulus, E (kPa)	Cell-cell adhesion, σ (nN/μm)	Bulk modulus, K (kPa)	Radius, R (μm)
Bladder normal cells	10	0.05-4.7		
Bladder cancer cells	0.3	0.05-36	5.5	10
Breast normal cells	2.3	0.05-7		
Breast cancer cells	1.2	0.05-11		

4.2.3 Cell sorting threshold

At the start of cell migration, after seeding and passive relaxation, normal and cancer cells in co-culture are randomly mixed. The initial sorting index varies between replicates due to the randomness of cell seeding. This variability was determined simulating the seeding of 20 replicates of normal/cancer cell co-cultures. One of this replicates is presented in Figure 4.1. The sorting index after seeding had a mean of 0.498±0.024, with values between 0.4 and 0.6.

This reflects the randomness of the initial configuration, as a sorting index of 0.5 is associated with cells having exactly the same proportion of cells of equal and different type surrounding them.
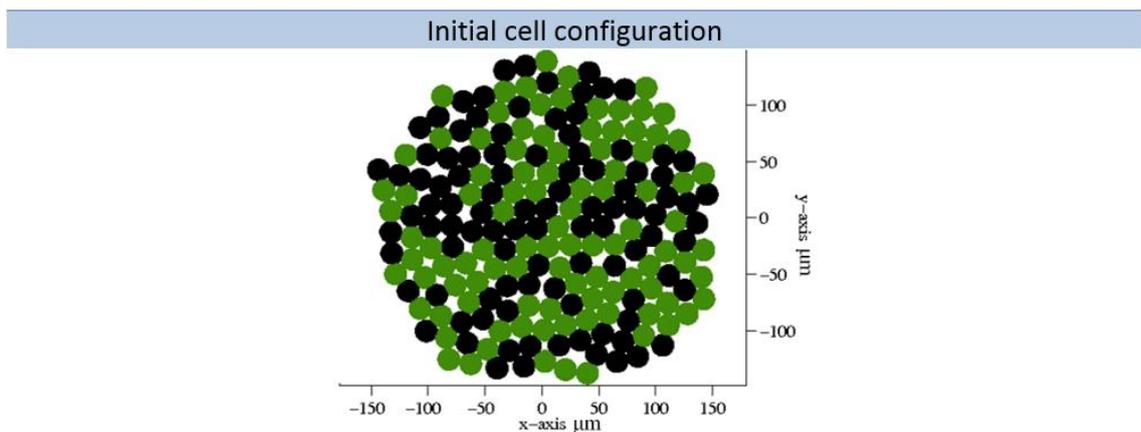
Figure 4.1. Example of initial configuration for one seeding replicate of a co-culture of bladder normal and cancer cells with equal intercellular adhesion energy of 0.05 nN/μm. The initial sorting index is 0.54.

During migration, cells rearrange their positions leading to changes in the sorting index. Since the sorting index decreases with cell sorting, sorting between normal and cancer cells is considered to have happened whenever the sorting index decreases to a value lower than 0.4 after two hours of migration.

4.3 Simulations

Cell migration was modelled synchronously for two hours of real time in an unconfined environment. A time step of 0.135 seconds, maximum cell displacement of 2.5 % of the cell radius per iteration, was considered since it is small enough to ensure both solution stability and accuracy – Appendix. Five seeding replicates were investigated per cell population. Normal and cancer cell co-cultures with 200 cells were studied from both the bladder and breast tissues. Intercellular forces, cell stress and sorting index were all calculated and saved every tenth iteration to reduce computational and memory costs. The following sections describe the several sorting studies performed.

4.3.1 Cell sorting based on different active traction

Traction forces measured for cancer cells are 20-100% higher than those measured for normal cells [30], [31]. This study investigates the effect of this force mismatch on the migration of bladder cell co-cultures. Cell-cell adhesion was assumed to be minimum and the same for the cell interactions normal-normal, cancer-cancer and normal-cancer. The cell properties considered are presented in Tables 4.2 and 4.3.

Table 4.2 – Young's modulus and intercellular adhesion properties used for the study.

	Bladder normal cells	Bladder cancer cells
Young's modulus (kPa)	10	0.3
Intercellular adhesion energy (nN/µm)	0.05	

Table 4.3 – Active traction properties used for the study.

Active traction force mismatch(%)	Active traction velocity (µm/min)	
	Normal cells	Cancer cells
20		6
30		6.5
40		7
50	5	7.5
60		8
70		8.5
80		9
90		9.5
100		10

4.3.2. Cell sorting based on absolute cell-cell adhesion

This study investigates the effect of cell-cell adhesion on the migration of bladder cell co-cultures. As in section 4.3.1, equal adhesion was assumed for all the cell-cell interactions. However, adhesion levels were varied between 0.05 and 4.7 nN/µm, the valid range found for bladder normal cells in Chapter 3 - section 3.3.2.2. Active velocity was assumed to be 5µm/min for normal cells and 10µm/min for cancer to maximize the possibility of cell sorting. The cell properties considered are presented in Tables 4.4 and 4.5.

Table 4.4 – Young's modulus and active velocity properties used for the study.

	Bladder normal cells	Bladder cancer cells
Young's modulus (kPa)	10	0.3
Active velocity (µm/min)	5	10

Table 4.5 – Intercellular adhesion properties used for the study.

Intercellular adhesion energy (nN/µm)
0.05
0.075
0.1
0.2
0.3
1.2
4.7

4.3.3. Cell sorting based on different cell-cell adhesion

This section investigates how different adhesion associated with cell interactions normal-normal and cancer-cancer, affects the sorting of normal and cancer cells in co-culture. Both co-cultures of cells from the bladder and from the breast were studied, Table 4.6. The adhesion associated to the cell interaction normal-cancer was assumed to be equal to the minimum between the normal-normal and the cancer-cancer adhesion values and kept constant at 0.05 nN/µm. Cell adhesion levels varied within the limits defined in Chapter 3 – section 3.3.2.2, Table 4.7. Two scenarios were tested: higher adhesion between normal cells, shaded in orange in Table 4.7, and higher adhesion between cancer cells, shaded in purple.

The active traction force mismatch between normal and cancer cells was minimum (20%) in order to explore how cell sorting in a co-culture is affected by differential intercellular adhesion solely.

Table 4.6 – Young's modulus and active velocity properties used for the study.

	Bladder cells		Breast cells	
	Normal	Cancer	Normal	Cancer
Young's modulus (kPa)	10	0.3	2.3	1.2
Active velocity (µm/min)	5	6	5	6

Table 4.7 – Intercellular adhesion properties used for the study. Two adhesion scenarios were considered: higher adhesion between normal cells, shaded in orange, and higher adhesion between cancer cells, shaded in purple.

Intercellular adhesion energy (nN/µm)					
Bladder cells			Breast cells		
Normal	Cancer	Absolute difference	Normal	Cancer	Absolute difference
0.075	0.05	0.025	0.075	0.05	0.025
0.05	0.075	0.025	0.05	0.075	0.025
0.3	0.05	0.25	0.3	0.05	0.25
0.05	0.3	0.25	0.05	0.3	0.25
1.05	0.05	1	1.05	0.05	1
0.05	1.05	1	0.05	1.05	1
2.5	0.05	2.45	2.5	0.05	2.45
0.05	2.5	2.45	0.05	2.5	2.45
4.7	0.05	4.65	7	0.05	6.95
0.05	4.7	4.65	0.05	7	6.95
0.05	36	35.95	0.05	11	10.95

4.3.4. Cell sorting based on the combined effect of different active traction and different cell-cell adhesion

This section explores the combined effect of differential intercellular adhesion and active force mismatch on the sorting of normal and cancer cells in co-culture. Sorting

was investigated for low adhesion differences between normal and cancer cells, lower than 1 nN/μm, in association with traction mismatches of 40 and 60%, Table 4.8.

Table 4.8 – Cell properties for combined effect of active traction force mismatch and differential cell-cell adhesion.

Intercellular adhesion energy (nN/μm)			
Bladder cells		**Breast cells**	
Active traction force mismatch (%)	Adhesion difference	Active traction force mismatch (%)	Adhesion difference
40	0.025	40	0.025
40	0.25	40	0.25
60	0.025	60	0.025
60	0.25	60	0.25

4.4 Results

4.4.1 Cell sorting based on different active traction

The sorting index evolution for maximum active traction force mismatch is showed as an example (Figure 4.2). A linear relationship provides the best fitting for this evolution with an R2 of 0.974.
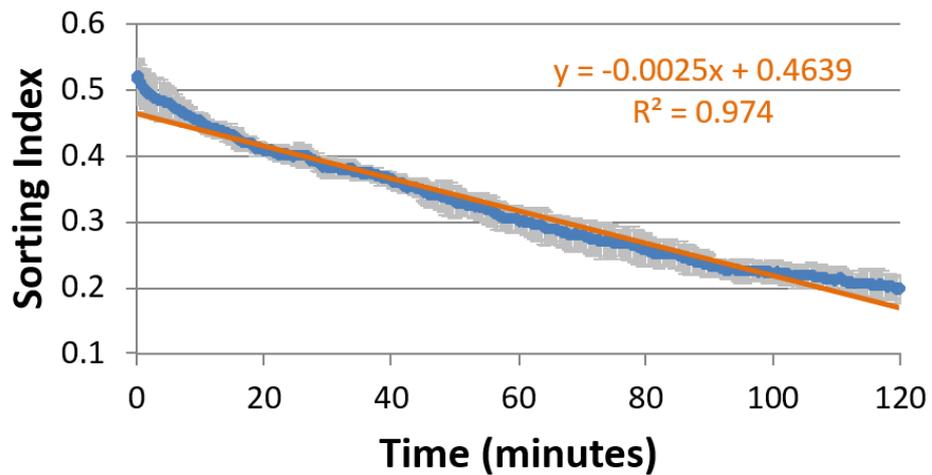
Figure 4.2. Sorting evolution for maximum active traction force mismatch, average of the five replicates in blue and region covered by the standard deviation in grey. Linear fitting in orange.

Cell sorting is higher for higher active traction force mismatch, see Figure 4.3. The coefficient of variation of the sorting index was determined by computing the ratio between the standard deviation and the average of the final sorting index values obtained for the various traction mismatches. A value of 27.2% was obtained. This is a quantitative measure of the variation in sorting with the active traction force mismatch between normal and cancer cells. It was found that a minimum mismatch of 70% is required for a significant sorting (sorting index less than 0.4) between normal and cancer cells in co-culture for low and uniform cell-cell adhesion.
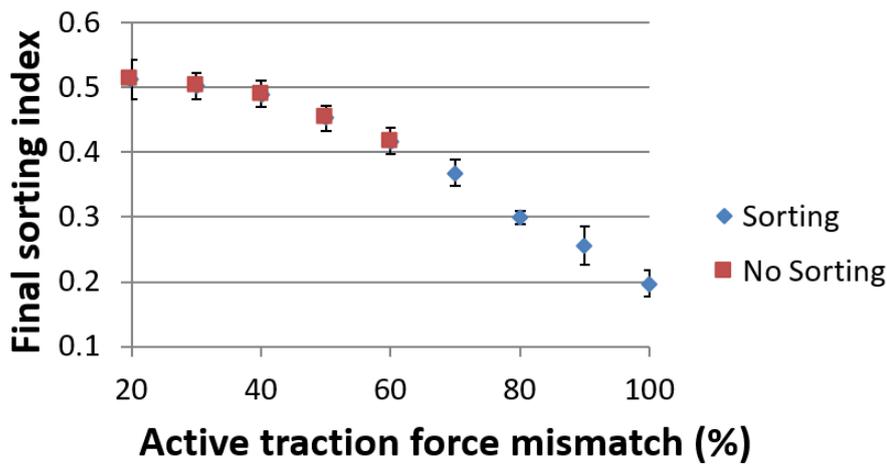
Figure 4.3. Relation between sorting index after two hours of migration and active traction force mismatch. Average and standard deviation of five seeding replicates.

Intercellular force and cell velocity are here analysed for three different active traction force mismatches: 20, 40 and 100%, see Figures 4.4, 4.5 and 4.6, respectively. Cell sorting was significant for the latter only.

Figures 4.4, 4.5 and 4.6 show the results obtained for one seeding replicate with initial cell distribution in Figure 4.1. Velocity and intercellular force distributions at the end of migration are presented, as well as the time evolution of the average magnitude of intercellular force and a visual representation of the direction of intercellular forces at the end of migration.

For 20 and 40% of active traction mismatch (Figures 4.4 and 4.5), cell velocity reaches a value equal to the average of the active velocities of normal and cancer cells, $5.5\pm2.5\text{x}10^{-2}$ µm/min for the former and 6.0 ± 0.31 µm/min for the latter. For the velocity of the heterogeneous cluster to be in between the active velocity of normal and cancer cells, normal cells need to migrate faster than when isolated and cancer cells slower. Intercellular forces emerge to make this possible, accelerating normal cells and dragging cancer cells behind. Intercellular force peaks at the beginning of cell migration and decreases as the cells align their migration direction. The active force of normal cells was fixed at 1.6 nN, associated with a velocity of 5 µm/min - section 4.3.1, while the active force of cancer cells was of 1.9 nN for 20% mismatch and 2.2 nN for 40%. Intercellular force reaches a magnitude equal to half the difference of the active force of normal and

cancer cells, $0.16\pm7.8\times10^{-3}$ nN for a mismatch of 20% and $0.28\pm8.3\times10^{-3}$ nN for 40%. In terms of direction, intercellular force has the same direction as cell migration for normal cells, therefore accelerating them, and opposite direction to cell migration for cancer cells, dragging them. For a mismatch of 40% cells rearrange more their positions according to their type and are less packed. This explains the higher variation in the magnitude and direction of intercellular forces when comparing to a 20% mismatch.

When there is cell sorting (active mismatch of 100% in Figure 4.6), three different regions are possible. One region in which cells migrate faster, at a velocity similar to the cancer cell active velocity, one in which cells migrate slower, at a velocity similar to the normal cell active velocity, and one last region in which cells migrate at an intermediate velocity. Intercellular forces decrease as cells sort and become locally high for the cells that do not sort. For instance, the cancer cells that stay at the rear migrating at a velocity similar to the one of normal cells have the highest intercellular force, ≈1.4 nN, that acts as a drag. Globally, cells travel at an average velocity of 7.5 ± 2.0 µm/min with intercellular forces of magnitude 0.24 ± 0.33 nN. The high standard deviations reflect the heterogeneity associated to intercellular force and velocity when there is a higher active traction force mismatch. It is the inability of cells to generate sufficient intercellular forces to drive a cohesive movement of the heterogeneous cluster that leads to sorting.
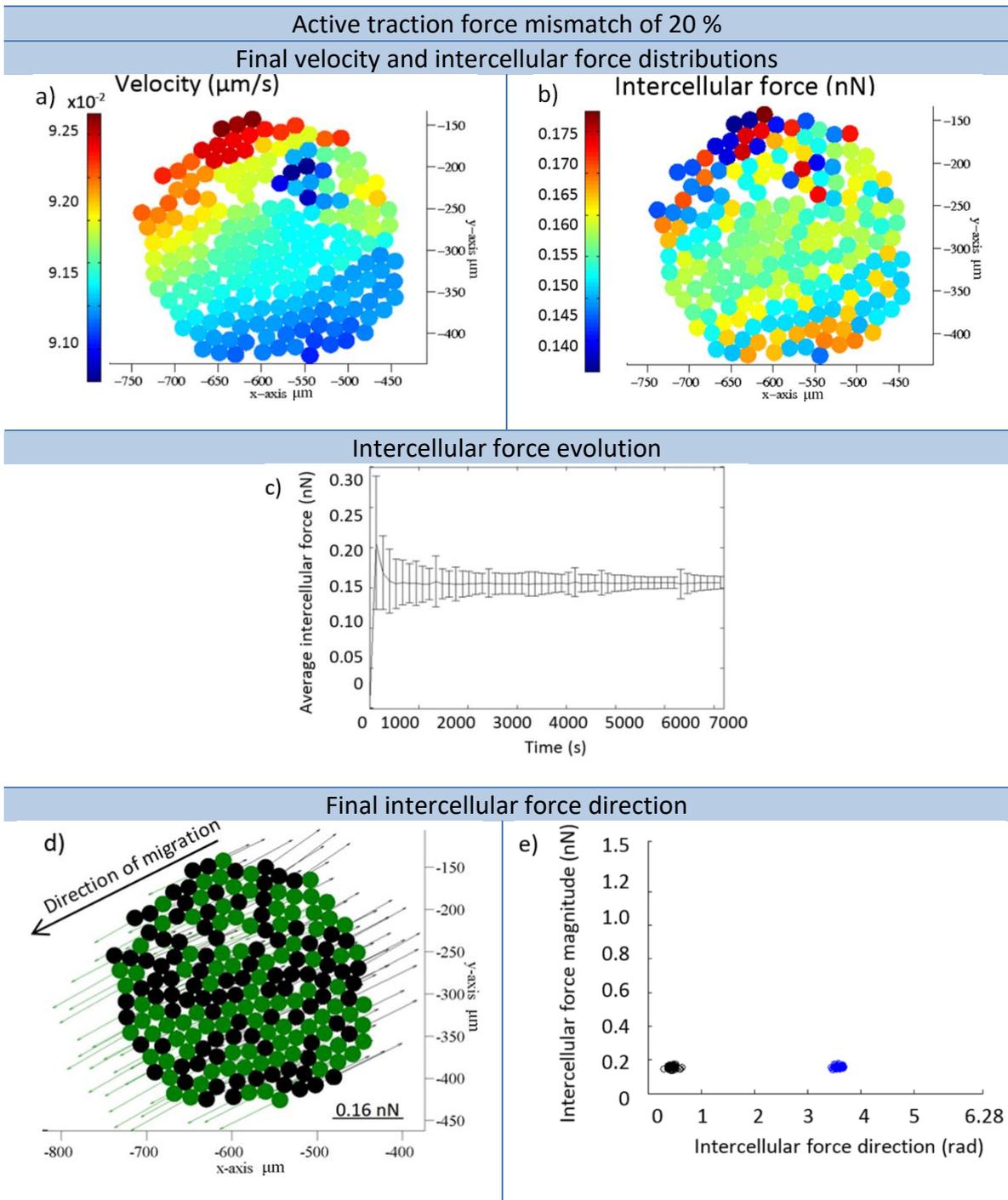
Figure 4.4. Final intercellular force and velocity for an active traction mismatch of 20%. a) Final velocity and b) intercellular force distributions: each cell is coloured according to velocity and force magnitudes respectively. c) Evolution of intercellular force, average for all the cells was computed and the associated standard deviation is shown. Intercellular force direction: d) normal cells in green and cancer cells in black, the arrows represent the resultant intercellular force for each cell and e) scatter plot in which blue circles correspond to normal cells and black circles to cancer cells.
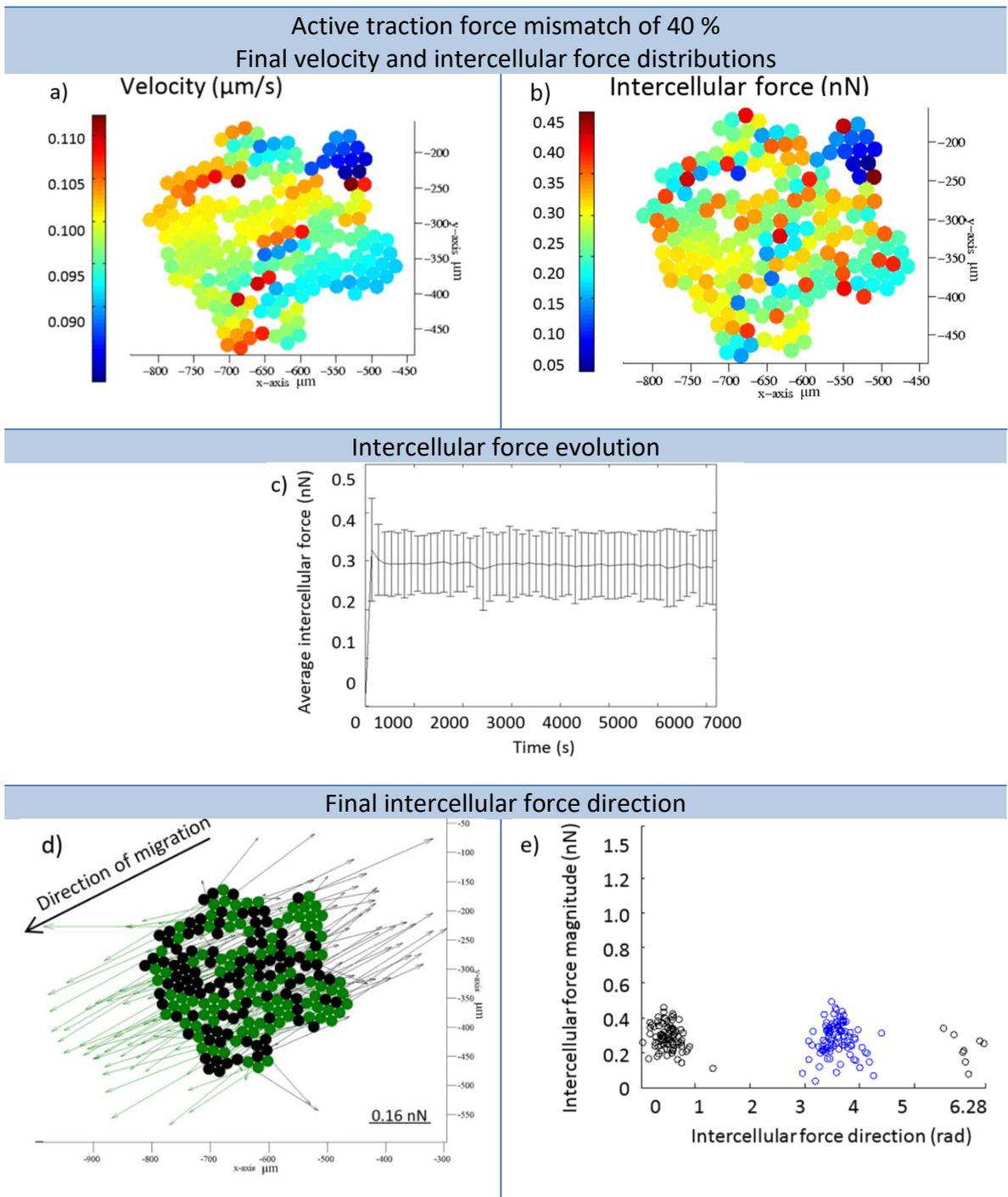
Figure 4.5. Final intercellular force and velocity for an active traction mismatch of 40%. a) Final velocity and b) intercellular force distributions: each cell is coloured according to velocity and force magnitudes respectively. c) Evolution of intercellular force, average for all the cells was computed and the associated standard deviation is shown. Intercellular force direction: d) normal cells in green and cancer cells in black, the arrows represent the resultant intercellular force for each cell and e) scatter plot in which blue circles correspond to normal cells and black circles to cancer cells.
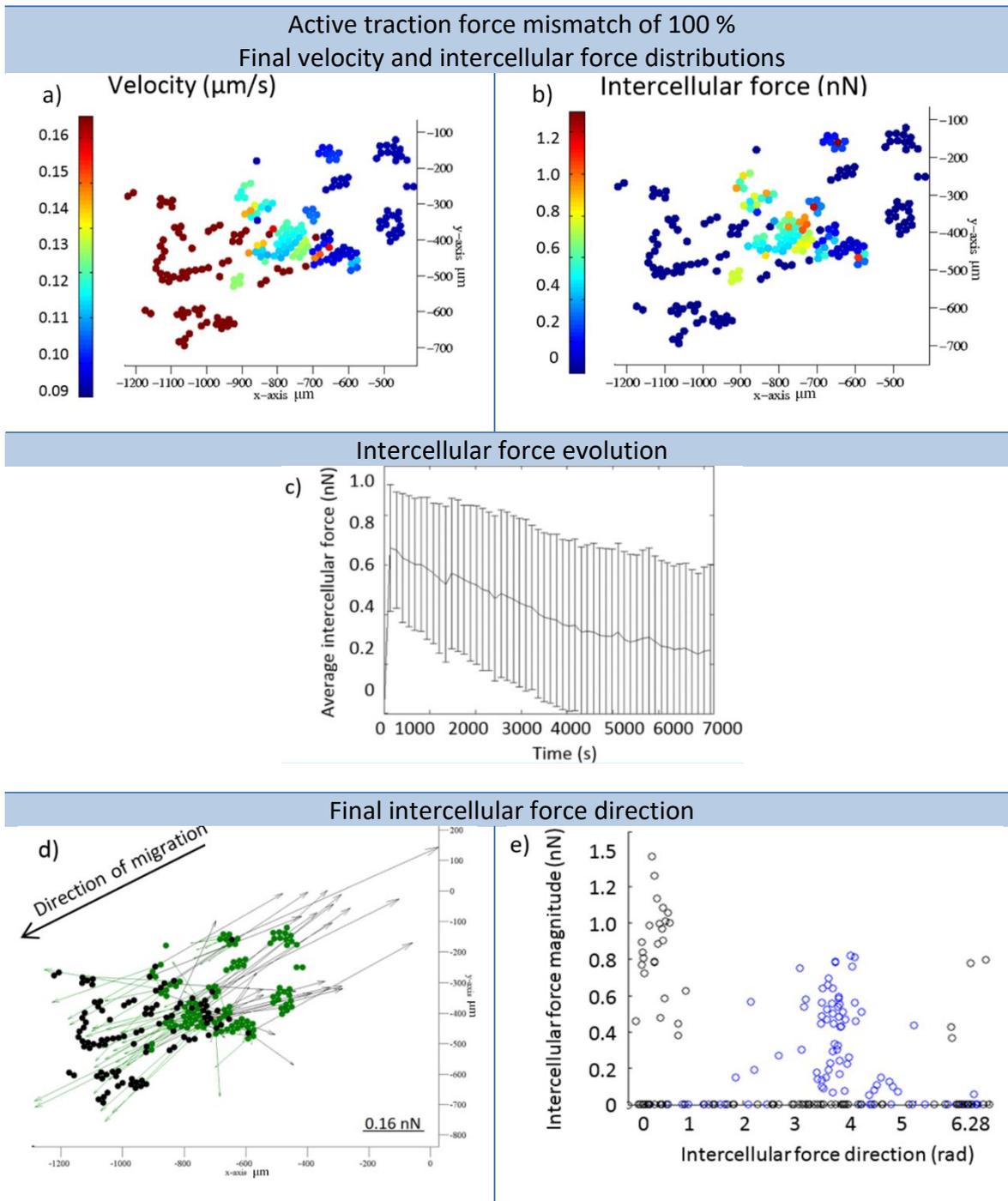
Figure 4.6. Final intercellular force and velocity for an active traction mismatch of 100%. a) Final velocity and b) intercellular force distributions: each cell is coloured according to velocity and force magnitudes respectively. c) Evolution of intercellular force, average for all the cells was computed and the associated standard deviation is shown. Intercellular force direction: d) normal cells in green and cancer cells in black, the arrows represent the resultant intercellular force for each cell and e) scatter plot in which blue circles correspond to normal cells and black circles to cancer cells.

4.4.2 Cell sorting based on absolute cell-cell adhesion

This section's aim is to explore the effect of the intercellular adhesion levels on cell sorting. Adhesion is considered to be the same between normal and cancer cells. However, different values are tested to understand the maximum adhesion leading to sorting of normal and cancer cells in co-culture. In section 4.4.1 it was found that sorting was higher for higher mismatch in the active forces of normal and cancer cells. Therefore, the high mismatch of 100% here considered maximizes the possibility of sorting.

In order to be able to find an accurate threshold for adhesion lower adhesion values were investigated. The coefficient of variation of the final sorting index was determined to quantify the variation in sorting with the absolute magnitude of cell-cell adhesion. A value of 26.8% was obtained for this coefficient.

Assuming the same adhesion between normal and cancer cells, the maximum adhesion possible for sorting in co-culture was found to be 0.1 nN/µm (Figure 4.7).
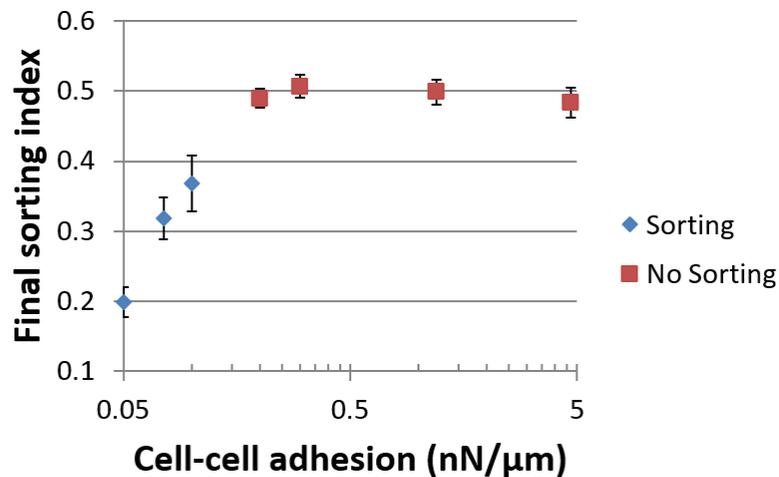
Figure 4.7. Sorting index after two hours of cell migration as a function of cell-cell adhesion. Normal and cancer cells have the same adhesion. Average and standard deviation of five seeding replicates.

4.4.3 Cell sorting based on different cell-cell adhesion

For bladder cell co-cultures the sorting index after two hours of migration varies 6% on average between seeding replicates of the same population and a maximum of 10%. For breast cell co-cultures it varies 7% on average and a maximum of 12%.

For the same adhesion difference, when comparing the higher normal cell adhesion scenario with the higher cancer cell adhesion scenario, sorting variations are in the same order of magnitude as the ones found between seeding replicates of the same population. For bladder cells the sorting index changes 7% on average and a maximum of 13% between both scenarios. On the other hand, for breast cells it varies 0.8% on average and a maximum of 1.3%. The smaller variation for breast cells is due to the fact that intercellular adhesion differences have less impact in the intercellular contact of cells with similar apparent Young's modulus.

For this reason, the sorting results of both adhesion scenarios were averaged. Sorting variations with the magnitude of the difference of adhesion are more relevant, $|\sigma_{cancer} - \sigma_{normal}|$ in Figure 4.8. The sorting variation with the adhesion difference is shown for bladder and breast cells. The coefficient of variation of the final sorting index was determined to quantify the variation in sorting with the difference of adhesion of normal and cancer cells. For bladder cells the sorting index changes 25.3% and for breast cells 20.3%. The adhesion difference values investigated were more refined for low magnitude to be able to find the threshold for sorting more accurately. A minimum difference of 1 nN/μm is required between the adhesion of normal and cancer bladder and breast cells for sorting to happen.
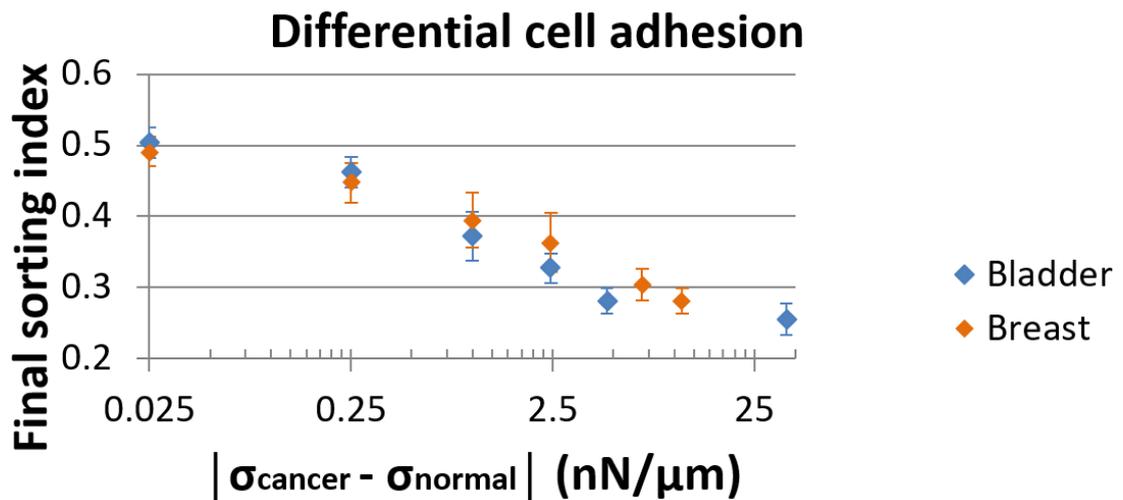
Figure 4.8. Sorting index after two hours of cell migration as a function of differential cell-cell adhesion. Higher normal cell adhesion and higher cancer cell adhesion scenarios were averaged. The standard deviation due to seeding replicates variation is shown.

In Chapter 3 cell stress was found to be related to cell-cell adhesion. For monolayers of cells with the same adhesion, it was found that maximum cell stress increases with the intercellular contact stiffness – section 3.4.2.3. When there is differential adhesion, for co-cultures, visible sorting was predicted within few hours after cell seeding – section 3.4.2.4. Sorting lead to lower levels of stress globally, but high stress was found locally for trapped cells, surrounded by cells of different type and not able to sort and for clusters of cells with high adhesion.

In the present study it was found that it is possible to find these cells in high state of stress after two hours of cell migration, see Figures 4.9 and 4.10. High compressive stress is observed for low adhesion cells that are surrounded by high adhesion cells. The high adhesion cells around them are in high level of tension. As an example, stress results are presented for bladder and breast cells with higher adhesion for normal cells than for cancer cells. High stress is locally found for cancer cells surrounded by normal cells. In addition, high stress is found for clusters of cells with high adhesion, the normal cells. Comparing breast and bladder stress levels, the ones associated with breast cultures are higher due to the lower mismatch in passive cell properties (lower levels of sorting between normal and cancer cells). Observing the stress evolution graphs in Figures 4.9 and 4.10 it is possible to see that normal cells are in tension, -6 Pa in average for breast

against -0.6 kPa for bladder, and cancer cells in compression, 5 Pa in average for breast against 0.6 Pa for bladder.

The main conclusion is that, since cell migration is not directly driven by stress levels but by traction and intercellular forces, it is possible to find high stress regions locally in a migrating co-culture.
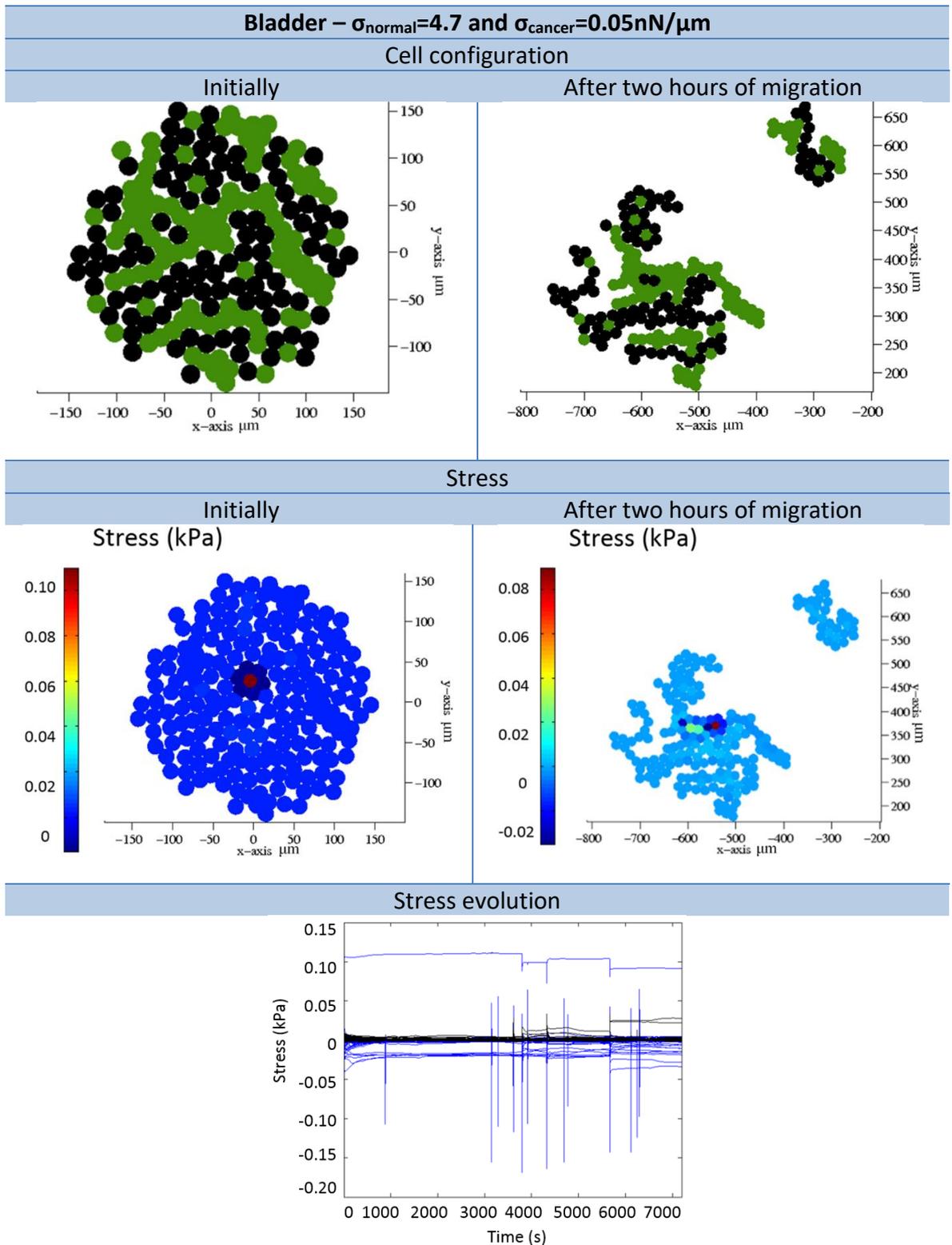
Figure 4.9. Stress results for bladder cells. Initial and final cell configurations and stress distributions. Stress evolution during the two hours of cell migration is also shown: each line corresponds to the evolution of stress for one cell, blue if normal and black if cancer cell.
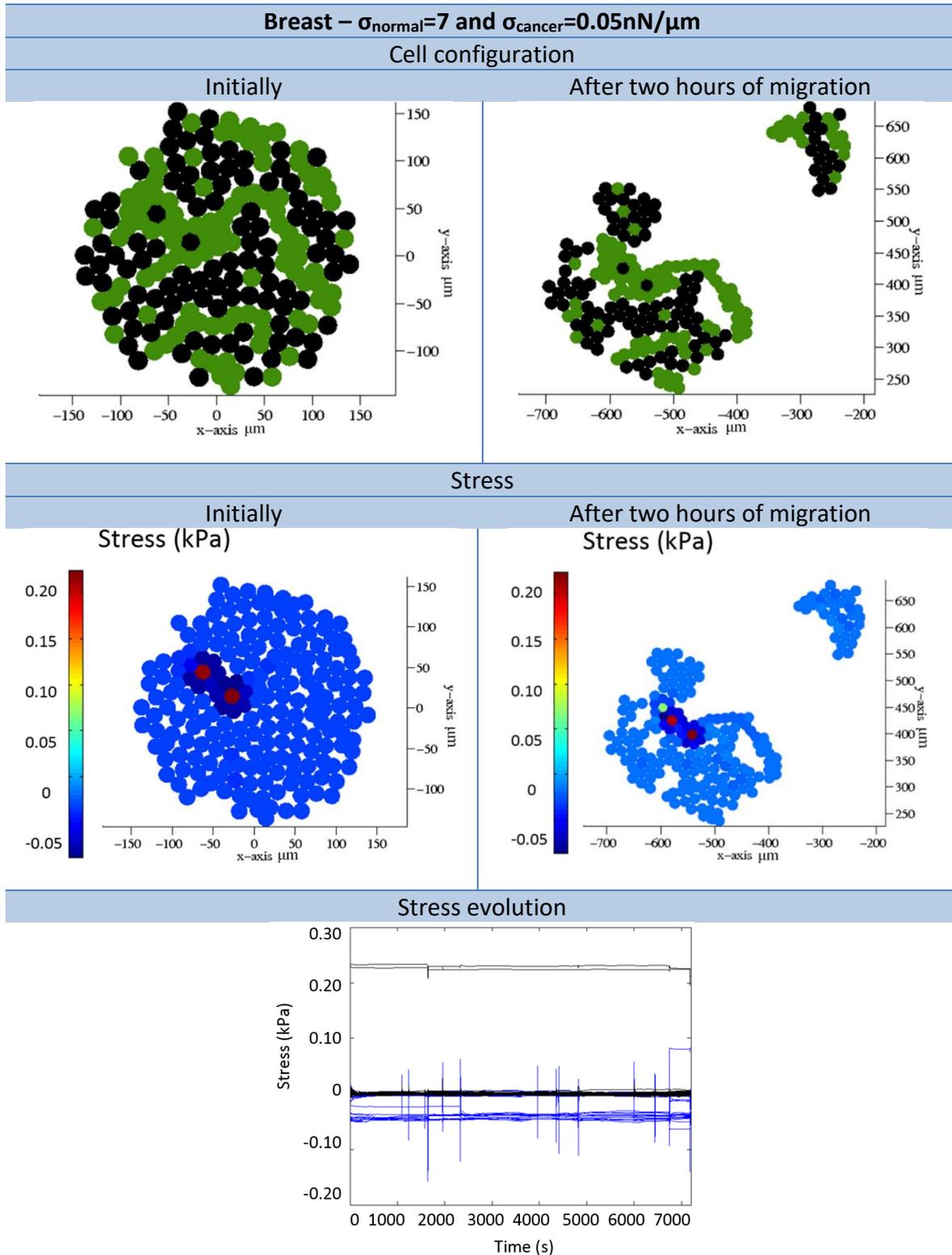
Figure 4.10. Stress results for breast cells. Initial and final cell configurations and stress distributions. Stress evolution during the two hours of cell migration is also shown: each line corresponds to the evolution of stress for one cell, blue if normal and black if cancer cell.

4.4.4 Cell sorting based on the combined effect of active traction force mismatch and different cell-cell adhesion

The minimum differential intercellular adhesion required for sorting tends to decrease with the increase in traction force mismatch, see Figures 4.11 and 4.12. The adhesion thresholds for 20 and 40% mismatch in traction force are equal for bladder and breast cells, 1 and 0.25 nN/μm. For 60% mismatch sorting happens for bladder cells for a differential adhesion with magnitude of 0.025 nN/μm (Figure 4.11). For breast cells a minimum differential adhesion of 0.25 nN/μm is required (Figure 4.12).
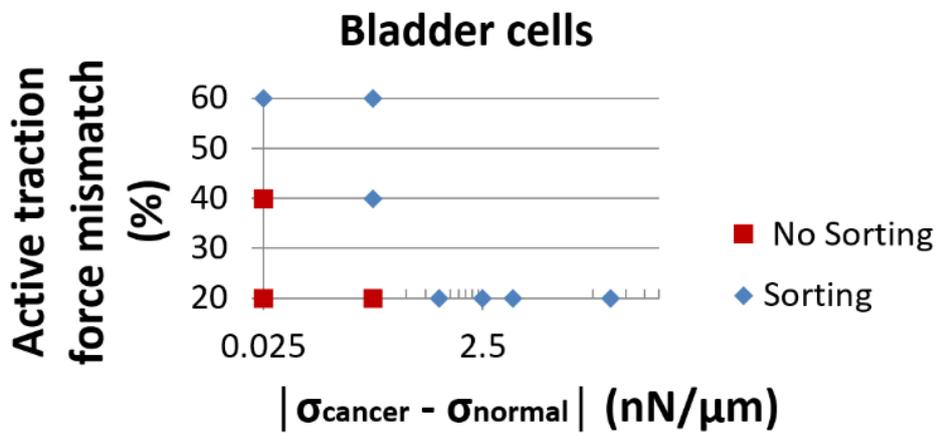
Figure 4.11. Sorting as a function of both active traction force mismatch and differential cell-cell adhesion for bladder cells.
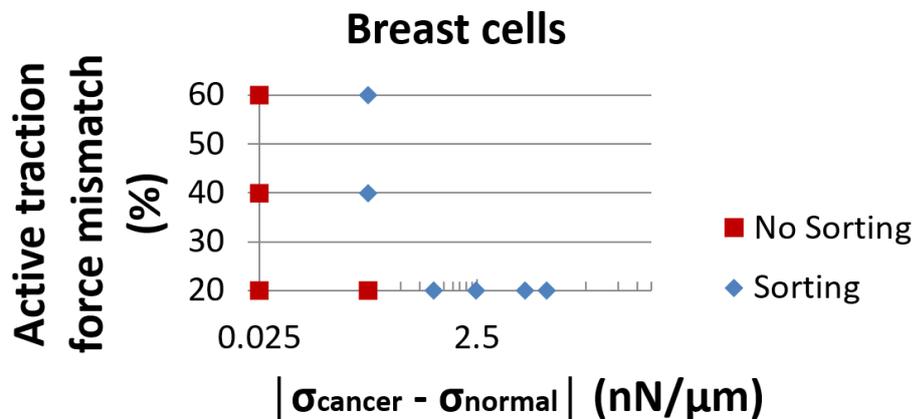
Figure 4.12. Sorting as a function of both active traction force mismatch and differential cell-cell adhesion for breast cells.

4.5 Discussion

4.5.1 Cell sorting based on different active traction

This work predicts the spontaneous sorting of normal and cancer cells in co-culture. This sorting is supported by experimental data from the literature [20], [129]. Cell sorting is quantified using the sorting index, which is lower for higher degrees of sorting between normal and cancer cells. In the beginning of cell migration computed sorting indexes were between 0.4 and 0.6 for cells with equal adhesion (Figure 4.1 in section 4.2.3), reflecting the randomness of the cell distribution. For this reason, in this work it was assumed that cell sorting happened significantly when the sorting index decreased to levels lower than 0.4 after two hours of cell migration. Even if cell sorting seems to develop continuously with the parameters studied (Figure 4.2), a limit was defined in order to be able to find quantitative thresholds for cell sorting.

This work proposes a linear evolution of the sorting index as normal and cancer cells sort. Other authors proposed power-laws for cell sorting with exponents between -0.18 and -0.22 [98], [103] and logarithmic functions [98], [99]. Although more data should be gathered, these results suggest that the temporal evolution of cell sorting should depend on the type of cells being studied.

It was found that sorting is higher for higher active traction mismatch, see Figure 4.3. A higher active traction mismatch requires higher intercellular forces between normal and cancer cells for the coordinated movement of the heterogeneous cluster. The fact that emergent intercellular forces between normal and cancer cells are proportional to the difference in active traction forces (Figures 4.4 and 4.5) shows that the sorting predicted by the model is directly related with this difference in traction. Since direction alignment is assumed, sorting happens when cells are not able to generate sufficiently high intercellular forces. This is further explored in the next sections by investigating the effect of cell-cell adhesion on cell sorting. A minimum active traction mismatch of 70%, correspondent with a traction force difference of 1nN, was found to be required for significant sorting between normal and cancer bladder cells in co-culture. To the authors knowledge this is the first time that spontaneous cell sorting in a normal/cancer cell co-culture was investigated as an emergent outcome of the mismatch found in traction

forces of normal and cancer cells in the experimental literature. This study shows that cell sorting can be driven by differences in cell motility and can happen in a co-culture of cells with equal intercellular adhesion. This was referred before by other authors [24], [98]. The present work complements the literature by defining sorting thresholds dependent on the range of values measured for parameters that characterize cell mechanics. The effect of cell adhesion on cell sorting is subject of sections 4.3.2. and 4.3.3.

4.5.2 Cell sorting based on absolute cell-cell adhesion

The results indicate that cell sorting between normal and cancer cells can happen without differential adhesion. All the cells are considered to adhere to each other to the same extent, whether the interaction is between two normal cells, two cancer cells or a normal and a cancer cell.

Under this condition it was found that sorting between normal and cancer bladder cells can happen as long as the intercellular adhesion energy has a value equal to or lower than 0.1 nN/μm, see Figure 4.7. To the author's knowledge, it is the first time that a threshold for sorting of normal and cancer cells was found for the same level of cell-cell adhesion.

As mentioned in section 4.5.1, cell sorting happens when intercellular cooperative forces are not enough to balance the traction force difference between normal and cancer cells. These intercellular forces emerge as a response to the traction difference but are dependent on the cell's passive properties, such as intercellular adhesion energy.

The effect of differential cell-cell adhesion will be investigated for both bladder and breast co-cultures inspired by the theory of Steinberg [21].

4.5.3 Cell sorting based on different cell-cell adhesion

Variations in the level of cell sorting were not found between the adhesion scenarios (higher adhesion for normal cells or higher adhesion for cancer cells). The relevant parameter is the difference in adhesion. Sorting is higher for higher adhesion difference, see Figure 4.8. It was found that a minimum difference of 1 nN/μm is required between

the adhesion of normal and cancer bladder and breast cells for a significant level of sorting to happen when there is minimum mismatch in traction of 20%.

These results are in agreement with the ones in Chapter 3 – section 3.4.2.4. It was reported that a higher mismatch in the passive properties, apparent Young's modulus and cell-cell adhesion, of normal and cancer cells could result in visual cell sorting within the first few hours after cell seeding, even without the onset of active cell migration. The higher mismatch in the passive properties of normal and cancer bladder cells explains the higher level of sorting observed for this cell type (Figure 4.8). Sorting decreases the level of cell stress and trapped cells are associated with regions of high local stress, see Figures 4.9 and 4.10. The present study complements the previous results by showing that it is still possible to find regions in a migrating monolayer with high stress levels, higher than the stress of the majority of the cells in two to three orders of magnitude. This is possible because cell migration is not assumed to be directly governed by the level of stress. In reality, it is possible that cells are able to remodel and change properties such as their traction force in response to high stress levels [132].

As mentioned in Chapter 3, tissue surface tension values were used in this work as a measure of intercellular adhesion energy. It is assumed that these are related to the expression levels of molecules that intermediate cell adhesion, such as cadherins. This follows from the Differential Adhesion Hypothesis (DAH) proposed by Steinberg [133]. The theory suggests that two tissues segregate due to differences in their surface tension. In particular, that the tissue with lower surface tension envelops the one with higher surface tension [133]. The developed model in this work is not able to reproduce this enveloping behaviour. One possible explanation is that cell migration is not considered to be driven by an effective energy that depends solely on cell-cell adhesion [94]. It is driven by active traction and an intercellular force resultant. These depend on cell traction, Young's modulus, adhesion and intercellular contacts between the cell and neighbouring cells. However, in agreement with Steinberg's theory, the proposed model does show that cell sorting depends on differential cell-cell adhesion.

4.5.4 Cell sorting based on the combined effect of active traction force mismatch and different cell-cell adhesion

In section 4.4.1 it was found that a minimum active traction force mismatch of 70% is required for sorting when cell adhesion levels are minimum and there is no differential adhesion. In addition, in section 4.4.3 it was found that a minimum difference of 1nN/μm between the adhesion of normal-normal and cancer-cancer cells was required for sorting with minimum active traction force mismatch. Cell sorting depends on both the mismatch between the traction force of normal and cancer cells and differences in intercellular adhesion. This combined effect is explored in the present section.

The difference of adhesion between normal and cancer cells leading to sorting depends on the traction mismatch. The higher the traction mismatch the lower the adhesion difference required for sorting tends to be, see Figures 4.11 and 4.12.

The thresholds for sorting are the same for bladder and breast cells. An exception is found for an active traction mismatch of 60%, for which breast cells require a higher adhesion difference, 0.25 nN/μm (Figure 4.12), than bladder cells, 0.025 nN/μm (Figure 4.11), to sort. This is due to the fact that normal and cancer breast cells have more similar apparent Young's modulus, 2.3 and 1.2 kPa, than normal and cancer bladder cells, 10 and 0.3 kPa.

The fact that sorting thresholds depend on both the active traction force mismatch and cell-cell adhesion suggests that it is their relation that is behind cell sorting. The present Chapter 4 complements Chapter 3 by showing that both passive and active cell properties influence the sorting of a migrating monolayer. Intercellular forces that depend on passive cell properties are developed in response to an active traction force mismatch. This is further explored in section 4.5.5.

4.5.5 Integrated perspective on cell sorting

The influence of several parameters on the sorting of normal and cancer cells in co-culture was quantified computing the coefficient of variation of the metric quantifying cell sorting, the sorting index, (Eq. 4.3). Sorting was more influenced by differences in the traction of normal and cancer cells (27.2%) and absolute cell-cell adhesion levels

(26.8%), followed by different adhesion of normal and cancer cells (25.3% for bladder and 20.3% for breast cells). The fact that cell sorting is possible in all these scenarios suggests a common underlying mechanism.

The mechanism proposed is that intercellular forces emerge in a culture in response to a mismatch in the passive and/or active properties of cells. Sorting is possible in the first few hours after seeding for high mismatch in the passive cell properties, Young's modulus and intercellular adhesion, Chapter 3 - section 3.4.2.4. The traction forces exerted later by cells can also drive cell sorting. A traction mismatch leads to the emergence of intercellular forces that make the coordinated movement of the heterogeneous cluster possible. If cells are not able to generate such forces, due to their passive properties, then sorting occurs. This complements the Differential Adhesion Hypothesis (DAH) that, using an analogy between cells and fluids, suggests that cell sorting can be uniquely governed by passive cell properties.

The model predicts that cell sorting can be driven by differences in the mechanical properties of individual cells. This prediction is in agreement with the computational work of Brodland et al [42]. They suggested that cancer cells need to be mechanically different from their neighbours and have an appropriate surface tension for individual cancer cells to sort from the primary tumour in metastasis. The model developed in this work complements the work of Brodland et al by considering mechanical properties of normal and cancer cells derived from experimental measurements.

Pawlizak et al. [127] also suggests a new theory with the potential to unify diverse factors that are thought to influence collective cell migration independently such as cell-cell adhesion, cell motility and cell density [134], [135]. The theory is based on cell jamming. In analogy with phase transitions in physics, it postulates that a cell monolayer can undergo a transition from a jammed solid-like state, in which cells have restricted movement, to an unjammed liquid-like state, in which cells can rearrange and ultimately dissociate from the others. According to this idea mesoscopic events, between the tissue and cell scales, should be regarded as due to long-range force transmission. Supporting the theory, complex force fields, heterogeneous and dynamic, have been measured for cell populations [33].

Individual-based models such as the one developed in this work arise as an interesting tool to investigate this theory. Forces at the cell scale can lead to emergence at the higher population scale, enabling the investigation of collective behaviour. The model proposed can bridge two scales by predicting how intercellular forces and stresses are distributed in a cell population based on local cell parameters. In the future, it would be interesting to model more cells and in a confined space, as did Mones et al. [136]. In comparison with the model developed by Mones et al., this model would additionally account for cell mechanics. Thereby, the model would generate integrative understanding of collective cell behaviour by exploring the relative roles of cell-cell adhesion, cell traction and cell density.

4.5.6 Discussion of model validation

In this work single cell velocity values were taken from the literature and converted in active force values. It was considered that the velocity at which adherent cells migrate is proportional to the magnitude of the force they exert on their substrate. This assumption disregards the fact that cell velocity can also depend on the properties of the cell substrate and on the dynamics of focal adhesions, the cell's ability to disassemble and reassemble the cell-substrate contacts. In addition, the Stoke's law [130] supposes the following:

- the cell drag can be approximated by the drag for a sphere with a radius of 10 μm,
- the extracellular environment has a viscosity of 0.1 kPa.s,
- the extracellular fluid flow is laminar,
- cells, or spheres, do not interfere with each other.

Since active force is considered as a proxy to traction force, the active force magnitudes considered can be compared with the ones that have been experimentally measured for traction forces. Maximum active forces on the order of 1-3 nN were considered in this work, associated to active velocities of 5-10 μm/min. The assumptions above seem to be acceptable as traction forces on the same order of magnitude have been measured at the leading edge of single cells, 2-3 nN [18]. For monolayers, magnitudes of 2 nN [18]

and 5nN have been measured for cells in the centre [137] and higher magnitudes of 12 nN [137] and 40 nN [18] for cells at the monolayer edge. Therefore the active forces considered seem to be in the same order of magnitude as the forces measured for cells belonging to a cell monolayer.

The maximum magnitude predicted for intercellular forces in this work is similar to that of active forces, order of the units of nN. Experimentally values one order of magnitude higher, of 20 nN for forces at focal adhesion of fibroblasts [138] and 40 nN between endothelial cells [139] have been reported.

Visually, extensive cell separation is predicted by the model in some cases that does not seem to correlate with *in-vitro* sorting experiments, for example for Figure 4.6 – active traction force mismatch of 100%. Several reasons can explain this disagreement.

In *in-vitro* sorting experiments homogenous cell clusters are formed within an initially mixed and confluent monolayer of cells. Cells seem to change their migration direction randomly and continuously, easily finding others of the same type, since they are confluent, and forming homogenous clusters, see Figure 2.6 in Chapter 2 [102]. However, in *in-vitro* collective cell migration experiments cell movement is normally not confined as extra space is required for the monolayer migration, see Figure 2.1 in Chapter 2 [33].

Following the latter approach, confluency was not replicated in this work as cell migration was not confined. In addition, a random component was not considered. Since randomness can influence the establishment of new cell-cell contacts, this fact possibly limits the extent to which cells can sort. Furthermore, a small number of cells (200) was modelled when comparing with real experiments. The higher the cell number the more complicated cell rearrangements become possibly making cell sorting more difficult. The number of cells modelled was chosen in the interest of computational time and, nonetheless, allowed the development of mechanistic hypotheses for collective cell migration and sorting. Furthermore, although it was considered that cells adapt the direction of their traction according to the one of neighbouring cells (Eq. 4.1), the traction magnitude was assumed to be constant. Therefore, the model is not able to fully replicate the dynamics of the observed phenomenon of Contact Inhibition of Locomotion (CIL). CIL refers to the changes in cell migration after cell-cell collision. In

particular, it refers to the cessation of movement in the direction of cell-cell contact and the repolarization towards the opposite direction [140]. In order to account for this time-dependent multifaceted behaviour, changes in both direction and magnitude of cell traction would have to be considered following the establishment of cell-cell contact. It is probable that, in reality, cells remodel, changing their traction properties when in contact with other cells. Therefore, not only cell traction but also Young's modulus and cell-cell adhesion are parameters that can potentially have different values when a cell is in isolation or within a monolayer. A binary distribution of cells was considered which means that 50% of the cells, the cancerous, were assigned higher traction force than the other 50%, the normal. It has been shown that the relative percentage of cells of different type in co-culture affects their sorting [36]. Different distributions, for example exponential [16], have been proposed to explain the heterogeneity of the traction forces measured in the case of monocultures. Ideally, to investigate collective behaviour the values incorporated in the model should be measured for cells within a monolayer. This is dependent on the available literature for the cell type studied, measurement techniques and technology development. In Chapter 5 the intra-population variability of cell mechanical properties is accounted for.

4.6 Conclusion

A computational model of collective cell migration developed based on passive intercellular forces (Chapter 3) was extended to include active migratory forces exerted by cells. The model was applied to normal and cancer cells in co-culture. Spontaneous sorting between normal and cancer cells was predicted based on individual cell mechanical parameters. Quantitative thresholds were defined for sorting which was primary driven by differences in the traction of normal and cancer cells and absolute cell-cell adhesion levels, followed by the differential adhesion of normal and cancer cells. The results supported an integrated mechanical mechanism for cell sorting.

It is now widely accepted that cell and tissue mechanics affects their physiology and that several diseases are related with changes in mechanics. Therefore, mechanistic understanding on how cell and tissue mechanics can be changed by drug treatments is

required. A recent review suggests the word mechanopharmacology to be used to highlight the relevance of biomechanics in drug development [141]. Complementing *in-vitro* experiments, *in-silico* mechanical models such as the one developed can be used as platforms for the testing of novel medicines, part of the Chapter 5 of this thesis.

Chapter 5 - Modelling the migration of mechanically heterogeneous cell populations

Summary

A population of cells is, by itself, a complex heterogeneous system, even if the cells belong to the same type. Cell heterogeneity is, in particular, a hallmark of cancer, representing a challenge to the disease treatment. There is heterogeneity between cells of different tumours but also within the same tumour.

The mechanistic and quantitative computational model developed in this work was used to investigate the role of mechanical heterogeneity in the migration of normal and cancer cell populations. Mechanically different normal and cancer cells were virtually cultured in mono and co-culture scenarios to investigate their collective migration. In addition, the effect of chemotherapeutic microtubule stabilizers was explored showing the potential of the model to act as a platform for the testing of anti-cancer drugs. Microtubule stabilizers are used to induce mitotic arrest but have been found to induce changes in the mechanical properties of cells. These changes have been incorporated in the model.

The results suggest that heterogeneity in single cell mechanics contributes to the plasticity of migration of cancer cell populations. The changes in cell mechanics promoted by microtubule stabilizers lead to changes in the collective migration of normal and cancer cells in co-culture. Since cancer metastasis is associated with changes in cell migration, this work suggests that the mechanical changes induced by microtubule stabilizers may contribute to their therapeutic effect in inhibiting metastasis.

5.1 Introduction

Heterogeneity in a population of cells of the same type can be due to factors intrinsic to the cells or extrinsic, driven by the microenvironment [142]. Intrinsic variability can be related with genetic variation in the form of mutations. On the other hand, extrinsic variability can take the form of phenotypic variations promoted by the interaction with other cells or the extracellular environment. Intrinsic and extrinsic factors cooperate for the cells' adaption and function. Therefore, a cell population is a complex dynamic

biological system in which there is a bi-directional cross-talk between heterogeneous cells and between them and their microenvironments. The behaviour of a cell population emerges from the collective and is not possible to predict from the behaviour of an individual cell.

In cancer, cell heterogeneity exists in the form of both genetic and phenotypic variation between different tumours, but also within the same tumour [143]. Tumour heterogeneity poses a challenge to drug development as the mechanisms in its origin and their clinical impact are to be fully understood [35].

Heterogeneity in a population of cells can be due to variation in cell mechanical properties, the subject of this work. Supporting this idea, heterogeneous fields have been measured for the traction forces exerted by populations of adherent epithelial cells in *in-vitro* culture [18], [137]. In addition, atomic force indentation results reported by Guo et al [32] suggest that intercellular interactions in a cell monolayer impact the Young's modulus of the individual cells. There is also evidence of heterogeneity in cell stiffness within tumours. Atomic force microscopy results obtained for breast [27] and for bladder cells [29] confirm this.

It was shown that microtubule stabilizers used for cancer treatment affect the mechanical properties of cells. An example is Paclitaxel, a commercially available chemotherapeutic drug used to treat several types of cancer, including breast [144] and bladder [145]. Ren et al [36] reported a 150% increase in the Young's modulus of lymphoma cells and Kraning-Rush et al [37] reported a 63% decrease in the traction forces exerted by breast cancer cells induced by Paclitaxel. Microtubule stabilizers stabilize the microtubules of the cytoskeleton against depolymerisation, thereby affecting the dynamics that is required for cell division and inducing mitotic arrest [146]. They aim to target the uncontrolled division characteristic of cancer cells. However, besides having a role in cell division, the cell's cytoskeleton has an important role in determining the mechanical properties of cells and in cell migration. Both changes in cell mechanical properties and cell migration have been associated with cancer [147].

The role of mechanics in the collective migration of mechanically heterogeneous cell populations is not understood. Neither is the impact of the mechanical changes induced by chemotherapeutic microtubule stabilizers.

In this Chapter a mechanistic and quantitative cell-based computational model is applied to mechanically heterogeneous cell populations from the bladder and the breast tissues. The mechanics of migration of heterogeneous cell populations is investigated in both monoculture and co-culture scenarios. Co-culture of normal and cancer cells is studied as a surrogate for tumour-host mechanical interactions. The influence of the mechanical changes induced by microtubule stabilizers on the migration of the cell collective is studied to investigate their potential contribution to metastasis treatment. The scientific questions that this chapter addresses are:

- What is the role of single cell mechanics in the migration of heterogeneous cell monocultures?
- What is the role of single cell mechanics in the migration of heterogeneous normal and cancer cell co-cultures?
- What is the impact of the changes in single cell mechanics induced by chemotherapeutic microtubule stabilizers in the mechanics of cancer migration?

5.2 General methods

5.2.1 Model description

In this Chapter the role of single cell mechanics in the collective migration of heterogeneous cell populations from the bladder and the breast tissues is investigated. Cell migration is modelled as described in Chapter 4 – section 4.2.1.

5.2.2 Model parameters

The values considered for the apparent Young's modulus of bladder and breast cells of a population followed a Gaussian distribution based on AFM measurements from the literature for the bladder [29] and the breast [27]. In these experiments 20 bladder cells and 30 breast cells from the same tissue section were indented several times. A model of contact mechanics was fitted to each force curve obtained in order to compute the Young's modulus. A Gaussian distribution was then fitted to the histogram of all the values of Young's modulus measured for all the cells.

Intercellular adhesion energy values were varied within the valid range found in Chapter 3 – section 3.3.2.2 according to cell volume restrictions. It was assumed that intercellular adhesion varies in a cell population following a Gaussian distribution with minimum and maximum values of 0.05 and 4.7 nN/μm for bladder normal cells, 0.05 and 19 nN/μm for bladder cancer cells, 0.05 and 6 nN/μm for breast normal cells and 0.05 and 7.5 nN/μm for breast cancer cells.

Saez et al [137] measured the traction forces exerted by assemblies of MDCK epithelial cells using micro pillar substrates. Maximum forces of 12 nN were reported for cells at the edge of the cluster on a substrate with micro pillars with spring constant of 23 nN/μm. Based on this observation, in this work the active traction force of normal cells was considered to achieve a maximum value of 12 nN. The active traction force of cancer cells was considered to reach a maximum value of 24 nN, according to the 100% maximum traction mismatch found between single normal and cancer cells of the same tissue [31]. Active traction forces in cell populations followed a distribution with shape as in Figure 5.1, in agreement with the distributions found in several works [18], [137], [148].
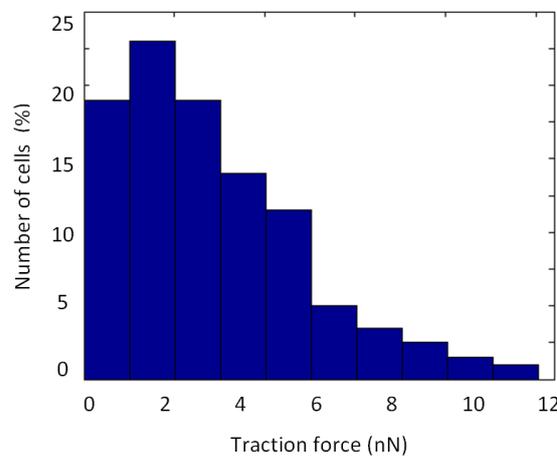
Figure 5.1. Traction force histogram for a population of 200 normal cells.

Since the traction force distribution is not normal, median and interquartile range were the measures considered for central tendency and statistical dispersion, respectively, throughout the Chapter. The interquartile range defines the region where the 50% central values reside. The median and interquartile range for Young's modulus, traction

force and cell-cell adhesion distributions for bladder and breast normal and cancer cell populations are presented in Tables 5.1 and 5.2.

Table 5.1 – Mechanical properties for bladder cell monocultures.

Input parameters	Bladder monocultures	
	Normal	**Cancer**
	Median (Interquartile Range)	Median (Interquartile Range)
Young's modulus (E, kPa)	10 (5.0)	0.3 (0.2)
Traction force (nN)	3.0 (3.5)	6.1 (7.1)
Cell-cell adhesion (nN/μm)	2.3 (1.0)	9.5 (5.2)

Table 5.2– Mechanical properties for breast cell monocultures.

Input parameters	Breast monocultures	
	Normal	**Cancer**
	Median (Interquartile Range)	Median (Interquartile Range)
Young's modulus (E, kPa)	2.2 (0.8)	1.2 (0.6)
Traction force (nN)	3.0 (3.5)	6.1 (7.1)
Cell-cell adhesion (nN/μm)	3.0 (1.4)	3.6 (1.9)

Mechanical properties from the parameter distributions were randomly assigned to cells in both monoculture and co-culture scenarios. The effect of microtubule stabilizers was considered by increasing the Young's modulus of cancer cells in 150% [36] and decreasing their active traction force in 63% [37].

5.3 Simulations

Cell migration was modelled synchronously for two hours of real time in an unconfined environment. Five seeding replicates were investigated per cell population. Heterogeneous populations of 200 cells were studied from both the bladder and breast tissues in both monoculture and co-culture scenarios. The effect of chemotherapeutic

microtubule stabilizers in the migration of normal and cancer cell co-cultures was modelled considering the induced change in cell mechanical properties reported for Paclitaxel. Intercellular forces, cell velocity and sorting index were all measured at the end of the two hours.

5.3.1. Migration of monocultures accounting for intra-population heterogeneity

The aim of this section was to investigate the mechanics of migration of cells in monoculture accounting for intra-population heterogeneity. Bladder and breast normal and cancer cell monocultures with properties in Tables 5.1 and 5.2 were studied.

5.3.2. Migration of co-cultures accounting for intra-population heterogeneity

In this section the migration of bladder and breast co-cultures composed of 50% normal and 50% cancer cells was investigated accounting for intra-population heterogeneity. The mechanical parameters of normal and cancer cells followed once more distributions with properties in Tables 5.1 and 5.2. The median and interquartile range of the mechanical parameters for all the cells of the co-culture, 100 normal and 100 cancer cells, are presented in Table 5.3.

Table 5.3 – Mechanical properties for co-cultures.

Input parameters	Co-cultures	
	Bladder	**Breast**
	Median (Interquartile Range)	Median (Interquartile Range)
Young's modulus (E, kPa)	0.7 (9.8)	1.7 (1.2)
Traction force (nN)	4.4 (6.4)	4.4 (6.4)
Cell-cell adhesion (nN/µm)	3.6 (7.3)	3.3 (1.7)

5.3.3. *In-silico* drug test on the migration of co-cultures

The possible effect of the commercially available microtubule stabilizer Paclitaxel on the collective migration of bladder normal and cancer cells in co-culture was investigated. The Young's modulus and traction force of cancer cells were modified to simulate treatment with the drug, Table 5.4.

Table 5.4 – Mechanical properties for bladder co-cultures without and with paclitaxel.

Input parameters	Effect of paclitaxel on co-culture	
	Bladder – Control	**Bladder - Paclitaxel**
	Median (Interquartile Range)	Median (Interquartile Range)
Young's modulus (E, kPa)	0.7 (9.8)	1.9 (9.3)
Traction force (nN)	4.4 (6.4)	2.8 (3.8)
Cell-cell adhesion (nN/μm)	3.6 (7.3)	3.6 (7.3)

5.4 Results

5.4.1. Migration of monocultures accounting for cell heterogeneity

Tables 5.5 and 5.6 present the median and interquartile range of the velocity and intercellular force distributions for bladder and breast cell populations, respectively. The results correspond to the average of the several seeding replicates. The boxplots in Figure 5.2 complement these results by showing the inter-replicate variation.

The median velocity for normal cell monocultures is 1.9×10^{-1} μm/s (11 μm/min), see Tables 5.5 and 5.6 and Figure 5.2. For cancer cell monocultures it is two times higher, regardless of the type of tissue. The same happens to the median intercellular force, it reaches 1.9 nN for normal cell monocultures and the double for cancer cell monocultures.

Intercellular force has an interquartile range of 1.9 nN for a normal monoculture and two times higher in a cancer monoculture, regardless of the type of tissue. In average, the velocity interquartile range is on the order of magnitude of 10^{-3} μm/s for normal cell and one order of magnitude higher for cancer cell monocultures, Tables 5.5 and 5.6. However, when considering the inter-replicate variation (Figure 5.2), it is possible to

observe that the velocity interquartile range is very dependent on the seeding for cancer cell monocultures. Its order of magnitude is of 10^{-2} µm/s in average but it ranges between 10^{-3} and 10^{-1} µm/s. In other words, the spatial distribution of mechanical properties of cancer cells in monoculture, different for different seeding replicates, significantly changes the cell velocity distribution.

Table 5.5 – Median and interquartile range of velocity and intercellular force distributions for bladder monocultures. The results correspond to the average of five seeding replicates.

	Bladder cell monocultures			
	Normal		**Cancer**	
	Median	Interquartile range	Median	Interquartile range
Velocity (µm/s)	1.9×10^{-1}	5.1×10^{-3}	3.6×10^{-1}	8.0×10^{-2}
Intercellular force (nN)	1.9	1.9	3.4	3.8

Table 5.6 – Median and interquartile range of velocity and intercellular force distributions for breast monocultures. The results correspond to the average of five seeding replicates.

	Breast cell monocultures			
	Normal		**Cancer**	
	Median	Interquartile range	Median	Interquartile range
Velocity (µm/s)	1.9×10^{-1}	3.8×10^{-3}	3.7×10^{-1}	3.6×10^{-2}
Intercellular force (nN)	1.9	1.9	3.7	3.7

Figures 5.3 and 5.4 show cell distributions after migration for equivalent seeding replicates of breast normal and cancer cell monocultures, respectively. Different seeding replicates of the same breast cancer cell population can have different collective migration mechanisms. Cluster formation of the type found for seeding replicate 3 and finger-like protrusions as found for seeding replicate 5 only happen for cancer cell populations. This explains the higher interquartile range found for the velocity of cancer

populations, when comparing to normal cell populations. For cancer the interquartile range was of 1.3×10^{-1} µm/s for seeding replicate 3, third cancer replicate in Figure 5.2 b), and 3.0×10^{-2} µm/s for replicate 5, fifth cancer replicate in Figure 5.2 b). For normal cell populations, the value of 5.0×10^{-3} µm/s was obtained for seeding replicate 3 and 7.0×10^{-3} µm/s for replicate 5. The red crosses in the boxplots of Figure 5.2 refer to outliers. Although there is higher velocity variability for seeding replicate 3 of the breast cancer monoculture, see Figure 5.2 b), there are no velocity outliers since cells did not sort individually. In fact, there are few outliers in velocity in general, as cells tend to migrate in clusters. The outliers in intercellular force correspond to cells with high active traction force, see Figure 5.4 c), in the extreme of the traction distribution (Figure 5.1).
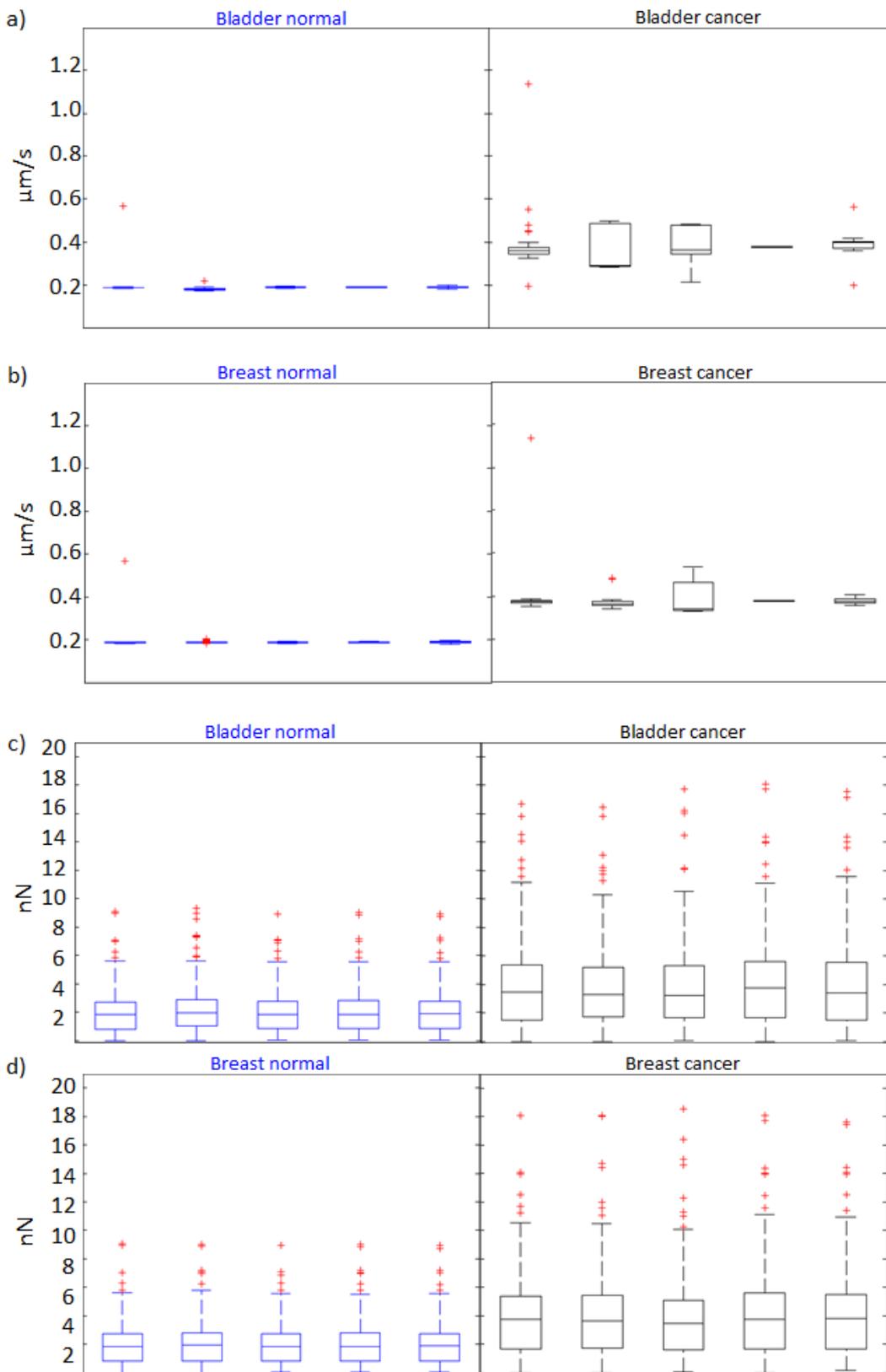
Figure 5.2. Velocity, a) and b), and intercellular force, c) and d), box plots for bladder and breast monocultures. Outliers are in red. Five seeding replicates were considered per monoculture.
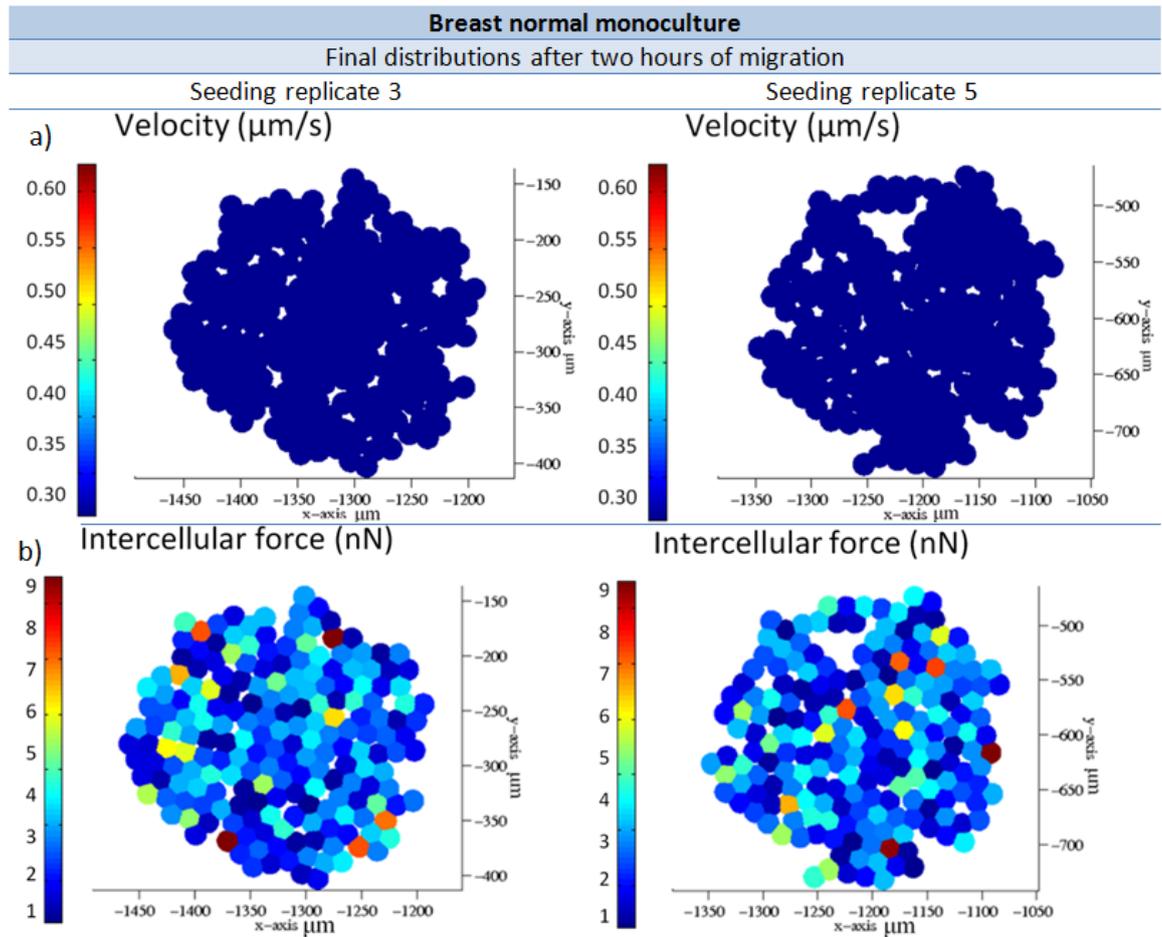
Figure 5.3. Final distribution of a) velocity and b) intercellular force for two seeding replicates of the breast normal monoculture.
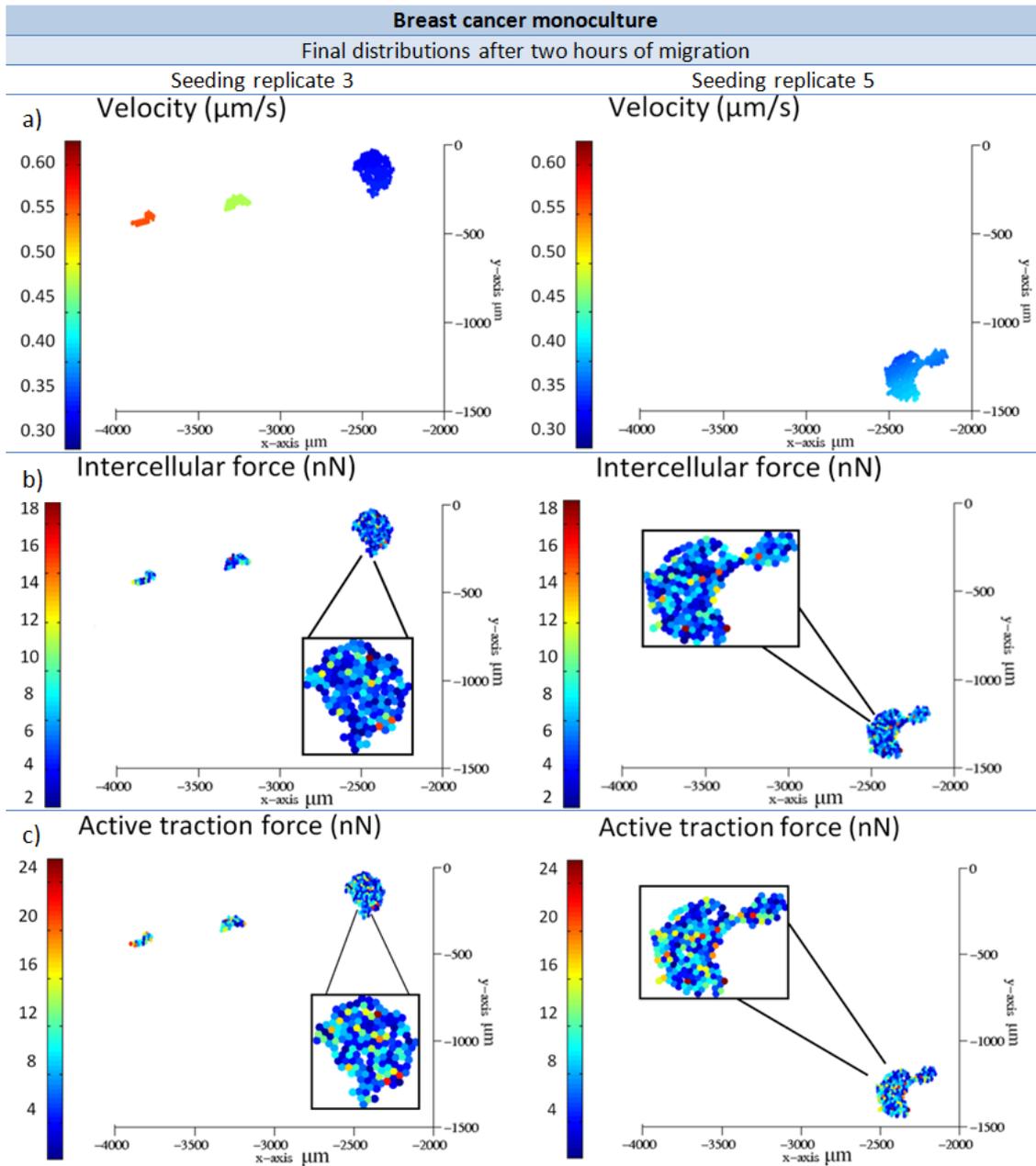
Figure 5.4. Final distribution of a) velocity, b) intercellular force and c) active traction force for two seeding replicates of the breast cancer monoculture.

5.4.2. Migration of co-cultures accounting for cell heterogeneity

Averaging the results from the several replicates, the median velocity found for co-cultures was on the order of magnitude of 3.0×10^{-1} μm/s (18 μm/min), Table 5.7. The interquartile range of the velocity distribution for both bladder and breast co-cultures is on the order of magnitude of 10^{-2} μm/s in average. However, when considering the

variation between replicates (Figure 5.5), it is possible to observe that the order of magnitude of the velocity interquartile range for breast co-cultures varies greatly. This was also observed for cancer cell monocultures (Figure 5.2). The velocity interquartile range is generally lower for breast co-cultures, order of magnitude of 10^{-3} μm/s, than for bladder co-cultures. However, seeding replicate 3 is an exception with an interquartile range on the order of 10^{-1} μm/s, third breast replicate in Figure 5.5 a).

Table 5.7 – Median and interquartile range of velocity and intercellular force distributions for bladder and breast co-cultures. The results correspond to the average of five seeding replicates.

| | Co-cultures | | | |
| | Bladder | | Breast | |
	Median	Interquartile range	Median	Interquartile range
Velocity (μm/s)	2.7×10^{-1}	3.2×10^{-2}	3.1×10^{-1}	4.3×10^{-2}
Intercellular force (nN)	2.6	2.8	3.3	3.1
Sorting Index (SI)	0.14	0.43	0.47	0.35

The sorting of normal and cancer cells is characterized by computed Sorting Indexes lower than 0.4 after two hours of cell migration (Chapter 4, section 4.2.3). Normal and cancer bladder cells in co-culture sort, Sorting Index (SI) with median of 0.14 - Table 5.7. On the contrary, sorting between normal and cancer breast cells in co-culture does not tend to happen, median Sorting Index of 0.47 in average. Sorting happened, nonetheless, for one of the five seeding replicates – seeding replicate 3 (median SI=0.3) in Figures 5.6 and 5.7. Normal and cancer cells breast cells migrate as different clusters at different velocities for seeding replicate 3, see Figure 5.7 a). For seeding replicate 5 there was no sorting between normal and cancer cells (median SI=0.5). One cluster of cells segregates from the main population resulting in a velocity outlier, see Figure 5.5 a). Intercellular forces are similar for both replicates, see Figure 5.5 b) and Figure 5.7 b).

The sorting of individual bladder normal and cancer cells in co-culture explains the high number of outliers in velocity when compared to breast cell co-cultures (Figure 5.5). Regarding intercellular force, it is higher for breast, median of 3.3 nN, than for bladder cell co-cultures, median of 2.6 nN - Table 5.7. In addition, it also varies more for the former, 3.1 against 2.8 nN. Intercellular forces decrease due to sorting in bladder cell co-cultures.
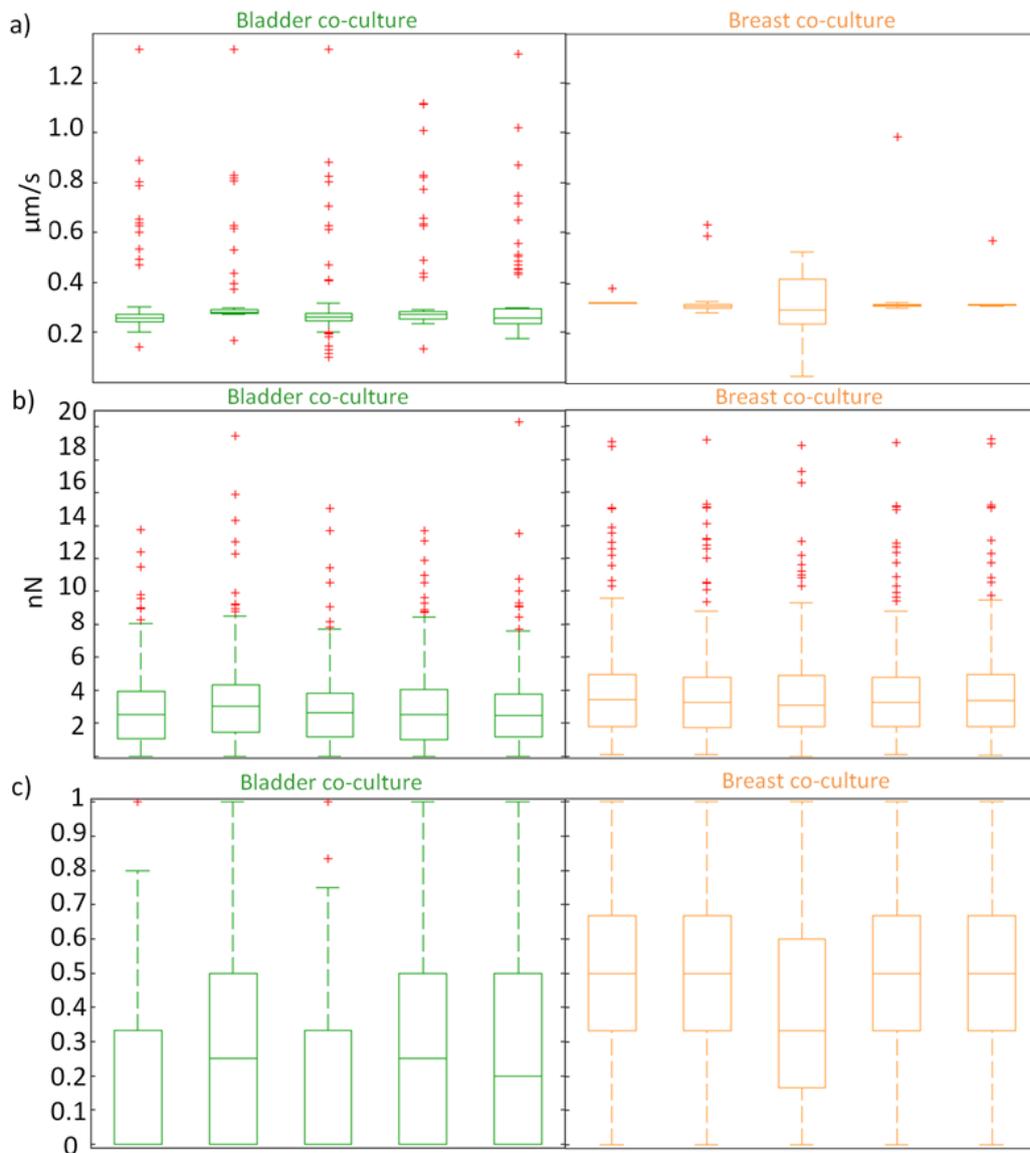
Figure 5.5. Velocity, a), intercellular force, b) and sorting index, c), box plots for bladder and breast co-cultures. Outliers are in red. Five seeding replicates were considered per co-culture.
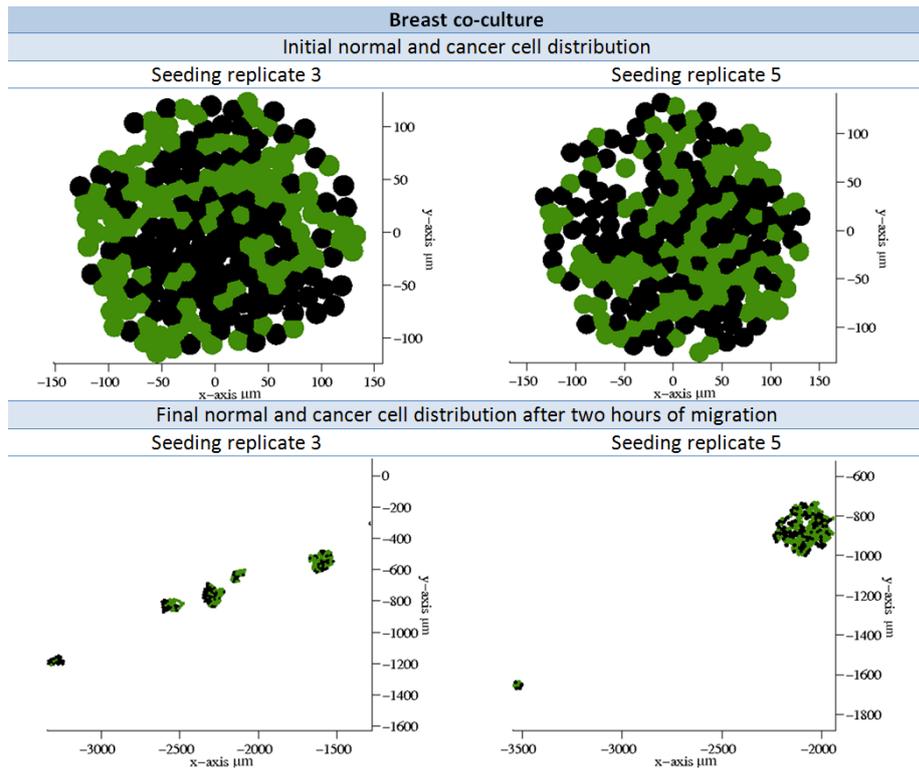
Figure 5.6 Initial and final distribution of normal (green) and cancer cells (black) for two seeding replicates of breast co-culture.
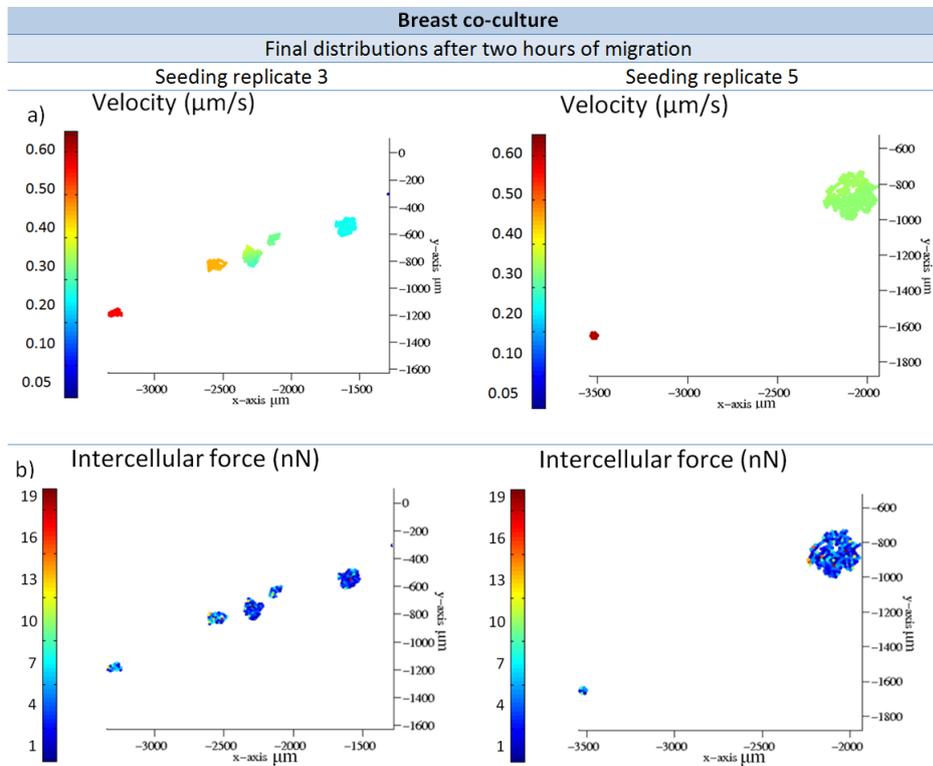
Figure 5.7. Final distributions of velocity and intercellular force for two seeding replicates of breast co-culture.

5.4.3. *In-silico* drug test on the migration of co-cultures

With the microtubule stabilizer Paclitaxel the velocity of bladder cell co-cultures decreases by 30%, Table 5.8. The median velocity, Table 5.8, becomes similar to the one found for monocultures of normal cells, $1.9x10^{-1}$ µm/s (11 µm/min) – Tables 5.5 and 5.6. The same happened with the interquartile range of the velocity distribution. It decreased to an order of magnitude of 10^{-3} µm/s, also found for monocultures of normal cells – Tables 5.5 and 5.6. In addition, the number of velocity outliers is reduced, see Figure 5.8.

The median intercellular force decreases by 23% to a value of 2.0 nN, Table 5.8, once more approaching the value of force found for normal cell monocultures – Tables 5.5 and 5.6. The same happens to the variation in intercellular force within the co-culture. The intercellular force interquartile range decreased from 2.8 to 1.9 nN.

With Paclitaxel the Sorting Index increases by 214%, revealing a decrease in the sorting of bladder normal and cancer cells. This explains the decrease in the number of velocity outliers.

Figures 5.9 and 5.10 show the results obtained for seeding replicate 5 of a bladder co-culture without and with treatment with Paclitaxel. Without the treatment the cells migrate in clusters with a median Sorting Index of 0.2 – control replicate 5 in Figure 5.8 c). Single cells separate from the cluster, not seen in Figure 5.10 a), migrating at a faster velocity of 1.2 µm/s, see Figure 5.8 a). With Paclitaxel normal and cancer cells do not sort, having a median Sorting Index of 0.5 – drug replicate 5 in Figure 5.8 c).

Table 5.8 – Median and interquartile range of velocity and intercellular force distributions for bladder co-cultures without and with paclitaxel. The results correspond to the average of five seeding replicates.

	Effect of paclitaxel			
	Bladder - Control		Bladder - Paclitaxel	
	Median	Interquartile range	Median	Interquartile range
Velocity (μm/s)	2.7×10^{-1}	3.2×10^{-2}	1.9×10^{-1}	5.2×10^{-3}
Intercellular force (nN)	2.6	2.8	2.0	1.9
Sorting Index (SI)	0.14	0.43	0.44	0.36
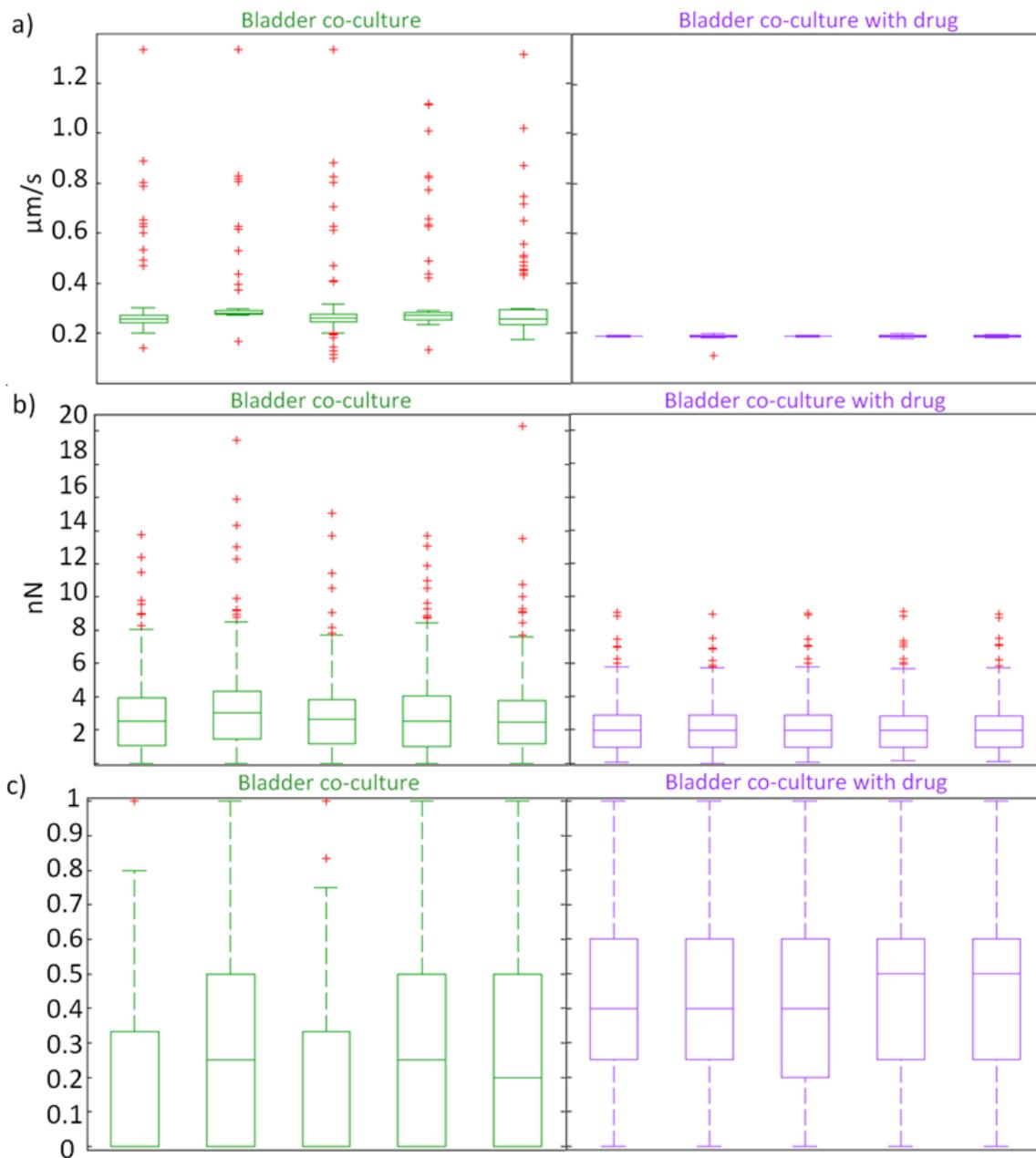
Figure 5.8. Velocity, a), intercellular force, b) and sorting index, c), box plots for bladder co-cultures without and with drug. Outliers are in red. Five seeding replicates were considered per co-culture.
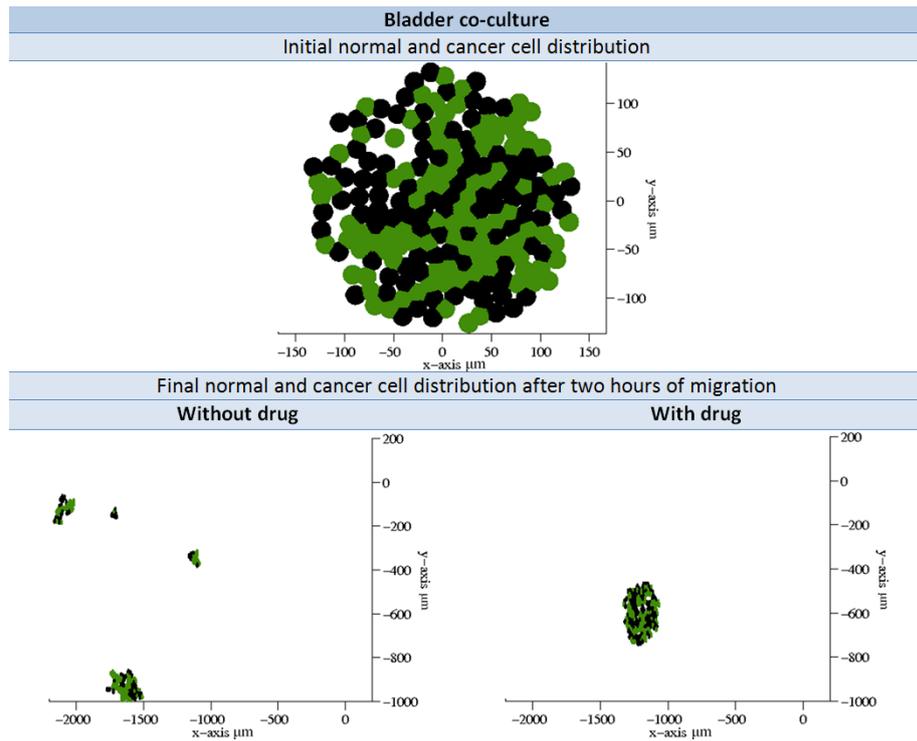
Figure 5.9. Initial distribution of normal, in green, and cancer cells, in black after seeding and final distribution for equivalent seeding replicates of bladder co-cultures without treatment with Paclitaxel (control) and with the treatment.
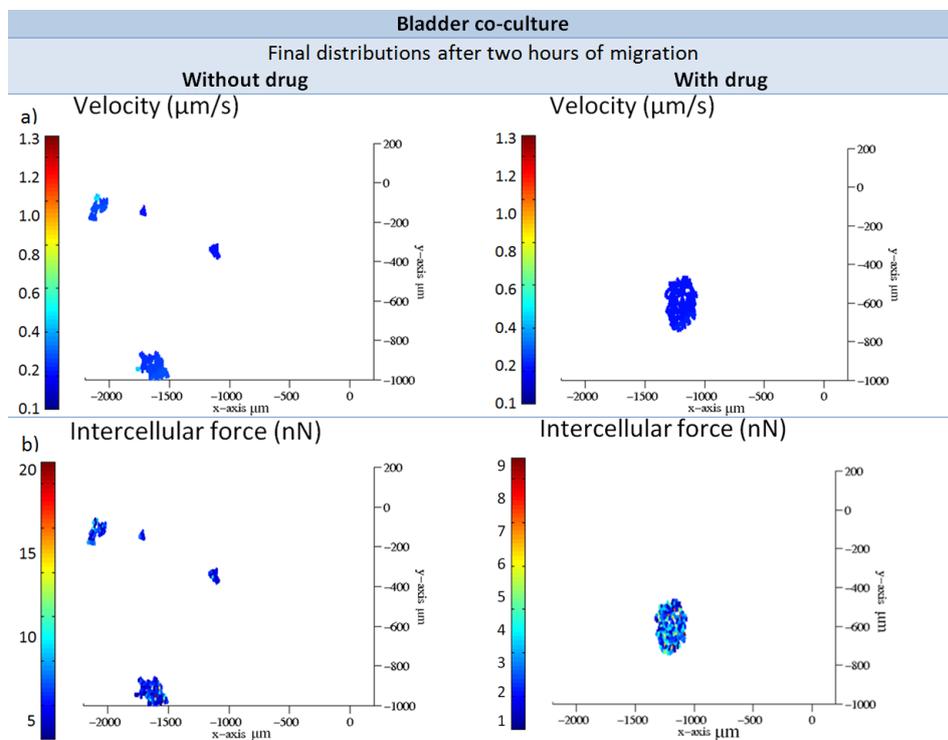
Figure 5.10. Final distributions for equivalent seeding replicates of bladder co-cultures without treatment with Paclitaxel (control) and with the treatment.

5.5 Discussion

5.5.1. Migration of monocultures accounting for intra-population heterogeneity

Outlier cell behaviour is often important to understand the emergence of a disease and population-based measurements generally lack the specificity to capture it. Cell heterogeneity calls for more effective specific treatments. Computational models such as the one developed in this study are able to account for cell heterogeneity playing an important part in the development of such treatments.

The model was applied to normal and cancer cell monocultures from both the bladder and breast tissues. The median values for the velocity and intercellular force are similar for bladder and breast cell populations (Tables 5.5 and 5.6). However, median velocity and intercellular force are two times higher for cancer cell than for normal cell populations, reflecting the mismatch between the active traction force of normal and cancer cells (Tables 5.1 and 5.2). This suggests that the active traction of individual cells has a greater influence on the velocity distribution than their passive and tissue specific mechanical properties: Young's modulus and cell-cell adhesion.

As seen in Tables 5.1 and 5.2, besides being higher for cancer than for normal cell populations, traction force also varies more for the former (higher interquartile range). As a result, intercellular force and velocity vary more within cancer cell monocultures. However, the cell velocity distribution varies greatly for the same population depending on the seeding replicate. The high heterogeneity in the active traction of cancer cell populations results in very different collective migration mechanisms such as migration in clusters and the formation of finger-like protrusions, see Figure 5.4. As presented in Chapter 4, cell sorting is related to differences in the traction force exerted by cells in physical contact. These different migratory behaviours can be seen for different seeding replicates of the same cell population. In other words, if the same cells are seeded in a different spatial arrangement, different migration mechanisms can take place. This suggests that the spatial distribution of mechanically different cells triggers different migration mechanisms. Further mechanistic and more quantitative understanding of the emergence of these different migration outcomes could be achieved in the future by

modelling a higher number of cells. This would increase the statistical power of the observations and better replicate *in-vitro* experiments.

Cancer cells are known to be highly heterogeneous, sensitive to their microenvironment and capable of changing their behaviour according to the stage of progression of the disease. Cancer cells need to adapt to their extracellular environment to be able to perform in diverse processes such as metastasis, invasion or intravasation (the process of entering into the bloodstream by crossing the membrane of blood vessels) [38], [149]. The results of this work suggest that the heterogeneity in the mechanical properties of cancer cells can explain their different migration behaviours. There is evidence that different cells in different spatial positions within the cluster adopt different roles in the collective migration. Other works suggest that cells at the leading edge develop leading features to direct the migration, such as higher sensitivity to growth factors [7]. Leader cells seem to have specific features, such as sensory and guiding properties, that differentiate them from the rest of the cells within the cluster. In fact, removing leader cells using micromanipulators from the front of a migrating population of Madin-Darby Canine Kidney (MDCK) epithelial cells disrupts their cohesive migration [150]. Mechanical changes have also been identified in leading cells in wound healing. Cells near the wound edge experience changes in their stiffness, which peaks approximately at 10-15 µm from the wound edge [151]. Several works report higher traction forces for cells on the edge of a migrating cell monolayer [18], [137]. The fact that the mechanical properties of cells seem to depend on their specific spatial position within the monolayer was not accounted for in this work. Mechanical properties following the parameter distributions were assigned to cells of the population regardless of their spatial position.

Changes in the mechanics of cancer cells are also related with different stages of the disease. Changes in cancer cell mechanics have, for instance, been reported during Epithelial-to-Mesenchymal Transition (EMT). EMT is the process through which epithelial polarized cells gain migratory characteristics and decrease their levels of cell-cell adhesion. This process is associated with both wound healing [152] and cancer progression [10]. EMT has been suggested as the mechanism that explains the transformation that cells from the carcinoma *in-situ* undergo when they individually

separate from the tissue and become invasive. The process has been related with changes in the apical tension of cells, which depends on the actomyosin contractility and the formation of actin stress fibres [153]. However, collective invasion also happens in cancer. Multicellular clusters of cancer cells can detach from the carcinoma and invade the surrounding tissues as a group keeping their cell-cell contacts [9]. In fact, EMT is seen as a continuous spectrum and the concept of partial EMT was created to understand the cells at the invasive front of a multicellular migrating cluster. These cells have gained migratory characteristics but have kept their cell-cell contacts stable. Furthermore, Mesenchymal-to-Epithelial Transition (MET) has been suggested as the mechanism through which individual moving cells form again multicellular aggregates in distant tissues after metastasis [9]. This shows the plasticity of cancer cell migration and suggests that cancer cells should go through several changes in their mechanical properties at different stages of the disease. The ability of cells to dynamically change their mechanical properties was not accounted for in this work. The mechanical properties of cells were considered as fixed, cell-type specific and not dependent on their position within the monolayer or stage of the disease. Nonetheless, the results support the idea that the mechanical heterogeneity of cancer cells enables diverse migration mechanisms. Cancer cells should be able to tune their mechanical properties to switch their migration mechanism according to their microenvironment.

5.5.2. Migration of co-cultures accounting for intra-population heterogeneity

The median velocity of cells in co-culture, order of magnitude of $3.0x10^{-1}$ µm/s (18 µm/min) – see Table 5.7, is in between the value found for normal and cancer monocultures - see Tables 5.5 and 5.6. This reflects the fact that co-cultures of 50% normal cells and 50% cancer cells were considered.

The sorting between normal and cancer bladder cells in co-culture explains the higher interquartile range obtained for velocity and the decrease in intercellular forces when comparing to breast co-cultures.

The same active traction force distribution was considered for bladder and breast cells. Therefore, the differences observed between them reflect the difference in the passive properties characteristic of the type of tissue – Table 5.3. A combination of mismatch in traction force and in the passive properties of normal and cancer cells lead to cell sorting in bladder cell co-cultures. Breast cells exerting the same traction forces do not tend to sort as they have more similar passive properties. This is reflected in the values of interquartile range for the Young's modulus and cell-cell adhesion distributions in Table 5.3. However, sorting between normal and cancer breast cells in co-culture happened for one of the five seeding replicates (seeding replicate 3). This means that sorting between normal and cancer cells in co-culture depends on the spatial distribution of active and passive cell mechanical properties. By changing the distribution of their mechanical properties in a cell cluster, normal and cancer cells can migrate as a cohesive group or sort. There are normal cells that are known to support cancer such as cancer associated fibroblasts. Gaggioli et al [154] found that fibroblasts can lead the invasion of cancer cells. Another example is the study of Carey et al from 2013 [155] in which a co-culture system of normal mammary epithelial and adenocarcinoma cells was developed. Collective cell migration features were identified in the migration of the heterogeneous clusters of normal and cancer cells. Cancer cells acted as leaders, developed protrusions and supported the invasion of otherwise non-invasive healthy epithelial cells. The study suggests that different roles in collective migration can be adopted by cells of different sub-populations within a tumour. Shin et al [156] investigated tumour heterogeneity co-culturing two different sub-populations of adenocarcinoma cells with different invasive properties. The authors concluded that the interaction between the two sub-populations of cancer cells promotes invasion and that the highly invasive cells guided the less invasive ones. Besides collective cell migration, also sorting is observed in cancer and it is important for metastasis. As mentioned in section 5.5.1, cancer cells exhibit different migration mechanisms and can migrate with decreased levels of cell-cell adhesion instead of collectively. Cancer cells that emerge in the normal tissue can sort from it, form clusters, enter in the bloodstream and thereby spread the disease. Spontaneous sorting of normal and cancer cells has also been observed *in-vitro* [20]. In Chapter 4 sorting between normal and cancer cells in co-culture was found to happen

due to differences in the mechanical properties of normal and cancer cells and thresholds were identified to explain sorting. The fact that cells of the same population are mechanically different was accounted for in the present Chapter 5. The results obtained complement the previous ones by suggesting that thresholds for sorting between cells can be dependent on the cell's microenvironment and, therefore, cell specific.

5.5.3. *In-silico* drug test on the migration of co-cultures

Studies suggest that the failure of drugs during their development phase is mainly due to their lack of efficacy and not their secondary effects [141]. Computational models such as the one developed in this work can serve as platforms for drug screening and save time and money when compared with clinical trials. In this section the impact of the changes in individual cell mechanics induced by microtubule stabilizers in collective cell migration was investigated.

Treatment with the microtubule stabilizer Paclitaxel was simulated by modifying the Young's modulus and traction force of individual cancer cells. Bladder cancer cells were seeded with normal bladder cells in a co-culture scenario. At the single cell level Paclitaxel was considered to affect more the cancer cell Young's modulus, 150%, than traction force, 63%. At the population level, the simulated drug affects a normal/cancer cell co-culture by increasing the median of the Young's modulus in 171% and decreasing the interquartile range in 5%. The median of the traction force distribution decreases by 36% and the variation in traction force by 41%. In Chapter 4 the sorting of normal and cancer cells in co-culture has been found to happen due to the variation in their mechanical properties. Variation in traction force (measured by the interquartile range) in a co-culture was more affected by the drug than the variation in Young's modulus. This suggests that the changes in collective migration observed for normal/cancer co-cultures with the drug are better explained by the changes that the drug promotes in the traction force of cancer cells than in their Young's modulus.

With the drug treatment both the median and interquartile range values associated to cell velocity (Table 5.8) decreased to values on the same order of magnitude as those found for monocultures of normal cells (Tables 5.5 and 5.6). Paclitaxel was also found to

inhibit cancer cell migration significantly experimentally: the distance travelled by cancer cells decreased with increased concentration of the drug [157]. The authors reported changes in the cell's morphology with the drug treatment, specifically, a decrease in cellular protrusions. These changes could be related with the effect on cell migration.

Also the median and interquartile range values for intercellular force (Table 5.8) decreased to the levels found for normal monocultures with the virtual drug treatment (Tables 5.5 and 5.5). These results suggest that Paclitaxel-type drugs reverse the mechanical and migration properties of cancer cells to properties similar to those of normal cells. It should be pointed out that there is no consensus on the effect of Paclitaxel on the mechanical properties of cells. There is a study reporting no influence on the cells traction force after treatment [158]. Information on the changes in cell mechanics promoted by Paclitaxel or other anti-cancer drugs lacks and the present work evidences the potential of such information. Furthermore, this work assumes that it is possible to use a chemotherapeutic agent to target cancer cells exclusively, without affecting contacting normal cells. In fact, one of the main challenges in cancer treatment remains to this day the toxicity of anti-cancer drugs [146]. One possibility being explored to protect healthy cells from adverse treatment effects is the use of a combination of several drugs in chemotherapy [159].

The computational model developed provided mechanistic and quantitative information about the effect of microtubule stabilizers on collective cell migration. With simulated drug treatment the sorting between bladder normal and cancer cells decreased 214%, Table 5.8. This supports the idea that the sorting between normal and cancer cells can be prevented using such drug. Changes in cell migration are associated with metastasis. Assuming that a decrease in the sorting of normal and cancer cells in the carcinoma *in-situ* reduces the possibility of metastasis, this result suggests that the changes in mechanical properties of cells induced by microtubule stabilizers can contribute to their therapeutic effect in metastasis inhibition [146]. Treatment with microtubule stabilizers such as Paclitaxel could keep the cancer localized [160], thereby, increasing the probability of treatment success.

However, it needs to be pointed out that the sorting of normal and cancer cells can be beneficial and, even required, in some circumstances. As discussed in previous sections there is plasticity in cancer cell migration and cells tune their properties according to their microenvironment and stage of the disease. As mentioned in section 5.5.2 there is evidence that the physical contact of normal cells and cancer cells can support cancer invasion and both cell types can migrate collectively. In this scenario, it would be beneficial to trigger the sorting of normal and cancer cells to stop this cooperation process. In addition, separating normal from cancer cells *in-vitro* can be useful to specifically treat cancer cells, purify tissue samples, generate primary tumour cell lines from biopsy samples for anti-cancer drugs testing and develop cell therapy personalized treatments [13], [161]. Therefore, drugs need to be designed depending on the particular application and cancer stage being targeted. The plasticity of migration of cancer cells needs to be further investigated, as it directly impacts the efficacy of anti-cancer drugs [162]. In addition, drug development should also account for features that are specific of the individual, the particular tumour and the cells it is composed of. Computational models such as the one developed in this work can account for these features and act as platforms for the testing of personalized drugs.

More generally, the results of this work emphasize the role of the cell's cytoskeleton in collective cell migration. Since the cytoskeleton contributes to the mechanical properties of cells, such as the apparent Young's modulus and traction force, it can be modified to change the migration mechanism of cells. Cells can remodel their cytoskeleton to change the number of stress fibres, adapt contractility forces and traction [163]. In fact, in the future the present population model could be combined with a single cell finite element model to explicitly model the mechanics of the cell's cytoskeleton. Thereby, the potential of Paclitaxel-type drugs to impact collective cell migration by changing the structure of the cells' cytoskeleton could be directly tested. Furthermore, cytoskeleton remodelling with the cell's microenvironment could be incorporated to increase mechanistic understanding on the plasticity of cancer cell migration. The present work proposes that the potential of drugs that target the mechanics of the cytoskeleton, such as microtubule stabilizers, to trigger changes in collective cell migration should be investigated. In conclusion, pharmaceutical

companies should explore further the changes in cell mechanics induced by anti-cancer drugs as they may contribute to their therapeutic effect.

5.6 Conclusion

A cell-centred computational model of collective cell migration that accounts for single cell mechanical heterogeneity was developed. The model was applied to the context of cancer, a disease that is particularly characterized by the heterogeneity that exists between cells of different tumours and cells belonging to the same tumour. The migration of normal and cancer cell populations was investigated. The virtual co-culture of normal and cancer cells was considered as a model for tumour-host interactions to increase understanding on the mechanics of cancer migration. Furthermore, the impact of chemotherapeutic microtubule stabilizers was tested.

The model predicts that the heterogeneity in single cell mechanics observed in cancer can be related with the diverse migration mechanisms cancer cells adopt. The results suggest that the cells' ability to tune their mechanical properties according to their microenvironment and the stage of progression of the disease can contribute to the plasticity of cancer cell migration. In addition, it is suggested that changes in cell mechanics promoted by anti-cancer drugs can lead to different cell migration and therefore contribute to their therapeutic effect in inhibiting metastasis. More generally, this work proposes that the cytoskeleton by contributing to cell mechanics contributes to the collective migration of cells.

Chapter 6 - General discussion

Summary

This Chapter presents a general discussion of the results of the thesis. The various sets of results are integrated and analysed in light of state of the art knowledge. Limitations and possible future improvements are discussed.

6.1 Modelling and simulation in drug development

Modelling and simulation in drug development is progressing from a scientific to a regulatory tool. The potential of modelling and simulation has been recognized by leading pharmaceutical companies and regulatory agents such as the USA Food and Drug Administration (FDA) [164] and the Japanese Pharmaceuticals and Medical Devices Agency (PMDA) [165]. A recent FDA work plan announces the investment in *in-silico* trials to support the advancement of novel therapeutics. The work plan follows the funding provided by the 21st Century Cures Act (H.R.34), a law enacted by the USA government in December 2016.

Mathematical and computational models provide a platform for *in-silico* drug testing. They can boost the advancement of precision medicine in the future by supporting the choice of the appropriate drug for a particular patient, predicting the efficacy and toxicity of the treatment, optimizing doses, testing drug-drug interactions in combined treatments and investigating alternative administration routes [166].

Drug development needs to adopt new strategies to reduce the time and money spent on investigating promising drugs that fail before their regulatory approval. A nine-year study including 7,455 drug development programs across 1,103 companies found that only one in ten programs entering Phase I in 2006 reached FDA approval by 2015 [167]. Of the 14 diseases investigated in the study, cancer was associated with the lowest likelihood of drug approval from Phase I (5.1%). Among other reasons, low success rates are explained by poor efficacy due to a lack of clear understanding of the drugs' mechanisms of action [168].

At an early stage of drug development computational models can be used to provide mechanistic knowledge about the disease, find potential drug candidates and understand mechanisms of action. Models can inspire novel *in-vitro*/animal experiments and clinical trials and be iteratively improved.

Physiological endpoints of mechanical nature, such as cellular contractile force, have recently been proposed to evaluate the effect of drugs [169]. It is known for a long time that cell mechanics affects cell behaviour [170]. Nonetheless, the relationship between biomechanics and drugs' mechanisms of action is still rarely investigated [141].

6.2 Discussion of model predictions

This work aimed to generate mechanistic and quantitative understanding of the role of cell mechanics in collective cell migration and sorting. For this purpose, a computational model was developed and applied to cancer. The ultimate goal was to make predictions able to inform the design of anti-cancer drugs.

Chapter 3 of this thesis describes the development of a computational model describing passive mechanical interactions between cells. Intercellular mechanical interactions are considered to drive cell spreading following the first few hours of *in-vitro* seeding. The model was applied to normal and cancer cells from the bladder and breast. Cells from both tissues were seeded in monocultures composed of identical normal or cancer cells. In addition, normal/cancer cell co-cultures were considered as a model for tumour-host interactions.

Predictions about population arrangement and mechanics were generated based on individual cell mechanical properties. It was found that intercellular stress in a monoculture depends on the cells' Young's modulus, cell-cell adhesion forces and local microenvironment (neighbouring cells and position within the monolayer). Intercellular stress is higher at the monolayer edge and in regions within the monolayer where the cells are less packed. Trepat et al [16] mathematically estimated the intercellular stress within an epithelial cell monolayer from experimentally measured traction forces. This was achieved considering the equilibrium between cell-substrate traction and cell-cell forces. The authors reported higher traction for the cells on the edge. Higher

intercellular stress was estimated for the cells within the monolayer as a result of the build-up of forces. In Trepat et al cell-cell forces were interpreted as the forces that balance cell traction. In this work, cell-cell forces emerge uniquely from intercellular mechanical interactions due to elastic repulsion and adhesion. This explains the disagreement between both results. In fact, although not considered in this work, it is also possible that passive cell stress originates active cell responses that maintain the monolayer uniformity and integrity, for instance, cytoskeleton remodelling [132] and the formation of protrusions [171]. These processes could have a role in preserving the integrity of the edge and closing monolayer wounds where the cells are less packed.

Intercellular stress was found to vary greatly within modelled co-cultures. For co-cultures of mechanically different cells, in addition to depending on cell packing and position within the monolayer, intercellular stress additionally depends on the cell type. The fact that heterogeneous traction fields were experimentally measured for populations of normal epithelial cells [16] suggests that mechanically different cells may be present in a monoculture. This idea is supported by this work and inspired the study of cell cultures considering intra-population mechanical variability in Chapter 5. The differentiation between passive and active force components poses a challenge to the validation of the model developed. Notwithstanding, models such as this one, that isolate the contributions of different factors, provide mechanistic understanding of their relative role.

In this work Young's modulus and cell-cell adhesion levels also explained the visual sorting of normal and cancer cells in the first few hours after seeding. Early cell sorting (Figure 3.15 in Chapter 3) can be driven by differences in the Young's modulus and intercellular adhesion of normal and cancer cells. Sorting, in turn, reduces the level of intercellular stress. Furthermore, cell sorting through passive cell spreading is dependent on the local microenvironment and seeding configuration. The model predicted the existence of trapped cells that do not sort and are completely surrounded by cells of other type. These cells are in a state of higher intercellular stress. As previously discussed, it is possible that high levels of passive stress give rise to responses that were not accounted for in this work and maintain the cells function. For example,

stress-driven changes in cell mechanical properties can take place, such as changes in cell stiffness or traction force generation [124].

In order to understand the relative role of passive cell mechanics and active force generation in the migration of co-cultures, the model was extended to describe migration after cell spreading in Chapter 4. The model includes traction forces actively exerted by cells and was applied to bladder and breast normal/cancer cell co-cultures. Mechanical and quantitative thresholds triggering the spontaneous sorting of normal and cancer cells were defined.

Following Vicsek's model [68], it was assumed that migrating cells in contact align the direction of their actomyosin machineries. Therefore, cell sorting emerges in the model due to the inability of cells with different mechanical properties to migrate in close contact and not as a result of their scattered movement.

Other works on collective cell migration focused on finding mechanistic explanations for the local movement alignment between contacting cells. Marth et al [172] computationally predicted the spontaneous emergence of collective cell migration from inelastic intercellular collisions. Contact inhibition of locomotion (CIL) describes the changes in cell migration following cell-cell contact, specifically, repolarization and migration away from other cells. There is evidence that CIL dysregulation in metastatic cancer cells is related with its invasive potential [173].

In order to investigate the possible relationship between the seemingly conflicting behaviours of CIL and collective cell migration, Desai et al 2013 [174] developed an individual-based model. The formation of collective cell chains following cell-cell collisions was predicted, observation that was posteriorly verified experimentally. The results suggest that CIL and collective cell migration are related and their interplay can explain the ability of cells to dynamically switch between migration modes.

Carmona-Fontaine et al [47] proposed that cell-cell attraction, in concert with CIL, is required to maintain cell clusters cohesive. Cell-cell attraction, or coattraction, is not to be confused with cell-cell adhesion as it emerges in response to a chemoattractant released by the individual cells, the complement fragment C3a. The authors suggest that a balance between short-range repulsion (CIL) and long-range attraction owing to the production and sensing of a chemoattractant (coattraction) is required for collective cell

migration. CIL drives repolarization in response to intercellular contact and coattraction keeps the cluster cohesive.

The computational predictions from Woods et al in 2014 [175] further show that directed collective cell migration does not require an external signal but, instead, chemotaxis towards an attractant produced by the cells itself.

On the whole, the results of these works suggest that directed collective cell migration can emerge uniquely from repulsive and attractive mechanical interactions between cells. In the future, the model presented in this thesis could be expanded to include a mechanistic explanation for cell movement alignment based on intercellular mechanical interactions.

The model developed allowed to make predictions related with the sorting of normal and cancer cells in co-culture based on their mechanical properties. Cell sorting was found to be higher the higher the active traction mismatch between both cell types. To the author's knowledge this was the first time that the spontaneous sorting of normal and cancer cells was related to the mismatch between traction forces derived from the experimental literature. The effect of cell-cell adhesion on sorting was also studied. If the levels of cell-cell adhesion are not sufficiently high, a mismatch in traction can lead to cell sorting, even without differential cell-cell adhesion (different levels of cell-cell adhesion for normal and cancer cells). Inspired by the DAH [21], the effect of differential cell-cell adhesion was also explored. It was found that the higher the traction mismatch, the lower the adhesion difference between normal and cancer cells required for their sorting. In addition to predicting that two tissues sort due to differences in their surface tension, the DAH predicts that the tissue with lower surface tension envelops the one with higher surface tension. Although, the role of differential cell-cell adhesion in cell sorting was confirmed with this work, the present model was not able to reproduce the enveloping behaviour predicted by the DAH. This could be explained by the fact that the model developed does not consider cell migration as solely governed by cell-cell adhesion [94] but also intercellular elastic interactions and active traction forces. Furthermore, following the set-up of *in-vitro* collective cell migration experiments [33], cell movement was not confined and confluency was not modelled. Nonetheless, even in sorting experiments in which cell movement is confined, the enveloping behaviour is

not always observed. Literature results show that the most aggressive cells enveloped the least aggressive ones in a 3D breast co-culture [155], [176] . However, brain tumour cells and stem cells have been found to organise themselves differently, in two poles, in a 3D tumour model [20]. Self-organization seems to be a complex behaviour dependent on factors such as the type of cell, the type of cadherin mediating cell-cell adhesion and recognition and the extracellular environment [104].

Globally, sorting was found to be more dependent on differences in the traction of normal and cancer cells and absolute cell-cell adhesion levels, followed by differential adhesion of normal and cancer cells. As a result, an integrated mechanism was proposed for the sorting of normal and cancer cells in Chapter 4. Intercellular forces emerge in a cell culture triggered by a mismatch in the passive and/or active mechanical properties of the cells. When there is a high mismatch in the passive properties of cells, Young's modulus and intercellular adhesion, cell sorting is possible in the first few hours after seeding – Chapter 3. The traction forces exerted by cells after the onset of active cell migration can also drive sorting – Chapter 4. A mismatch in traction gives rise to intercellular forces that allow normal and cancer cells to migrate cohesively. Sorting happens when the passive properties of cells prevent them from generating such intercellular cooperative forces.

It is possible that cells adapt their traction forces in response to the intercellular forces that build-up in a co-culture of cells with different motility. The inclusion of modelled feedback between passive and active cell mechanical properties would allow remodelling based on the mechanical microenvironment to be explored. Besides being affected by the local environment, cell mechanical properties can also be intrinsically different between cells that belong to the same population [27], [29]. This intrinsic heterogeneity can, for example, be due to genetic variation generated by mutations. Although also present in the normal tissue, cell heterogeneity is characteristic of cancer [142]. For that reason, its implications need to be understood to inform the development of anti-cancer drugs.

The migration of mechanically heterogeneous cell populations was investigated in Chapter 5 of the present work. Normal and cancer cells from the bladder and breast tissues were modelled in both monoculture and normal/cancer cell co-culture scenarios.

In addition to the variation of cell mechanical properties depending on the tissue of origin and malignancy, intra-population variability based on the experimental literature was considered. The results suggest that different spatial distributions of mechanical properties can trigger different migration mechanisms in cancer cell populations. Different behaviours emerged in different seeding replicates such as collective migration, segregation in various clusters or formation of finger-like protrusions. This suggests that the plasticity often associated to the migration of cancer cell populations can be related to the heterogeneity of their mechanical properties. Cancer cells vary these properties, for instance through cytoskeleton remodelling, at different stages of the disease to switch migration mode. In fact, changes in cell mechanics were reported during Epithelial-to-Mesenchymal Transition (EMT) [153], the transformation that explains how individual cells segregate from the carcinoma *in-situ* and become invasive. It would be interesting in the future to use the model developed to further investigate how the different migration modes emerge. Mechanistic and quantitative understanding could support the development of techniques to control the migration of cancer cells and trigger particular migration modes in particular circumstances. For this purpose, a higher number of cells, and therefore a higher number of seeding replicates, should be modelled in order to increase the statistical power of the predictions.

Although mechanical properties were considered to vary within a cell population, they were assigned randomly to cells independently of their position within the monolayer. This approach is in apparent contrast with experimental results that found that mechanical properties differ for cells on the edge or within a monolayer. For instance, as previously mentioned, higher traction forces have been measured for cells on the edge of a migrating cell monolayer [18], [137]. Nonetheless, it is probable that this spatial distribution emerges as a result of cells sensing their local microenvironment through mechanotransduction pathways [177], directing their migration machineries and remodelling. An extended version of the computational model developed including these cell processes has the potential to explain the emergence of such heterogeneous and dynamic force fields. Furthermore, the formation, characterization and importance of specialized leader cells could also be explored. The results of this work propose that, even without remodelling, the intrinsic intra-population variability of mechanical

properties can explain the variety of migration modes that cancer cell populations adopt.

The effect of intra-population heterogeneity was also investigated in normal/cancer cell co-cultures. The sorting of normal and cancer cells was found to depend on the spatial distribution of passive and active cell mechanical properties. The results obtained in Chapter 5 complement those of Chapter 4 by suggesting that mechanical thresholds for cell sorting should be dependent on the cell microenvironment, and, therefore, cell specific.

The predictions of the model developed indicate that the mechanical properties of individual cells are reflected in the migration at the population level. Therefore, they are potential targets for the treatment of diseases affecting cell migration, such as cancer. The effect of chemotherapeutic microtubule stabilizers on the sorting of normal and cancer bladder cells in co-culture was tested *in-silico* using the model developed. Microtubule stabilizers impair cell division by affecting the dynamics of the cytoskeleton. However, there is evidence that, by targeting the cytoskeleton, microtubule stabilizers such as Paclitaxel modify the mechanical properties of cells: Young's modulus [36] and traction force [37]. The effect of microtubule stabilizers was modelled accounting for the changes in mechanical properties they induce in cancer cells. The results suggest that this family of drugs reverses the mechanical and migratory properties of cancer cells from the bladder to properties similar to those of normal cells. Since the sorting of normal and cancer cells in co-culture is driven by differences between cells, sorting is reduced by the drug treatment. A decrease in the sorting of normal and cancer cells in carcinoma *in-situ* could reduce the possibility of metastasis. Thereby, the changes in mechanical properties induced by microtubule stabilizers could promote metastasis inhibition. The relationship between cell mechanics and the therapeutic effect of these drugs should be further explored.

In addition to metastasis prevention, the results of this work can be used for situations in which cell sorting is required. For instance, cell sorting can be triggered to purify tumour samples composed of a mixture of cancer cells, stem cells and normal epithelial cells. This purification is required to create primary tumour cell lines for the development of anti-cancer drugs. Cell sorting could be prevented or triggered

depending on the application. The quantitative and mechanistic understanding provided by the model developed can, therefore, be beneficial in different scenarios and inform the design of different drugs.

Experimental studies confirm that Paclitaxel inhibits the proliferation of cancer cells [178], [179]. Combined drug treatments have also been explored. Paclitaxel combined with Harmine resulted in more effective inhibition of gastric cancer cells migration and invasion than the treatment with both drugs separately [180]. However, Paclitaxel has also been associated with metastasis promotion in some situations [181], [182]. Further research is required to better understand and maximize the anti-cancer potential of the drug.

In this computational work it was assumed that the modelled chemotherapeutic agent was 100% efficient in affecting the mechanical properties of cancer cells. Nevertheless, the effect is dependent on several factors such as the drug uptake and the drug concentration. Different delivery mechanisms such as the use of micelles have been experimentally explored to improve the drug uptake [183]. Furthermore, microtubule stabilizers seem to have a concentration-dependent effect. Low concentrations of Paclitaxel have been found to be clinically relevant and less susceptible to generate treatment toxicity [184]. There are studies reporting EMT [185] and metastasis inhibition [160] using low doses of Paclitaxel. Low-Dose Metronomic (LDM) chemotherapy has been proposed as a less toxic alternative to conventional chemotherapy [186]. It consists on the frequent and continuous administration of low doses of chemotherapeutic drugs. The concentration-dependency of the effect of microtubule stabilizers was not considered in this work. In the future, a coupled model could provide further insight into the range of possible cell population behaviours triggered by microtubule stabilizers. For this purpose, the mechanical model developed in this work could be coupled with a pharmacological model of the drug's mechanism of action.

6.3 Messages to take forward

More generally, the results of this thesis provide evidence of the role of the cytoskeleton in the collective migration of cells. The cytoskeleton is a structural, load-bearing and dynamic structure. It bridges the cell and the extracellular environment and takes part in the formation of protrusions, cell migration, division and intracellular transport of organelles. The functionality of the cytoskeleton requires the generation of forces by the actomyosin machinery. Cytoskeleton remodelling is, hence, associated with changes in the mechanics of cells such as elasticity [153] and force generation properties [163]. In fact, the hypothesis that microtubule stabilizers impact collective cell migration by changing the structure of the cytoskeleton could be tested in the future. For this purpose, the model developed could be combined with a single cell finite element model that explicitly describes the structure and mechanics of the cytoskeleton. Thereby, the cytoskeleton structure, passive and active cell mechanical properties and migration behaviour could be related and understood in an integrated perspective. Furthermore, cytoskeleton remodelling triggered by the cell's microenvironment could be included to investigate the several migration modes exhibited by cancer cells.

This work proposes that pharmaceutical companies should perform mechanopharmacology [141] studies on the changes in cell mechanical properties induced by drugs known to be chemotherapeutic, as they may play role in their therapeutic effect. Equally, the anti-cancer potential of drugs known to target the mechanics of cells should also be explored.

Collective cell behaviour in cancer is much less understood than in morphogenesis. Being a slowly evolving and complex disease makes the design of cancer experiments more difficult [75]. This is an opportunity for the development of computational models able to generate knowledge and inspire novel experiments. Although migration and sorting are required for cancer metastasis and invasion [41], [42], modelling in cancer has been mainly focused on tumour growth [39], [40]. The computational model of the present work adds to the ones existent by investigating the mechanics of sorting between normal and cancer cells based on cell mechanical properties experimentally measured [42]. In fact, with the advancement of measurement technologies the

mechanical fidelity of computational models should increase. Computational models should develop hand in hand with experimental technologies. Experimental technologies will provide increasingly accurate measurements and models will continue to demonstrate the gaps in knowledge that, in turn, inspire novel experiments. The model developed in this work highlights that single cell mechanical properties should be further studied to understand complex diseases such as cancer. Given the potential of cell-cell adhesion forces, traction forces and cell Young's modulus to determine cell migration modes and sorting, techniques to measure these mechanical properties must continue to evolve. In addition, this work proposes the integration of concepts related with collective cell migration and sorting. Experimental [102] and computational models [24], [103] investigating the relation between both phenomena offer insight on the mechanisms behind the dynamics of cell migration.

Although the focus of this work was on cancer metastasis, the model predictions can be translated to other biological scenarios involving collective cell migration and sorting, such as morphogenesis. The segregation of the cells that will compose the several tissues is required in biological development. It is possible that collective cell migration and sorting in cancer and in morphogenesis are based on shared core principles. Therefore the model developed could be tuned to better understand and treat congenital diseases.

Chapter 7 - Conclusions

Summary

This Chapter concludes the thesis by summarising the main findings and the messages to take forward.

The aim of this thesis was to improve the understanding of the mechanics of collective cell migration and sorting in cancer. The role of the mechanical properties of individual cells in determining mechanics and migration at the cell-population level was investigated. A quantitative and mechanistic computational model was developed for this purpose.

In Chapter 3 a model describing cell-cell passive mechanical interactions was presented. These interactions were related with cell spreading in the first hours following seeding. Normal and cancer cells were considered in both monoculture and co-culture scenarios. The changes in the mechanical properties of cells associated with malignancy were accounted for. The model predicts intercellular stress to be dependent on the cells' Young's modulus, cell-cell adhesion levels and local microenvironment (neighbouring cells and position within the monolayer). The presence of mechanically different normal and cancer cells in co-culture results in a higher variation of intercellular stress in comparison to monocultures. In addition, the differences in Young's modulus and intercellular adhesion of normal and cancer cells explain their early sorting.

In Chapter 4 the migratory traction forces exerted by cells after spreading were incorporated in the model. Quantitative mechanical thresholds were defined for the sorting of normal and cancer cells in co-culture. Sorting was found to depend primarily on differences in the traction of normal and cancer cells and absolute cell-cell adhesion levels, followed by the differential adhesion of normal and cancer cells. The predictions supported an integrated mechanism for the sorting of normal and cancer cells. The differences in the passive properties of cells, Young's modulus and intercellular adhesion, generate intercellular forces that drive sorting in the first few hours after seeding – Chapter 3. The migratory traction forces exerted by cells later were also found

to contribute to sorting. The mismatch in traction force can generate cooperative intercellular forces that allow normal and cancer cells to migrate collectively. The generation of these intercellular forces is, in turn, dependent on the passive properties of cells. If cells are not able to generate intercellular forces, sorting of normal and cancer cells occurs.

In Chapter 5 the intra-population variability of the mechanical properties of cells was included. The results suggest that the plasticity of migration of cancer cell populations is related with the heterogeneity of cell mechanics. Different spatial distributions of mechanical properties can trigger different migration modes in cancer cell populations. In normal/cancer cell co-cultures sorting also depends on the spatial distribution of passive and active mechanical properties. This result complements the ones found in Chapter 4 by proposing that mechanical thresholds for cell sorting depend on the cell microenvironment being, therefore, cell specific. The effect of microtubule stabilizers on sorting was tested *in-silico* accounting for the changes induced in the mechanical properties of cancer cells. Microtubule stabilizers were predicted to reverse both the mechanical and migration properties of cancer cells to properties similar to the ones of normal healthy cells. The sorting of normal and cancer cells, is thereby, reduced.

This study shows that individual cell mechanical properties can explain a variety of population-scale measurements and behaviours. The results emphasize the importance of investigating the changes in cell mechanics that accompany malignant transformation and their role in cancer progression. The relation between biomechanics and the effect of drugs is rarely investigated. In this work the effect of the cell changes induced by microtubule stabilizers on the population behaviour was studied. It is proposed that pharmaceutical companies would benefit from exploring the cell mechanical changes induced by anti-cancer drugs as they may contribute to their therapeutic effect. Furthermore, cell heterogeneity should be regarded in the design of anti-cancer drugs as it allows the diversity of behaviours cancer cell populations' exhibit.

A computational model integrating collective cell migration and sorting was developed. The model is unique in investigating the migration of normal and cancer cell populations based on the cell mechanical changes observed in cancer. It represents a step forward towards a quantitative and mechanistic description of collective cell migration and

sorting. Such a description has the potential to enable the development of techniques to control the migration of cancer cells and support treatment. The findings can, nonetheless, be translated to other applications. The framework can be tuned to investigate collective cell migration and sorting in other biological scenarios, such as in morphogenesis.

Chapter 8 - References

[1]   X. Guan, "Cancer metastases: Challenges and opportunities," *Acta Pharm. Sin. B*, vol. 5, no. 5, pp. 402–418, 2015.

[2]   P. Steeg and D. Theodorescu, "Metastasis: a therapeutic target for cancer," *Nat. Clin. Pract. Oncol.*, vol. 5, no. 4, pp. 206–219, 2008.

[3]   X. Trepat, Z. Chen, and K. Jacobson, "Cell Migration," vol. 2, no. 4, pp. 2369–2392, 2015.

[4]   J. Jiang, L. Li, Y. He, and M. Zhao, "Collective cell migration: Implications for wound healing and cancer invasion," *Burn. Trauma*, vol. 1, no. 1, p. 21, 2013.

[5]   S. R. K. Vedula *et al.*, "Emerging modes of collective cell migration induced by geometrical constraints.," *Proc. Natl. Acad. Sci. U. S. A.*, vol. 109, no. 32, pp. 12974–9, 2012.

[6]   N. A. Hale, Y. Yang, and P. Rajagopalan, "Cell migration at the interface of a dual chemical-mechanical gradient," *ACS Appl. Mater. Interfaces*, vol. 2, no. 8, pp. 2317–2324, 2010.

[7]   D. A. Chapnick and X. Liu, "Leader cell positioning drives wound-directed collective migration in TGFβ-stimulated epithelial sheets.," *Mol. Biol. Cell*, vol. 25, no. 10, pp. 1586–1593, 2014.

[8]   P. Pandya, J. L. Orgaz, and V. Sanz-Moreno, "Modes of invasion during tumour dissemination," *Molecular Oncology*, vol. 11. pp. 1–23, 2016.

[9]   N. V Krakhmal, M. V Zavyalova, E. V Denisov, S. V Vtorushin, and V. M. Perelmuter, "Cancer Invasion: Patterns and Mechanisms.," *Acta Naturae*, vol. 7, no. 2, pp. 17–28, 2015.

[10]   J. P. Thiery, "Epithelial-mesenchymal transitions in tumour progression.," *Nat. Rev. Cancer*, vol. 2, no. 6, pp. 442–454, 2002.

[11]   J. M. Halbleib and W. J. Nelson, "Cadherins in development: Cell adhesion, sorting, and tissue morphogenesis," *Genes Dev.*, vol. 20, no. 23, pp. 3199–3214,

2006.

[12]   E. Méhes and T. Vicsek, "Collective motion of cells: from experiments to models," *Integr. Biol.*, vol. 6, no. 9, pp. 831–854, 2014.

[13]   A. Mitra, L. Mishra, and S. Li, "Technologies for deriving primary tumor cells for use in personalized cancer therapy," *Trends Biotechnol.*, vol. 31, no. 6, pp. 347–354, 2013.

[14]   P. M. Vitorino, "Modular Control of Endothelial Sheet Cohesion and Collective Cell Migration," *Stanford Univ. Thesis*, vol. 1, pp. 3268–3281, 2009.

[15]   A. Zaritsky *et al.*, "Propagating Waves of Directionality and Coordination Orchestrate Collective Cell Migration," *PLoS Comput. Biol.*, vol. 10, no. 7, pp. 15–19, 2014.

[16]   X. Trepat *et al.*, "Physical forces during collective cell migration," *Nat. Phys.*, vol. 5, no. 6, pp. 426–430, 2009.

[17]   W.-J. Rappel, "Cell–cell communication during collective migration," *Proc. Natl. Acad. Sci.*, vol. 113, no. 6, p. 201524893, 2016.

[18]   O. du Roure *et al.*, "Force mapping in epithelial cell migration.," *Proc. Natl. Acad. Sci. U. S. A.*, vol. 102, no. 7, pp. 2390–2395, 2005.

[19]   E. Urich, C. Patsch, S. Aigner, M. Graf, R. Iacone, and P.-O. Freskgård, "Multicellular self-assembled spheroidal model of the blood brain barrier.," *Sci. Rep.*, vol. 3, p. 1500, 2013.

[20]   D. P. Ivanov *et al.*, "In vitro co-culture model of medulloblastoma and human neural stem cells for drug delivery assessment," *J. Biotechnol.*, vol. 205, pp. 3–13, 2015.

[21]   M. S. Steinberg, "Does Differential Adhesion Govern Self -assembly Processes in Histogenesis? Equilibrium Configurations and the Emergence of a Hierarchy Among Populations of Embryonic Cells," *J. Exp. Zool.*, vol. 173, no. 4, pp. 395–433, 1970.

[22]   D. A. Beysens, G. Forgacs, and J. A. Glazier, "Cell sorting is analogous to phase

ordering in fluids.," *Proc. Natl. Acad. Sci.*, vol. 97, no. 17, pp. 9467–9471, 2000.

[23] E. Evans and A. Yeung, "Apparent viscosity and cortical tension of blood granulocytes determined by micropipet aspiration.," *Biophys. J.*, vol. 56, no. 1, pp. 151–60, 1989.

[24] A. J. Kabla, "Collective Cell Migration: Leadership, Invasion and Segregation," *J. R. Soc. Interface*, vol. 9, no. 77, pp. 3268–3278, 2011.

[25] G. Wayne Brodland and H. H. Chen, "The mechanics of cell sorting and envelopment," *J. Biomech.*, vol. 33, no. 7, pp. 845–851, 2000.

[26] W. Xu, R. Mezencev, B. Kim, L. Wang, J. McDonald, and T. Sulchek, "Cell Stiffness Is a Biomarker of the Metastatic Potential of Ovarian Cancer Cells," *PLoS One*, vol. 7, no. 10, 2012.

[27] M. Lekka *et al.*, "Cancer cell detection in tissue sections using AFM," *Arch. Biochem. Biophys.*, vol. 518, no. 2, pp. 151–156, 2012.

[28] Q. S. Li, G. Y. H. Lee, C. N. Ong, and C. T. Lim, "AFM indentation study of breast cancer cells," *Biochem. Biophys. Res. Commun.*, vol. 374, no. 4, pp. 609–613, 2008.

[29] M. Lekka, P. Laidler, D. Gil, J. Lekki, Z. Stachura, and a Z. Hrynkiewicz, "Elasticity of normal and cancerous human bladder cells studied by scanning force microscopy.," *Eur. Biophys. J.*, vol. 28, no. 4, pp. 312–316, 1999.

[30] Z. Li *et al.*, "Quantifying the traction force of a single cell by aligned silicon nanowire array," *Nano Lett.*, vol. 9, no. 10, pp. 3575–3580, 2009.

[31] C. M. Kraning-Rush, J. P. Califano, and C. A. Reinhart-King, "Cellular traction stresses increase with increasing metastatic potential," *PLoS One*, vol. 7, no. 2, 2012.

[32] X. Guo, K. Bonin, K. Scarpinato, and M. Guthold, "The effect of neighboring cells on the stiffness of cancerous and non-cancerous human mammary epithelial cells," *New J. Phys.*, vol. 16, 2014.

[33] D. T. Tambe *et al.*, "Collective cell guidance by cooperative intercellular forces.,"

Nat. Mater., vol. 10, no. 6, pp. 469–75, 2011.

[34] A. Marusyk and K. Polyak, "Tumor heterogeneity: Causes and consequences," *Biochim. Biophys. Acta - Rev. Cancer*, vol. 1805, no. 1, pp. 105–117, 2010.

[35] R. a Burrell, N. McGranahan, J. Bartek, and C. Swanton, "The causes and consequences of genetic heterogeneity in cancer evolution.," *Nature*, vol. 501, no. 7467, pp. 338–45, 2013.

[36] J. Ren, H. Huang, Y. Liu, X. Zheng, and Q. Zou, "An atomic force microscope study revealed two mechanisms in the effect of anticancer drugs on rate-dependent Young's modulus of human prostate cancer cells," *PLoS One*, vol. 10, no. 5, pp. 1–14, 2015.

[37] C. M. Kraning-Rush, S. P. Carey, J. P. Califano, B. N. Smith, and C. A. Reinhart-King, "The role of the cytoskeleton in cellular force generation in 2D and 3D environments.," *Phys. Biol.*, vol. 8, no. 1, p. 15009, 2011.

[38] P. Katira, R. T. Bonnecaze, and M. H. Zaman, "Modeling the mechanics of cancer: effect of changes in cellular and extra-cellular mechanical properties.," *Front. Oncol.*, vol. 3, no. June, p. 145, 2013.

[39] P. Katira, M. H. Zaman, and R. T. Bonnecaze, "How changes in cell mechanical properties induce cancerous behavior," *Phys. Rev. Lett.*, vol. 108, no. 2, pp. 1–5, 2012.

[40] G. Sciumè, W. G. Gray, M. Ferrari, P. Decuzzi, and B. A. Schrefler, "On Computational Modeling in Tumor Growth," *Arch. Comput. Methods Eng.*, vol. 20, no. 4, pp. 327–352, 2013.

[41] A. Szabó, K. Varga, T. Garay, B. Hegedus, and A. Czirók, "Invasion from a cell aggregate-the roles of active cell motion and mechanical equilibrium.," *Phys. Biol.*, vol. 9, no. 1, p. 16010, 2012.

[42] G. W. Brodland and J. H. Veldhuis, "The Mechanics of Metastasis: Insights from a Computational Model," *PLoS One*, vol. 7, no. 9, 2012.

[43] R. Mayor and S. Etienne-Manneville, "The front and rear of collective cell

migration," *Nat. Rev. Mol. Cell Biol.*, vol. 17, no. 2, pp. 97–109, 2016.

[44] B. A. Camley and W.-J. Rappel, "Physical models of collective cell motility: from cell to tissue," *J. Phys. D. Appl. Phys.*, vol. 50, no. 11, p. 113002, 2017.

[45] V. Hakim and P. Silberzan, "Collective cell migration: a physics perspective," *Reports Prog. Phys.*, vol. 80, no. 7, p. 76601, 2017.

[46] T. E. Dick *et al.*, "Equation-Based Models of Wound Healing and Collective Cell Migration," in *Complex Systems and Computational Biology Approaches to Acute Inflammation*, 2013, pp. 185–207.

[47] C. Carmona-Fontaine *et al.*, "Complement Fragment C3a Controls Mutual Cell Attraction during Collective Cell Migration," *Dev. Cell*, vol. 21, no. 6, pp. 1026–1037, 2011.

[48] F. A. Meineke, C. S. Potten, and M. Loeffler, "Cell migration and organization in the intestinal crypt using a lattice-free model," *Cell Prolif.*, vol. 34, no. 4, pp. 253–266, 2001.

[49] J. Jeon, V. Quaranta, and P. T. Cummings, "An off-lattice hybrid discrete-continuum model of tumor growth and invasion," *Biophys. J.*, vol. 98, no. 1, pp. 37–47, 2010.

[50] G. P. G. Latini, R. Cocci Grifoni, *Transport Properties of Organic Liquids*. WIT Press, 2006.

[51] H. R. Hertz, D. . Jones, and G. . Schott, "Miscellaneous papers," *Macmillan Co. Ltd*, vol. 92, pp. 156–171, 1896.

[52] J. Galle, M. Loeffler, and D. Drasdo, "Modeling the effect of deregulated proliferation and apoptosis on the growth dynamics of epithelial cell populations in vitro.," *Biophys. J.*, vol. 88, no. 1, pp. 62–75, 2005.

[53] D. Drasdo and S. Hoehme, "Modeling the impact of granular embedding media, and pulling versus pushing cells on growing cell clones," *New J. Phys.*, vol. 14, 2012.

[54] R. M. Hochmuth, "Micropipette aspiration of living cells," *J. Biomech.*, vol. 33, no.

1, pp. 15–22, 2000.

[55]   S. M. Mijailovich *et al.*, "A finite element model of cell deformation during magnetic bead twisting," vol. 2115, pp. 1429–1436, 2002.

[56]   H. Zhang and K.-K. Liu, "Optical tweezers for single cells.," *J. R. Soc. Interface*, vol. 5, no. 24, pp. 671–90, 2008.

[57]   K. A. Addae-Mensah and J. P. Wikswo, "Measurement techniques for cellular biomechanics in vitro.," *Exp. Biol. Med. (Maywood).*, vol. 233, no. 7, pp. 792–809, 2008.

[58]   G. Thomas, N. a Burnham, T. A. Camesano, and Q. Wen, "Measuring the mechanical properties of living cells using atomic force microscopy.," *J. Vis. Exp.*, no. 76, pp. 1–8, 2013.

[59]   T. Neumann, "Determining the elastic modulus of biological samples using atomic force microscopy," *JPK Instruments Appl. Rep.*, pp. 1–9, 2008.

[60]   S. Nawaz, P. S??nchez, K. Bodensiek, S. Li, M. Simons, and I. A. T. Schaap, "Cell Visco-Elasticity Measured with AFM and Optical Trapping at Sub-Micrometer Deformations," *PLoS One*, vol. 7, no. 9, 2012.

[61]   K. L. Johnson, K. Kendall, and A. D. Roberts, "Surface Energy and the Contact of Elastic Solids," *Proc. R. Soc. A Math. Phys. Eng. Sci.*, vol. 324, no. 1558, pp. 301–313, 1971.

[62]   Y. S. Chu, S. Dufour, J. P. Thiery, E. Perez, and F. Pincet, "Johnson-Kendall-Roberts theory applied to living cells," *Phys. Rev. Lett.*, vol. 94, no. 2, pp. 1–4, 2005.

[63]   G. Schaller and M. Meyer-Hermann, "A modelling approach towards epidermal homoeostasis control," *J. Theor. Biol.*, vol. 247, no. 3, pp. 554–573, 2007.

[64]   T. Beyer and M. Meyer-Hermann, "Modeling emergent tissue organization involving high-speed migrating cells in a flow equilibrium," *Phys. Rev. E - Stat. Nonlinear, Soft Matter Phys.*, vol. 76, no. 2, pp. 1–27, 2007.

[65]   F. Liao, H. Xu, N. Torrey, P. Road, and L. Jolla, "Velocity alignment leads to high persistence in confined cells," vol. 2, no. 74, 2015.

[66] D. Stichel *et al.*, "An individual-based model for collective cancer cell migration explains speed dynamics and phenotype variability in response to growth factors," *npj Syst. Biol. Appl.*, vol. 3, no. 1, p. 5, 2017.

[67] D. Cai, W. Dai, M. Prasad, J. Luo, N. S. Gov, and D. J. Montell, "Modeling and analysis of collective cell migration in an in vivo three-dimensional environment.," *Proc. Natl. Acad. Sci. U. S. A.*, vol. 113, no. 15, pp. E2134-41, 2016.

[68] T. Vicsek, A. Czirók, E. Ben-Jacob, I. Cohen, and O. Shochet, "Novel type of phase transition in a system of self-driven particles." .

[69] A. Czirók, E. Ben-Jacob, I. Cohen, and T. Vicsek, "Formation of complex bacterial colonies via self-generated vortices," *Phys. Rev. E*, vol. 54, no. 2, pp. 1791–1801, 1996.

[70] V. Tarle, A. Ravasio, V. Hakim, and N. S. Gov, "Modeling the finger instability in an expanding cell monolayer," *Integr. Biol.*, vol. 7, no. 10, pp. 1218–1227, 2015.

[71] G. Gregoire and H. Chate, "Onset of collective and cohesive motion," no. 2, pp. 1–4, 2004.

[72] I. Y. Wong *et al.*, "Collective and individual migration following the epithelial–mesenchymal transition," *Nat. Mater.*, vol. 13, no. 11, pp. 1063–1071, 2014.

[73] Y. Hegerfeldt, M. Tusch, E.-B. Bröcker, and P. Friedl, "Collective Cell Movement in Primary Melanoma Explants," *Cancer Res.*, vol. 62, no. 7, pp. 2125–2130, 2002.

[74] P. Friedl, J. Locker, E. Sahai, and J. E. Segall, "Classifying collective cancer cell invasion.," *Nat. Cell Biol.*, vol. 14, no. 8, pp. 777–83, 2012.

[75] P. Friedl and D. Gilmour, "Collective cell migration in morphogenesis, regeneration and cancer.," *Nat. Rev. Mol. Cell Biol.*, vol. 10, no. july, pp. 445–457, 2009.

[76] T. A. Ulrich, E. M. De Juan Pardo, and S. Kumar, "The mechanical rigidity of the extracellular matrix regulates the structure, motility, and proliferation of glioma cells," *Cancer Res.*, vol. 69, no. 10, pp. 4167–4174, 2009.

[77] N. Gavara and R. S. Chadwick, "Relationship between cell stiffness and stress fiber

amount, assessed by simultaneous atomic force microscopy and live-cell fluorescence imaging," *Biomech. Model. Mechanobiol.*, vol. 15, no. 3, pp. 511–523, 2016.

[78] C. K. Shih, "Cell Motility and Local Viscoelasticity of Fibroblasts," vol. 89, no. December, pp. 4330–4342, 2005.

[79] Q. Luo, D. Kuang, B. Zhang, and G. Song, "Cell stiffness determined by atomic force microscopy and its correlation with cell motility," *Biochim. Biophys. Acta - Gen. Subj.*, vol. 1860, no. 9, pp. 1953–1960, 2016.

[80] P. Friedl, K. Wolf, and J. Lammerding, "Nuclear mechanics during cell migration," *Curr. Opin. Cell Biol.*, vol. 23, no. 1, pp. 55–64, 2011.

[81] J. Lammerding, "Mechanics of the nucleus," *Compr. Physiol.*, vol. 1, no. 2, pp. 783–807, 2011.

[82] R. Omidvar, M. Tafazzoli-shadpour, M. A. Shokrgozar, and M. Rostami, "Atomic force microscope-based single cell force spectroscopy of breast cancer cell lines: An approach for evaluating cellular invasion," *J. Biomech.*, vol. 47, no. 13, pp. 3373–3379, 2014.

[83] L. Bastatas *et al.*, "AFM nano-mechanics and calcium dynamics of prostate cancer cells with distinct metastatic potential," *Biochim. Biophys. Acta - Gen. Subj.*, vol. 1820, no. 7, pp. 1111–1120, 2012.

[84] H. W. Yu *et al.*, "β-PIX controls intracellular viscoelasticity to regulate lung cancer cell migration," *J. Cell. Mol. Med.*, vol. 19, no. 5, pp. 934–947, 2015.

[85] C.-Y. Liu, H.-H. Lin, M.-J. Tang, and Y.-K. Wang, "Vimentin contributes to epithelial-mesenchymal transition cancer cell mechanics by mediating cytoskeletal organization and focal adhesion maturation," *Oncotarget*, vol. 6, no. 18, pp. 15966–15983, 2015.

[86] A. L. Sieminski *et al.*, "Migration of tumor cells in 3D matrices is governed by matrix stiffness along with cell-matrix adhesion and proteolysis," *Proc. Natl. Acad. Sci. U. S. A.*, vol. 103, no. 15, pp. 15–16, 2006.

[87] S. K. Mitra, D. A. Hanson, and D. D. Schlaepfer, "Focal adhesion kinase: In command and control of cell motility," *Nat. Rev. Mol. Cell Biol.*, vol. 6, no. 1, pp. 56–68, 2005.

[88] A. Techasen *et al.*, "Loss of E-cadherin promotes migration and invasion of cholangiocarcinoma cells and serves as a potential marker of metastasis," *Tumor Biol.*, vol. 35, no. 9, pp. 8645–8652, 2014.

[89] A. Stockinger, A. Eger, J. Wolf, H. Beug, and R. Foisner, "E-cadherin regulates cell growth by modulating proliferation-dependent -beta-catenin transcriptional activity," vol. 154, no. 6, pp. 1185–1196, 2001.

[90] R. T. Bryan *et al.*, "Cadherin switching dictates the biology of transitional cell carcinoma of the bladder : ex vivo and in vitro studies," no. February, pp. 184–194, 2008.

[91] P. Friedl and R. Mayor, "Tuning Collective Cell Migration by Cell – Cell Junction Regulation," pp. 1–18, 2017.

[92] E. Bazellières *et al.*, "Control of cell – cell forces and collective cell dynamics by the intercellular adhesome," vol. 17, no. 4, 2015.

[93] T. J. Sego, U. Kasacheuski, D. Hauersperger, A. Tovar, and N. I. Moldovan, "A heuristic computational model of basic cellular processes and oxygenation during spheroid-dependent biofabrication," *Biofabrication*, vol. 9, no. 2, p. 24104, 2017.

[94] Y. Zhang, G. L. Thomas, M. Swat, A. Shirinifard, and J. A. Glazier, "Computer simulations of cell sorting due to differential adhesion," *PLoS One*, vol. 6, no. 10, pp. 26–28, 2011.

[95] A. K. Harris, "Is cell sorting caused by differences in the work of intercellular adhesion? A critique of the steinberg hypothesis," *J. Theor. Biol.*, vol. 61, no. 2, pp. 267–285, 1976.

[96] G. W. Brodland, "The Differential Interfacial Tension Hypothesis (DITH): a comprehensive theory for the self-rearrangement of embryonic cells and tissues.," *J. Biomech. Eng.*, vol. 124, no. 2, pp. 188–197, 2002.

[97]   F. Graner, "Can Surface Adhesion Drive Cell-rearrangement? Part I: Biological Cell-sorting," *Journal of Theoretical Biology*, vol. 164, no. 4. pp. 455–476, 1993.

[98]   C. P. Beatrici and L. G. Brunnet, "Cell sorting based on motility differences," *Phys. Rev. E - Stat. Nonlinear, Soft Matter Phys.*, vol. 84, no. 3, pp. 1–5, 2011.

[99]   F. Graner and J. A. Glazier, "Simulation of Biological Cell Sorting Using a 2-Dimensional Extended Potts-Model," *Physical Review Letters*, vol. 69, no. 13. pp. 2013–2016, 1992.

[100] M. Krieg *et al.*, "Tensile forces govern germ-layer organization in zebrafish.," *Nat. Cell Biol.*, vol. 10, no. 4, pp. 429–36, 2008.

[101] M. L. Manning, R. A. Foty, M. S. Steinberg, and E.-M. Schoetz, "Coaction of intercellular adhesion and cortical tension specifies tissue surface tension.," *Proc. Natl. Acad. Sci. U. S. A.*, vol. 107, no. 28, pp. 12517–22, 2010.

[102] E. Méhes, E. Mones, V. Németh, and T. Vicsek, "Collective motion of cells mediates segregation and pattern formation in co-cultures," *PLoS One*, vol. 7, no. 2, 2012.

[103] J. M. Belmonte, G. L. Thomas, L. G. Brunnet, R. M. C. De Almeida, and H. Chaté, "Self-propelled particle model for cell-sorting phenomena," *Phys. Rev. Lett.*, vol. 100, no. 24, pp. 20–23, 2008.

[104] E. Méhes and T. Vicsek, "Segregation mechanisms of tissue cells: from experimental data to models," *Science (80-.).*, vol. 338, no. 6104, pp. 212–215, 2012.

[105] P. M. Altrock, L. L. Liu, and F. Michor, "The mathematics of cancer: integrating quantitative models," *Nat Rev Cancer*, vol. 15, no. 12, pp. 730–745, 2015.

[106] E. Scarpa and R. Mayor, "Collective cell migration in development," *J. Cell Biol.*, vol. 212, no. 2, pp. 143–155, 2016.

[107] M. Lekka, "Discrimination Between Normal and Cancerous Cells Using AFM," *Bionanoscience*, vol. 6, no. 1, pp. 65–80, 2016.

[108] J. Kashef and C. M. Franz, "Quantitative methods for analyzing cell-cell adhesion

in development," *Dev. Biol.*, vol. 401, no. 1, pp. 165–174, 2015.

[109] R. Winklbauer, "Cell adhesion strength from cortical tension - an integration of concepts," *J. Cell Sci.*, vol. 128, no. 20, pp. 3687–3693, 2015.

[110] R. David, O. Luu, E. W. Damm, J. W. H. Wen, M. Nagel, and R. Winklbauer, "Tissue cohesion and the mechanics of cell rearrangement," *Development*, vol. 141, no. 19, pp. 3672–3682, 2014.

[111] B. Hegedüs, F. Marga, K. Jakab, K. L. Sharpe-Timms, and G. Forgacs, "The Interplay of Cell-Cell and Cell-Matrix Interactions in the Invasive Properties of Brain Tumors," *Biophys. J.*, vol. 91, no. 7, pp. 2708–2716, 2006.

[112] "MATLAB and Statistics Toolbox Release 2012b." The MathWorks, Inc, Natick, Massachusetts, US.

[113] I. N. Bronshtein and K. A. Semendyayev, *A Guide Book to Mathematics*. Springer New York, 1973.

[114] H. V. O. Bart Smeets, Tim Odenthal, Engelbert Tijskens, Herman Ramon, "Quantifying the mechanical micro-environment during three-dimensional cell expansion on microbeads by means of individual cell-based modelling," *Comput. Methods Biomech. Biomed. Engin.*, vol. 16, no. 10, pp. 1071–1084, 2013.

[115] T. Beyer and M. Meyer-Hermann, "Multiscale modeling of cell mechanics and tissue organization," *IEEE Eng. Med. Biol. Mag.*, vol. 28, no. 2, pp. 38–45, 2009.

[116] S. M. Zehnder, M. Suaris, M. M. Bellaire, and T. E. Angelini, "Cell volume fluctuations in MDCK monolayers," *Biophys. J.*, vol. 108, no. 2, pp. 247–250, 2015.

[117] M. H. Zaman, R. D. Kamm, P. Matsudaira, and D. A. Lauffenburger, "Computational Model for Cell Migration in Three-Dimensional Matrices," *Biophys. J.*, vol. 89, no. 2, pp. 1389–1397, 2005.

[118] G. Coceano *et al.*, "Investigation into local cell mechanics by atomic force microscopy mapping and optical tweezer vertical indentation," *Nanotechnology*, vol. 27, no. 6, p. 65102, 2016.

[119] R. Vargas-Pinto, H. Gong, A. Vahabikashi, and M. Johnson, "The effect of the

endothelial cell cortex on atomic force microscopy measurements," *Biophys. J.*, vol. 105, no. 2, pp. 300–309, 2013.

[120] D. R. Pier Carlo Braga, *Atomic Force Microscopy : Biomedical Methods and Applications*. Humana Press, 2004.

[121] T. G. Kuznetsova, M. N. Starodubtseva, N. I. Yegorenkov, S. A. Chizhik, and R. I. Zhdanov, "Atomic force microscopy probing of cell elasticity," *Micron*, vol. 38, no. 8, pp. 824–833, 2007.

[122] P. Van Liedekerke, M. Palm, N. Jagiella, and D. Drasdo, "Simulating tissue mechanics with Agent Based Models : concepts and perspectives," *Comput. Part. Mech.*, vol. 2, no. 4, pp. 401–444, 2015.

[123] G. Fenteany, P. A. Janmey, and T. P. Stossel, "Signaling pathways and cell mechanics involved in wound closure by epithelial cell sheets," *Curr. Biol.*, vol. 10, no. 14, pp. 831–838, 2000.

[124] A. F. Mertz, Y. Che, S. Banerjee, J. M. Goldstein, K. a Rosowski, and S. F. Revilla, "Cadherin-based intercellular adhesions organize epithelial cell–matrix traction forces," *Proc. Natl. Acad. Sci.*, vol. 110, no. 3, pp. 842–847, 2013.

[125] E. M. Strohm and M. C. Kolios, "Measuring the mechanical properties of cells using acoustic microscopy.," *Conf. Proc. IEEE Eng. Med. Biol. Soc.*, vol. 2009, pp. 6042–6045, 2009.

[126] D. Hartono, Y. Liu, P. L. Tan, X. Y. S. Then, L.-Y. L. Yung, and K.-M. Lim, "On-chip measurements of cell compressibility via acoustic radiation," *Lab Chip*, vol. 11, no. 23, p. 4072, 2011.

[127] S. Pawlizak *et al.*, "Testing the differential adhesion hypothesis across the epithelial-mesenchymal transition," *New J. Phys.*, vol. 17, no. 8, 2015.

[128] W. G. Martin, Tracey Amanda, Ye, Lin, Sanders, Andrew J., Lane, Jane and Jiang, "Cancer invasion and metastasis: molecular and cellular perspective," in *Metastatic Cancer Clinical and Biological Perspectives*, Austin, Texas: Landes Bioscience, 2013, pp. 135–168.

[129] O. F. Kandarakov, M. V Kalashnikova, A. A. Vartanian, and A. V Belyavsky, "Homogeneous and Heterogeneous In Vitro 3D Models of Melanoma," *Mol. Biol. Orig. Russ. Text ©*, vol. 49, no. 6, pp. 895–898, 2015.

[130] T. H. O. Bruce R. Munson, Donald F. Young, *Fundamentals Of Fluid Mechanics, John Wiley & Sons, Inc., 4th edition*, 4th editio. John Wiley & Sons, Inc., 2002.

[131] A. G. Clark and D. M. Vignjevic, "Modes of cancer cell invasion and the role of the microenvironment," *Curr. Opin. Cell Biol.*, vol. 36, pp. 13–22, 2015.

[132] S. L. Lee *et al.*, "Physically-Induced Cytoskeleton Remodeling of Cells in Three-Dimensional Culture," *PLoS One*, vol. 7, no. 12, 2012.

[133] R. A. Foty and M. S. Steinberg, "The differential adhesion hypothesis: A direct evaluation," *Dev. Biol.*, vol. 278, no. 1, pp. 255–263, 2005.

[134] M. Sadati, N. Taheri Qazvini, R. Krishnan, C. Y. Park, and J. J. Fredberg, "Collective migration and cell jamming," *Differentiation*, vol. 86, no. 3, pp. 121–125, 2013.

[135] A. F. Pegoraro, J. J. Fredberg, and J. A. Park, "Problems in biology with many scales of length: Cell-cell adhesion and cell jamming in collective cellular migration," *Exp. Cell Res.*, vol. 343, no. 1, pp. 54–59, 2016.

[136] E. Mones, A. Czirók, and T. Vicsek, "Anomalous segregation dynamics of self-propelled particles," *New J. Phys.*, vol. 17, no. 6, 2015.

[137] A. Saez *et al.*, "Traction forces exerted by epithelial cell sheets," *J. Phys. Condens. Matter*, vol. 22, no. 19, p. 194119, 2010.

[138] U. S. Schwarz *et al.*, "Measurement of cellular forces at local adhesion using elastic micro- patterned substrates," *Mater. Sci. Eng. C*, vol. 23, no. 3, pp. 387–394, 2003.

[139] Z. Liu *et al.*, "Mechanical tugging force regulates the size of cell-cell junctions," *Proc. Natl. Acad. Sci.*, vol. 107, no. 22, pp. 9944–9949, 2010.

[140] A. Roycroft and R. Mayor, "Forcing contact inhibition of locomotion," *Trends Cell Biol.*, vol. 25, no. 7, pp. 373–375, 2015.

[141] A. G. Ramaswamy Krishnan, Jin-Ah Park, Chun Y. Seow, Peter V-S. Lee and

Stewart, "Cellular Biomechanics in Drug Screening and Evaluation: Mechanopharmacology," *Trends Pharmacol. Sci.*, vol. 37, no. 2, pp. 87–100, 2015.

[142] B. Snijder, R. Sacher, P. Rämö, E.-M. Damm, P. Liberali, and L. Pelkmans, "Population context determines cell-to-cell variability in endocytosis and virus infection," *Nature*, vol. 461, no. 7263, pp. 520–523, 2009.

[143] V. R. Zellmer and S. Zhang, "Evolving concepts of tumor heterogeneity," *Cell Biosci.*, vol. 4, no. 1, p. 69, 2014.

[144] S. Ward, E. Simpson, S. Davis, D. Hind, A. Rees, and A. Wilkinson, "Taxanes for the adjuvant treatment of early breast cancer: Systematic review and economic evaluation," *Health Technol. Assess. (Rockv).*, vol. 11, no. 40, p. iii-79, 2007.

[145] F. A. Yafi, S. North, and W. Kassouf, "First- and second-line therapy for metastatic urothelial carcinoma of the bladder," *Curr. Oncol.*, vol. 18, no. 1, pp. e25-34, 2011.

[146] K. E. Gascoigne and S. S. Taylor, "How do anti-mitotic drugs kill cancer cells?," *J. Cell Sci.*, vol. 122, no. 15, pp. 2579–2585, 2009.

[147] S. Suresh, "Biomechanics and biophysics of cancer cells," *Acta Mater.*, vol. 55, no. 12, pp. 3989–4014, 2007.

[148] A. Saez, A. Buguin, P. Silberzan, and B. Ladoux, "Is the Mechanical Activity of Epithelial Cells Controlled by Deformations or Forces?," *Biophys. J.*, vol. 89, no. 6, pp. L52–L54, 2005.

[149] D. Wirtz, K. Konstantopoulos, and P. C. P. P. C. Searson, "The physics of cancer: the role of physical interactions and mechanical forces in metastasis," *Nat. Rev. Cancer*, vol. 11, no. 512, p. 522, 2011.

[150] N. Yamaguchi, T. Mizutani, K. Kawabata, and H. Haga, "Leader cells regulate collective cell migration via Rac activation in the downstream signaling of integrin β1 and PI3K.," *Sci. Rep.*, vol. 5, p. 7656, 2015.

[151] A. A. Wagh *et al.*, "Localized elasticity measured in epithelial cells migrating at a wound edge using atomic force microscopy Localized elasticity measured in epithelial cells migrating at a wound edge using atomic force microscopy," vol. 1,

no. May 2008, pp. 54–60, 2012.

[152] J. W. O'Connor and E. W. Gomez, "Biomechanics of TGFβ-induced epithelial-mesenchymal transition: implications for fibrosis and cancer," *Clin. Transl. Med.*, vol. 3, no. 1, p. 23, 2014.

[153] D. Schneider *et al.*, "Tension monitoring during epithelial-to-mesenchymal transition links the switch of phenotype to expression of moesin and cadherins in NMuMG cells," *PLoS One*, vol. 8, no. 12, 2013.

[154] C. Gaggioli *et al.*, "Fibroblast-led collective invasion of carcinoma cells with differing roles for RhoGTPases in leading and following cells," *Nat. Cell Biol.*, vol. 9, no. 12, pp. 1392–1400, 2007.

[155] A. Manuscript, "Leading malignant cells initiate collective epithelial cell invasion in a three-dimensional heterotypic tumor spheroid model," *Clin. Exp. Metastasis.*, vol. 30, no. 5, pp. 615–630, 2014.

[156] Y. Shin, S. Han, E. Chung, and S. Chung, "Intratumoral phenotypic heterogeneity as an encourager of cancer invasion.," *Integr. Biol. (Camb).*, vol. 6, no. 7, pp. 654–61, 2014.

[157] S. Mi *et al.*, "Microfluidic co-culture system for cancer migratory analysis and anti-metastatic drugs screening," *Sci. Rep.*, vol. 6, no. 1, p. 35544, 2016.

[158] A. Rape, W. Guo, and Y. Wang, "Microtubule depolymerization induces traction force increase through two distinct pathways," *J. Cell Sci.*, vol. 124, no. 24, pp. 4233–4240, 2011.

[159] M. V. Blagosklonny, "The power of chemotherapeutic engineering: Arresting cell cycle and suppressing senescence to protect from mitotic inhibitors," *Cell Cycle*, vol. 10, no. 14, pp. 2295–2298, 2011.

[160] X. S. Hongchi Jiang, Weiyang Tao, Mu Zhang, Shangha Pan, Jagat R Kanwar, "Low-Dose Metronomic Paclitaxel Chemotherapy Suppresses Breast Tumors and Metastases in Mice," *Cancer Invest.*, vol. 28, no. 1, pp. 74–84, 2010.

[161] I. Turin *et al.*, "In Vitro Efficient Expansion of Tumor Cells Deriving from Different

Types of Human Tumor Samples," *Med. Sci.*, vol. 2, no. 2, pp. 70–81, 2014.

[162] W. Sun, C. T. Lim, and N. A. Kurniawan, "Mechanistic adaptability of cancer cells strongly affects anti-migratory drug efficacy," *J. R. Soc. Interface*, vol. 11, no. 99, pp. 20140638–20140638, 2014.

[163] K. Burridge and E. S. Wittchen, "The tension mounts: Stress fibers as force-generating mechanotransducers," *J. Cell Biol.*, vol. 200, no. 1, pp. 9–19, 2013.

[164] J. V. S. G. Christine E. Garnett, Joo Yeon Lee, "Contribution of Modeling and Simulation in the Regulatory Review and Decision-Making: U.S. FDA Perspective," in *Clinical Trial Simulations, AAPS Advances in the Pharmaceutical Sciences Series, vol. 1*, Springer, New York, NY, 2011.

[165] M. Sato *et al.*, "Quantitative modeling and simulation in PMDA: A Japanese regulatory perspective," *CPT Pharmacometrics Syst. Pharmacol.*, vol. 6, no. 7, pp. 413–415, 2017.

[166] D. Barbolosi, J. Ciccolini, B. Lacarelle, F. Barlési, and N. André, "Computational oncology — mathematical modelling of drug regimens for precision medicine," *Nat. Rev. Clin. Oncol.*, vol. 13, no. 4, pp. 242–254, 2015.

[167] J. A. David W. Thomas, Justin Burns, A. Caroll, C. Dow-Hygelund, and M. Hay, "Clinical development success rates 2006-2015," *Biomedtracker, Biotechnol. Innov. Organ. (BIO), Amplion*, no. June, p. https://www.bio.org/sites/default/files/Clinical%2, 2016.

[168] C. Printz, "Failure rate: Why many cancer drugs don't receive FDA approval, and what can be done about it," *Cancer*, vol. 121, no. 10, pp. 1529–1530, 2015.

[169] C. Y. Park *et al.*, "High-throughput screening for modulators of cellular contractile force," *Integr. Biol.*, vol. 7, no. 10, pp. 1318–1324, 2015.

[170] J. Wolff, "The classic: On the inner architecture of bones and its importance for bone growth," *Clin. Orthop. Relat. Res.*, vol. 468, no. 4, pp. 1056–1065, 2010.

[171] A. M. Goldyn, B. A. Rioja, J. P. Spatz, C. Ballestrem, and R. Kemkemer, "Force-induced cell polarisation is linked to RhoA-driven microtubule-independent focal-

adhesion sliding," *J. Cell Sci.*, vol. 122, no. 20, pp. 3644–3651, 2009.

[172] W. Marth and A. Voigt, "Collective migration under hydrodynamic interactions - a computational approach," *Arxiv*, pp. 1–18, 2016.

[173] J. W. Astin *et al.*, "Competition amongst Eph receptors regulates contact inhibition of locomotion and invasiveness in prostate cancer cells.," *Nat. Cell Biol.*, vol. 12, no. 12, pp. 1194–204, 2010.

[174] R. A. Desai, S. B. Gopal, S. Chen, and C. S. Chen, "Contact inhibition of locomotion probabilities drive solitary versus collective cell migration," *J. R. Soc. Interface*, vol. 10, no. 88, p. 20130717, 2013.

[175] M. L. Woods, C. Carmona-Fontaine, C. P. Barnes, I. D. Couzin, R. Mayor, and K. M. Page, "Directional collective cell migration emerges as a property of cell interactions," *PLoS One*, vol. 9, no. 9, 2014.

[176] A. P. Vamvakidou, M. J. Mondrinos, S. P. Petushi, F. U. Garcia, P. I. Lelkes, and A. Tozeren, "Heterogeneous Breast Tumoroids: An In Vitro Assay for Investigating Cellular Heterogeneity and Drug Delivery," *J. Biomol. Screen.*, vol. 12, no. 1, pp. 13–20, 2007.

[177] G. Charras and E. Sahai, "Physical influences of the extracellular environment on cell migration," *Nat. Rev. Mol. Cell Biol.*, vol. 15, no. 12, pp. 813–824, 2014.

[178] F. Petrella *et al.*, "Paclitaxel-releasing mesenchymal stromal cells inhibit in vitro proliferation of human mesothelioma cells.," *Biomed. Pharmacother.*, vol. 87, pp. 755–758, 2017.

[179] C. Lv *et al.*, "Low-Dose Paclitaxel Inhibits Tumor Cell Growth by Regulating Glutaminolysis in Colorectal Carcinoma Cells," *Front. Pharmacol.*, vol. 8, no. May, pp. 1–10, 2017.

[180] K. Sun, X.-H. Tang, and Y.-K. Xie, "Paclitaxel combined with harmine inhibits the migration and invasion of gastric cancer cells through downregulation of cyclooxygenase-2 expression.," *Oncol. Lett.*, vol. 10, no. 3, pp. 1649–1654, 2015.

[181] L. Volk-Draper *et al.*, "Paclitaxel therapy promotes breast cancer metastasis in a

TLR4-dependent manner," *Cancer Res.*, vol. 74, no. 19, pp. 5421–5434, 2014.

[182] Q. Li *et al.*, "Low doses of paclitaxel enhance liver metastasis of breast cancer cells in the mouse model," *FEBS J.*, vol. 283, no. 15, pp. 2836–2852, 2016.

[183] Q. Z. Yanjun Chen, Qiaoxin Yue, Gejing De , Jie Wang , Zhenzhen Li , Shuiming Xiao , Huatao Yu , Hai Ma , Feng Sui, "Inhibition of breast cancer metastasis by paclitaxel-loaded pH responsive poly(β-amino ester) copolymer micelles," *Nanomedicine*, vol. 12, no. 2, 2016.

[184] B. A. Weaver, "How Taxol/paclitaxel kills cancer cells," *Mol. Biol. Cell*, vol. 25, no. 18, pp. 2677–2681, 2014.

[185] A. Hirose *et al.*, "Low-dose paclitaxel inhibits the induction of epidermal-mesenchymal transition in the human cholangiocarcinoma CCKS-1 cell line," *Oncol. Lett.*, vol. 6, no. 4, pp. 915–920, 2013.

[186] K. Lien, S. Georgsdottir, L. Sivanathan, K. Chan, and U. Emmenegger, "Low-dose metronomic chemotherapy: A systematic literature analysis," *Eur. J. Cancer*, vol. 49, no. 16, pp. 3387–3395, 2013.

[187] D. P. Stonko, L. Manning, M. Starz-Gaiano, and B. E. Peercy, "A mathematical model of collective cell migration in a three-dimensional, heterogeneous environment," *PLoS One*, vol. 10, no. 4, pp. 1–19, 2015.

[188] S. Aland, H. Hatzikirou, J. Lowengrub, and A. Voigt, "A Mechanistic Collective Cell Model for Epithelial Colony Growth and Contact Inhibition," *Biophys. J.*, vol. 109, no. 7, pp. 1347–1357, 2015.

[189] F. J. Vermolen and A. Gefen, "A semi-stochastic cell-based formalism to model the dynamics of migration of cells in colonies," *Biomech. Model. Mechanobiol.*, vol. 11, no. 1–2, pp. 183–195, 2012.

[190] R. Rey and J. M. García-Aznar, "A phenomenological approach to modelling collective cell movement in 2D," *Biomech. Model. Mechanobiol.*, vol. 12, no. 6, pp. 1089–1100, 2013.

Appendix

Model stability and accuracy

Simulations

The effect of the time step on the model stability and accuracy was investigated. Co-cultures of 200 bladder cells were considered. The aim was to challenge the model and explore the instability of the solution. For this reason, a high adhesion mismatch between normal and cancer cells was considered since it is associated with high cell forces, see Table A.1. Equal active velocity was assigned to normal and cancer cells. Intercellular force and velocity were computed for all the cells every iteration to detect potential oscillating behaviour.

Table A.1 – Cell properties for the model stability and accuracy study.

	Bladder normal cells	Bladder cancer cells
Young's modulus (kPa)	10	0.3
Intercellular adhesion energy (nN/μm)	0.05	36
Active velocity (μm/min)	5	

Results

The time step is associated with the maximum force possible in the model and consequently, the maximum displacement allowed for cells per iteration. As previously mentioned in Chapter 3, a maximum force of 500 nN, time step of 0.189 seconds, is required to model the migration of all the cell populations investigated in this work. However, this value of time step, associated with a maximum cell displacement per iteration of 8.9% of the cell radius, did not enable force relaxation (as shown in Figure A.1). For this reason, lower values of time step were tested until relaxation was observed, which happened for a time step of 0.135 seconds. In order to confirm the solution accuracy a time step with half of this value was also tested, see Table A.2.

The results in Figure A.1 refer to one of the seeding replicates as an example.

Since all the cells have the same active velocity, 5 µm/min=0.083 µm/s, their velocity should approach this value as they align their migration direction. Intercellular forces should increase at the beginning of cell migration and then decrease as cells move synchronously. As observed in Figure A.1, this does not occur for time step 1. Force relaxation does not happen and cells reach an average velocity of 0.27±0.83 µm/s. However, force relaxation happens for both time step 2 and 3. The average velocity approaches $0.083±5.6x10^{-4}$ µm/s and $0.083±3.2x10^{-4}$ µm/s for time steps 2 and 3, respectively. The force and velocity peaks observed for time step 3 are explained by cell contact changes.

It can be concluded that a time step of 0.135 seconds, maximum cell displacement of 2.5 % of the cell radius per iteration, is small enough to ensure both solution stability and accuracy. This time step requires an iteration number on the order of magnitude of $53x10^3$ to model two hours of real time cell migration. Modelling five seeding replicates of a 200 cell population requires globally 2.4G of maximum virtual memory and 29 hours of CPU time.

The results obtained for time step 1 are better understood by investigating the level of force for each cell, see Figure A.2. High levels of force and velocity are obtained for cancer cells and result from the solution instability. Oscillations in intercellular force occur every iteration, more evident for the cells with higher force, the cancer cells. Cells follow an adhesion-repulsion cycle, adhering to each other in one iteration and repelling in the next one (Figure A.3).
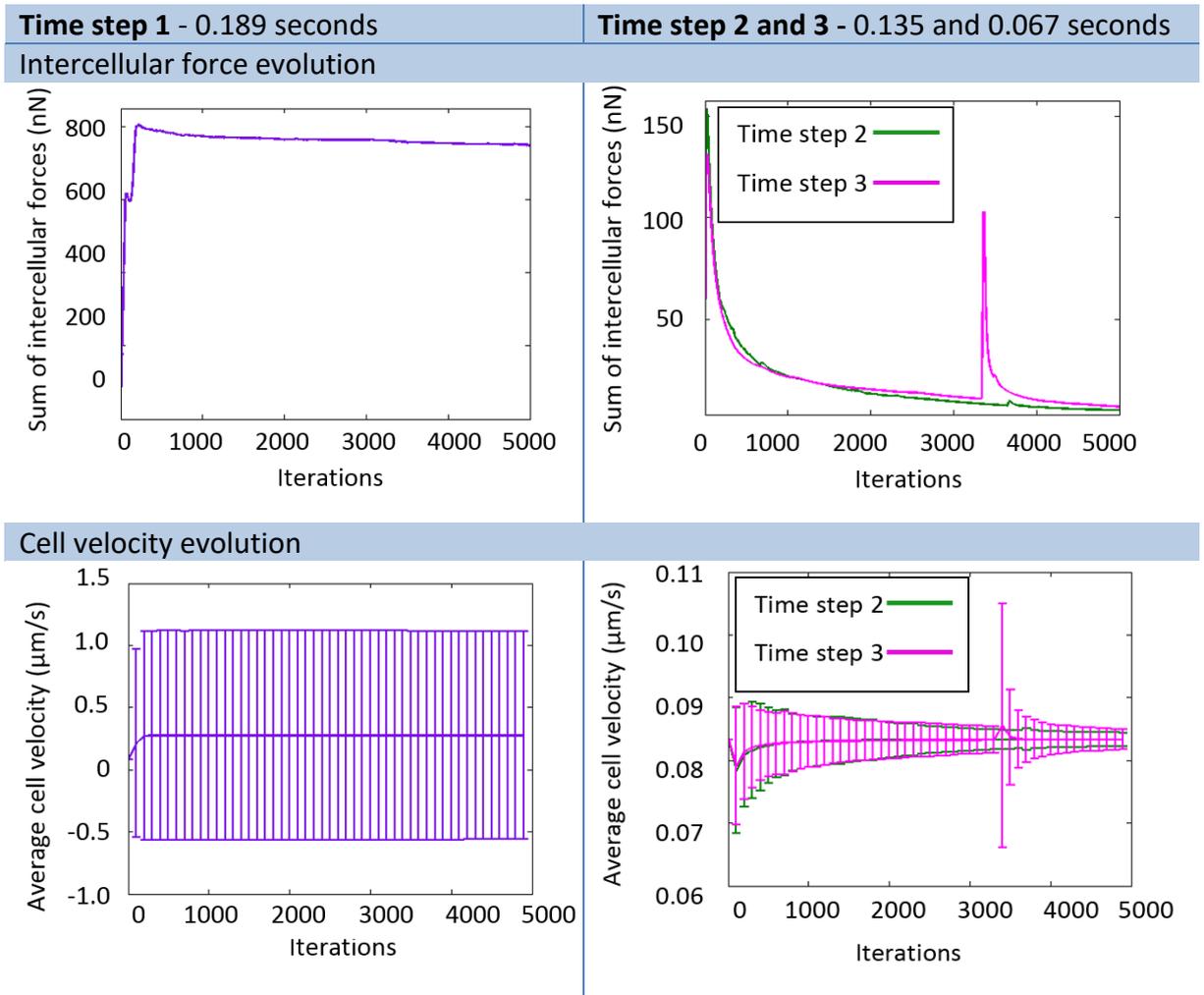
| Time step 1 - 0.189 seconds	Time step 2 and 3 - 0.135 and 0.067 seconds
Intercellular force evolution	

| Cell velocity evolution | |

Figure A.1. Intercellular force and cell velocity evolution for the three time step values considered. Force was computed as the sum of intercellular forces for all the cells modelled. Cell velocity was averaged for all the cells and the associated standard deviation is shown.

Table A.2 – Maximum displacement per iteration for each time step studied.

|	Time step 1	Time step 2	Time step 3
Time step (seconds)	0.189	0.135	0.067
Maximum cell displacement per iteration (µm)	0.89	0.25	0.085
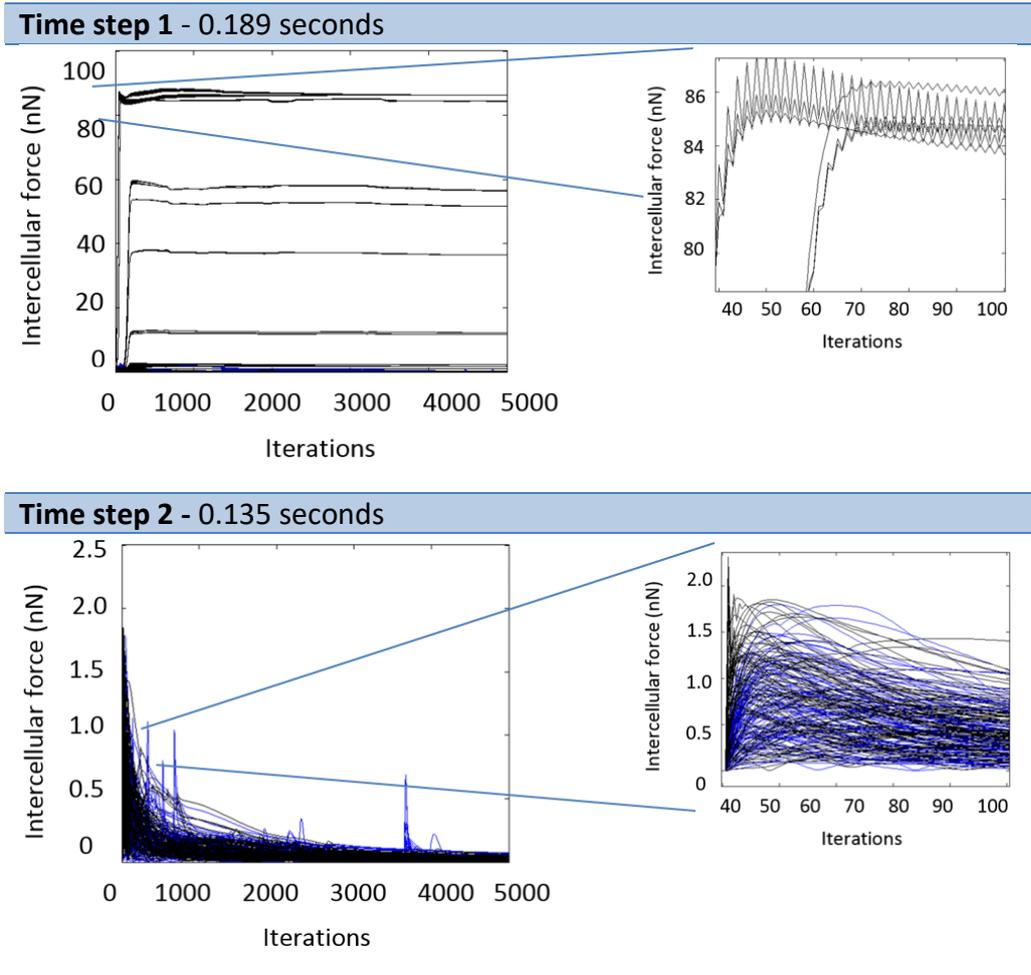
Figure A.2. Level of force per cell shows that force oscillates every iteration for time step 1. This is not observed for time step 2. Each line corresponds to the evolution of intercellular force for one cell. For normal cells intercellular force is in blue and for cancer cells intercellular force is in black.
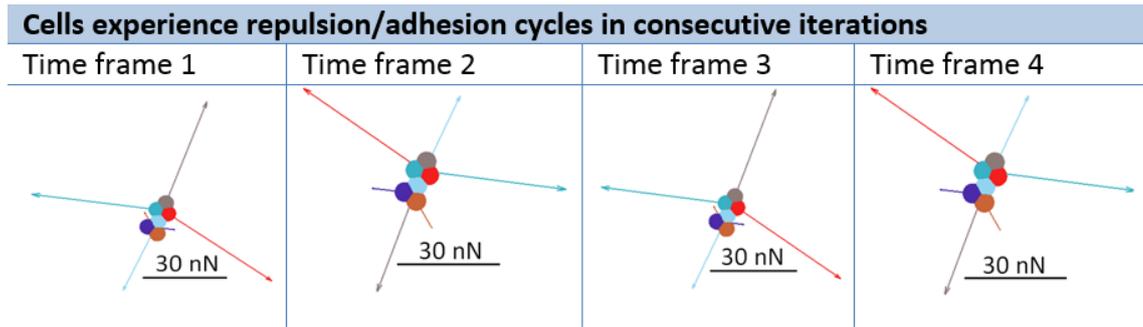
Figure A.3. Cells with higher intercellular force are shown for four consecutive iterations using time step 1. These cells experience a repulsion/adhesion cycle. They are shown in different colour together with their intercellular force vector.

Discussion

The value for the time step should be chosen according to the time scale of the phenomenon modelled, being directly constrained by the model formulation. The time step used when modelling cell populations vary greatly being in the order of magnitude of 10^{-2} to 10^{1} s [98], [187], [188].

For the collective cell migration model developed in this work it was found that the cell displacement per iteration should not exceed 2.5 % of the cell radius, which is achieved with a time step of 0.135 seconds. This time step ensures both the solution stability and accuracy, see Figure A.1.

Vermolen et al [189] proposed a model for collective migration. It is suggested by the authors that collective migration emerges from cells generating a mechanical signal that is sensed by the others through the substrate. Intercellular repulsions were included based on the Hertz model. An adaptive time step scheme was used in which the time step is limited by the cell with the highest velocity. The maximum displacement for cells was defined as 25% of their diameter, 20 times higher than the one established in this work. Although it is stated that reducing the time step in half did not alter the results, oscillatory behaviour of the kind mentioned in this Appendix (Figure A.2), is reported for cells in high proximity.

On the other hand, Rey et al [190] developed a collective cell migration model that describes intercellular interactions based on the interatomic Morse potential. Model

stability and accuracy was found for displacements of less than 0.6 % of the cell radius per iteration, a value much closer to the one reported here.

The suitable time step is specific of the model chosen. In the context of intercellular mechanical interactions repulsion/adhesion instabilities depend on the force-distance curve defining contact. It is important to ensure that the change in the intercellular force is sufficiently small to ensure both the solution stability and accuracy.